ANÁLISE DE UM AMORTECEDOR DE COLUNA DE LÍQUIDO SINTONIZADO EM UMA TURBINA EÓLICA SUJEITA A CARREGAMENTO ALEATÓRIO

Por,

Mansour Hassan Alkmim

DISSERTAÇÃO DE MESTRADO EM CIÊNCIAS MECÂNICAS

UNIVERSIDADE DE BRASÍLIA

FACULDADE DE TECNOLOGIA
DEPARTAMENTO DE ENGENHARIA MECÂNICA

UNIVERSIDADE DE BRASÍLIA
FACULDADE DE TECNOLOGIA
DEPARTAMENTO DE ENGENHARIA MECÂNICA

ANÁLISE DE UM AMORTECEDOR DE COLUNA DE LÍQUIDO SINTONIZADO EM UMA TURBINA EÓLICA SUJEITA A CARREGAMENTO ALEATÓRIO

MANSOUR HASSAN ALKMIM

ORIENTADOR: ADRIANO TODOROVIC FABRO

DISSERTAÇÃO DE MESTRADO EM CIÊNCIAS MECÂNICAS

PUBLICAÇÃO: ENM.DM

Brasília, 5 de outubro de 2017

UNIVERSIDADE DE BRASÍLIA
FACULDADE DE TECNOLOGIA
DEPARTAMENTO DE ENGENHARIA MECÂNICA

ANÁLISE DE UM AMORTECEDOR DE COLUNA DE LÍQUIDO SINTONIZADO EM UMA TURBINA EÓLICA SUJEITA A CARREGAMENTO ALEATÓRIO

MANSOUR HASSAN ALKMIM

DISSERTAÇÃO DE MESTRADO SUBMETIDA AO DEPARTAMENTO DE ENGENHARIA MECÂNICA DA FACULDADE DE TECNOLOGIA DA UNIVERSIDADE DE BRASÍLIA, COMO PARTE DOS REQUISITOS NECESSÁRIOS PARA A OBTENÇÃO DO GRAU DE MESTRE EM CIÊNCIAS MECÂNICAS.

APROVADO POR:

Adriano Todorovic Fabro DSc. (ENM/ UnB)
(Orientador)

Aline Souza de Paula DSc. (ENM/ UnB)
(Examinadora interna)

Sergio Henrique da Silva Carneiro DSc. (FGA/ UnB)
(Examinador externo)

Brasília 5 de outubro de 2017

Acknowledgments

I would like to express my sincere appreciation and respect to my supervisors DSc. Adriano T. Fabro and DSc. Marcus V. G. de Morais for their guidance, advise and encouragement in carrying out this research. A especial thanks to DSc. Aline S. de Paula for the opportunities that opened many doors for me during graduation.

I also would like to thanks my colleagues from the Dynamic System's Group with whom I shared my time at University of Brasilia.

Finally, a especial note of gratitude goes to my family for their moral and financial support through out my life.

We know the past but cannot control it. We control the future but cannot know it.

- Claude Shannon

Resumo

Os sistemas passivos de dissipação de energia abrangem uma variedade de materiais e dispositivos para melhorar o amortecimento de estruturas. Entre os atuais sistemas de dissipação de energia passiva, o amortecedor de coluna de líquido sintonizado (TLCD), uma classe de controle passivo que utiliza líquido em um reservatório de forma "U", tem sido amplamente pesquisado em diversas aplicações. O principal objetivo desta dissertação é desenvolver técnicas de análise numéricas e experimentais para um TLCD com aplicação em turbinas eólicas submetido a cargas de vento aleatório.

A análise numérica está dividida em duas etapas. A primeira etapa considera o modelo determinístico da turbina e TLCD. Um algoritmo de otimização é utilizado para encontrar parâmetros ótimos do TLCD submetido a espectros de vento aleatório. Em seguida, um exemplo numérico com um modelo de turbina eólica simplificado é estudado para ilustrar a eficácia do TLCD e é mostrado que diferentes espectros de vento podem afetar significativamente os resultados de otimização, isto é, os parâmetros do TLCD. Os resultados no tempo e frequência da análise de vibração aleatória mostram uma redução satisfatória dos níveis de vibração de resposta.

Na segunda etapa, considera-se o modelo não determinista com objetivo de quantificar incertezas nos parâmetros do TLCD e da estrutura. A função de resposta em frequência do sistema com TLCD é investigada considerando dois casos de incerteza de parâmetros. Para o primeiro caso, os resultados mostraram que a incerteza só é predominante perto da região de ressonância e antirressonância e pode interferir na condição ideal do TLCD. Para o segundo caso, as incertezas estão presentes em todas a faixa de frequência.

Finalmente, uma análise experimental é realizada. A caracterização dos parâmetros modais do TLCD e da estrutura é realizada e os resultados numéricos e teóricos se mostram em boa concordância. Em seguida, A resposta do sistema acoplado é investigada. Os resultados mostram que o efeito da massa adicional é o predominante. Embora o efeito do TLCD tenha sido pequeno, ele apresenta uma redução de vibração próximo a sua frequência natural.

Palavras-chaves: vibração aleatória, análise estocástica, otimização, quantificação de incertezas

Abstract

Passive energy dissipation systems encompass a range of materials and devices for enhancing damping. Among the current passive energy dissipation systems, tuned liquid column damper (TLCD), a class of passive control that utilizes liquid in a "U" shape reservoir to control structural vibration of the primary system, has been widely researched in a variety of applications. The main objective of this thesis is to develop numerical and experimental analysis techniques for a liquid column damper subjected to random wind loads with particular application in wind turbines.

The numerical analysis in this thesis is divided in two stages. The first stage consider the deterministic model of the wind turbine and TLCD. An optimization approach is used to search for optimized parameters considering different wind spectrums. Then, a numerical example with a simplified wind turbine model is given to illustrate the efficacy of TLCD and it is shown that different wind spectra can significantly affect the optimization results, i.e. the TLCD parameters. Time and frequency domain results from the random vibration analysis are shown with satisfactory reduction of the response vibration levels.

In the second stage, nondeterministic model is studied with goal to quantify uncertainties in the damper and structure parameters. The frequency response function is investigated considering two cases of parameter uncertainty. The results showed that, for the former, the uncertainty is only predominant near the resonance and anti-resonance region and can indeed interfere in the optimum condition of the absorber. For the latter, the uncertainties are presented in frequency range.

Finally, an experimental characterization of the TLCD and structure is carried out. The characterization of the modal parameters of the TLCD and the structure is performed and the numerical and theoretical results that show good agreement. Then, the response of the coupled system is investigated. Results showed that the effect of added mass is predominant. While the effects of TLCD were minimal, it showed a vibration reduction which validated the correctly tuned TLCD near its natural frequency.

Key-words: random vibration, stochastic analysis, optimization, uncertainty quantification

Contents

List of Figures

List of Tables

List of Simbols

H	Frequency response function
h	Impulse response function
j	Imaginary number
t	Time [s]
ω	Frequency [rad/s]
f	Frequency [Hz]
T	Period [s^{-1}]
τ	Time interval [s]
Δ	Sampling time interval [s]
P	Probability distribution function
p	Probability density function
x	Input function in time domain (Chapter 3)
x	Displacement of the structure (Chapter 5)
y	Output function in time domain
E	Expected value $E[x]$
R	Correlation function $R(\tau)$
S	Spectral density $S(\omega)$
v	mean wind velocity
z_0	hub height
ρ_{air}	air density
C_D	drag coefficient

β	roughness coefficient
c	Weibull mode parameter
ψ	Turbulence intensity
v_{hub}	Mean value of the hub height velocity
w	Transverse displacement response
c	Weibull mode parameter
ϕ	Spatial displacement
Y	Temporal displacement
E	Elastic modulus
L	Tower length
I	Moment of inertia
J	Rotary mass moment of inertia
M	Cantilever beam tip mass
m	Cantilever beam distributed mass
D	Cantilever beam width
t_h	Cantilever beam thickness
A_h	Cantilever beam cross section
ρ_s	Steel density
λ	Roots of the eigenvalue problem
ω_n	Natural frequency cantilever beam
T	Kinetic energy
M^*	Generalized mass
V	Potential (strain) energy
K^*	Generalized stiffness
u	Displacement of fluid
ρ	Water density
ξ	Head loss coefficient

A	Cross section area of TLCD
b	Horizontal length of TLCD
l	Total length of TLCD
g	Gravity constant
m_a	Mass of TLCD
c_a	damping of TLCD
k_a	stiffness of TLCD
ω_a	Natural frequency of TLCD
ζ_a	Damping ratio of TLCD
m_e	Mass of structure
c_e	damping of structure
k_e	stiffness of structure
ω_e	Natural frequency of structure
ζ_e	Damping ratio of structure
F	Excitations force
α	Length ratio
μ	Mass ratio
γ	Tuning ratio
Ξ	performance index (cost function)
ω_e	Natural frequency of structure
Φ	Mass normalized mode shape (eigenvectors)
Ψ	General normalization mode shape (eigenvectors)

1 Introduction

The current Brazilian energy scenario is undergoing impactful changes. There is a clear need to adjust the current energy sector that presents an imbalance. Brazil depends almost exclusively on hydroelectric power. According to data released by PNE 2030 (National Energy Plan), most of the energy produced in the country comes from hydroelectric plants. By the year 2030, it is expected that hydroelectric plants will have a share of 77.4 % of the energy matrix (Pottmaier et al., 2013).

Despite all the benefits of the hydroelectric plants, there are uncertainties about their future supply. Major projects such as S. Luiz do Tapajós and Belo Monte have faced serious socio-environmental conflicts such as the transposition of rivers, impacts on the fauna and conflicts with local communities. Another critical aspect of hydroelectric plants is the existence of a great dependence on the climatic conditions and the location of this energy, found primarily in the Amazon region. Moreover, recent examples of poor management of water levels in reservoirs led to the reactivation of thermoelectric plants that generate environmental and economic damages.

Since there is a need to diversify the Brazilian energy matrix, other energy sources that are efficient and renewable are sought. Among the possible options that stand out, wind and solar energy are becoming good options due to good geographical and economic conditions (Jong et al., 2013).

The increasing height of wind turbine increases the need of new methods to ensure structural reliability. Wind turbines are structures that convert the mechanical movement generated by the force of the winds into electric energy. The wind reaches the rotor blades that transfer the rotational motion to an electric generator responsible for producing electricity.

During the design phase, wind turbines must meet a wind speed that produces the maximum output power. Occasionally, the wind forces can be dangerously high which forces the control system to limit the movement of the blades in order to avoid overloading of the rotor, the gearbox and the generator. Usually, wind turbines have angular control systems in the turbines and brakes that maintain integrity and prevent excessive vibration of the towers. These systems are useful because they regulate rotor speed based on wind speed under certain operating conditions. Generally, wind turbines have small damping values compared to other structures. The damping ratio resulting from aerodynamic

damping corresponds to 1-2 % (Altay et al., 2014).

Concerns over the integrity of wind turbines throughout the years have become a key point during design phase. The advance of the technology in wind turbines have caused an increase in its size and efficiency. In this way, challenges arise to avoid excessive vibration of both propellers and towers. Higher and more slender structures also raise concerns over their integrity and longevity.

The dynamic behavior of wind turbines has led to several technical studies in recent years. The reduction of vibration, with the purpose of increasing its lifespan, motivates the use of several passive or semi-active vibration control techniques. Among the various vibration control proposals, tuned liquid column dampers (TLCDs) have been considered in several publications in recent years and have become a feasible option with relative low cost and good efficiency.

Analyzing the dynamic response in the frequency domain has proven to be a feasible initial approach of understanding the wind turbine behavior. Design optimization can be carried out rapidly in the frequency domain to increase the damper efficiency. A more rigorous analysis can be carried out after the initial parameter optimization in the frequency domain is completed. This approach increase qualitative and quantitative understanding and can lead to reduced design costs and better optimized schemes.

Some of the questions we hope to address in this thesis are:

- To what extent will the vibration suppression take place with the added damper?
- Is the simplified model of wind turbine acceptable? Why?
- How much can the vibration suppression be improved from optimized parameters?
- How much variability the TLCD's parameters have? How does it influence the turbine performance?
- How the model and dynamic response of the structure compare with experimental data?

1.1 The objectives of the study

The main objective of the study is to develop numerical and experimental techniques to investigate the behavior of a liquid column damper subjected to random wind loads with particular application in wind turbines. For this reason, we have the following secondary objectives:

- a numerical analysis considering the deterministic model of the wind turbine and TLCD with goal of controlling the structure for small displacement without consi-

dering the rotational inertia from the blades. An optimization approach is adopted which allows the search of optimized parameter considering different wind spectrums.

- a numerical analysis considering the nondeterministic model with goal of quantifying uncertainties in the TLCD's damper and structure stiffness.
- an experimental phase is carried out with goal of characterization of the TLCD and structure and then compare it with numerical result.

1.2 Organization of the Thesis

This thesis is organized as follows.

Chapter 1 presents the introduction and objectives.

Chapter 2 presents some of the main structural control techniques in suppressing vibration of structures. First, the state of the art of structural control is presented. Then, the relevant types of control systems are discussed. Emphasis will be given to passive controls and more specifically on the tuned liquid absorbers and their use in wind turbines which is the subject of this work. A literature review is presented considering the use of absorbers in several applications and their development in recent years.

Chapter 3 presents a review on fundamental concepts of random vibration and probability theory. The aim is to review the key principles of the probability theory and thus facilitate its application to solve problems in random vibration.

Chapter 4 deals with the effects of the probabilistic aspect of wind in low atmospheric layers on flexible structures. The problems is confined to along-wind response of structures. Moreover, cross-wind response or aero-elastic coupled problems are left out of discussion. The idea is to discuss some general notions, which should cast some light on the complexity of the phenomenon.

Chapter 5 discusses how winds influence the dynamic behavior of the structure and how to optimize the TLCD with respect to different wind spectrums. It is therefore of interest to study how a simplified dynamic model could estimate the structural response. The simplified model has to be reduced to the elementary coordinates but still have to describe the relevant physical process under consideration with good accuracy. Such a simplified model can be used as an early design of new wind turbines. This work focus on the structural dynamic aspect of structures such as lattice towers with concentrated mass at the top, hence, the model does not include the gyroscopic effects due to turbine blade rotation.

In Chapter 6 we propose the use of a optimization algorithm for the TLCD's parameters subjected to an arbitrary wind spectra, given by its power spectral density (PSD). A simple verification is made considering the analytical solution of undamped

primary structure under white noise excitation. Finally, a numerical example with a simplified wind turbine model is given to illustrate the efficacy of TLCD. Time and frequency domain results from the random vibration analysis are also shown.

In Chapter 7, parametric uncertainties in a TLCD applied in wind turbines are investigated. The assumption that uncertainties in structures have negligible response can be unacceptable in real situations and, beside that, uncertainties in the performance-related cannot be included in the damper parameter optimization. For this reason, to increase the credibility of the model, these uncertainties are included to help describe the range of potential outputs of the system at some probability level and estimate the relative impacts of input variable uncertainties. Two different cases are studied, the first one we only consider uncertainties in the absorber damping ratio and, in the second case, we consider both uncertainties in the absorber damping ratio and the structural stiffness.

Finally, in Chapter 8, an experimental setup built in the Vibration Laboratory of the Dynamic Systems Group (GDS) is proposed. An experimental procedure is carried out to characterize the modal parameters of the TLCD and structure. Finally, the response of the coupled system is investigated.

2 Structural Control

Structural control can be an important part of designing new structure and retrofitting existing ones. Design for strength alone does not necessarily ensure that the structure will respond well dynamically. It was during the Second World War that concepts such as vibration isolation, vibration absorption and vibration damping were developed and effectively applied to aircraft structures. The technology quickly moved into civil engineering. Similar to the general controls literature, the structure control tends to represent diverse interests and viewpoints, though all share common goal: the protection of buildings and the people around them.

This chapter presents some of the main structural control techniques in suppressing vibration of structures. First, a brief introduction is presented. Then, the relevant types of control systems are discussed. Emphasis will be given to passive controls and more specifically on the tuned liquid absorbers and their use in wind turbines, which is the subject of this work. A brief bibliographic review is made about the use of absorbers in several applications and their development in recent years.

2.1 Introduction

The need to build larger and more complex structures has created challenges for engineers who have to deal with unwanted vibrations and at the same time maintain safe constructions. For this reason, vibration absorption methods are used extensively. Engineers from various parts of the world have been using vibration control methods in recent decades mainly in the following areas:

- tall and slender structures (bridges, chimneys, towers) that tend to be dangerously excited by the wind in one or more of its natural modes;
- stairs and walkways subject to the resonance due to the movement of pedestrians. These vibrations are generally not dangerous to the structure itself, but can become very unpleasant to people;
- metal structures that vibrate at a harmonic frequencies by the action of machines, such as sieves, centrifuges, fans, etc;

- decks and boats excited in one of their natural modes by the main engines, equipment embarked or even by the rhythm of the waves.

In recent years, innovations that enhance the functionality and security of structures against natural and human disasters are at various stages of research and development. Globally, they can be grouped into three areas, passive control, active control, and semi-active or hybrid control.

Due to economic reasons, it is acceptable that structures suffer damage as long as there is no collapse and its useful life is preserved. However, when the structure function is compromised no damage is allowed. In this case, over large or continuous loads the structures should be able to absorb and dissipate energy in a stable manner for several cycles without damage being caused to it and being sufficiently strong to avoid or minimize inelastic actions.

For instance, during a seismic event or in the presence of strong winds, a finite amount of energy is added to the structure. This energy is transformed into both kinetic and potential energy (deformation) that must be absorbed or dissipated by heat. If there is no damping, the structure will vibrate indefinitely. However, there is always a level of damping inherent in the structure that dissipates part of the energy and therefore reduces the amplitude of vibration until the motion ceases. The performance of the structure is improved if part of the energy can be absorbed, not only by the structure, but by some type of complementary device (Constantinou et al., 1998).

Structural control is a technique commonly used by civil and mechanical engineers that involves a dissipation or energy absorption device. Among the types of structural control, the dynamic absorbers have applications restricted to elastic structures. Dynamic absorbers are oscillatory systems that when attached to the structure and properly tuned in frequency close to a vibration mode or a harmonic excitation, a transfer of kinetic energy from the primary structure to the absorber occurs. Dynamic absorbers can have various forms, namely, tuned mass dampers (TMD), tuned liquid damper (TLD), tuned liquid column dampers (TLCD), or any combination of these devices each tuned to a specific frequency (Hartog, 1985).

A passive control strategy consist of motion control forces at the system fixation points. It does not require an external power source, the energy required to generate these forces comes from the movements of the attachment points during dynamic excitation. The relative displacement of these attachment points determines the amplitude and direction of the control forces.

Active control also develops motion control forces. However, the magnitude and direction of these forces is determined by a controller based on sensor information and a control strategy (algorithm) as shown in Figure 2.1. The active control uses some kind of external power source proportional to the magnitude of the vibrating body excitation to perform its function. A command produced by the signal processor informs the actuator

of the amount of displacement or force proportional to the signal to be executed in order to control the displacement and keep the system in a constant and controlled state. The feedback signal can be obtained in a number of ways based on distance, displacement, speed, acceleration, force, among others. An active control system, in principle, has a better and more versatile control response.

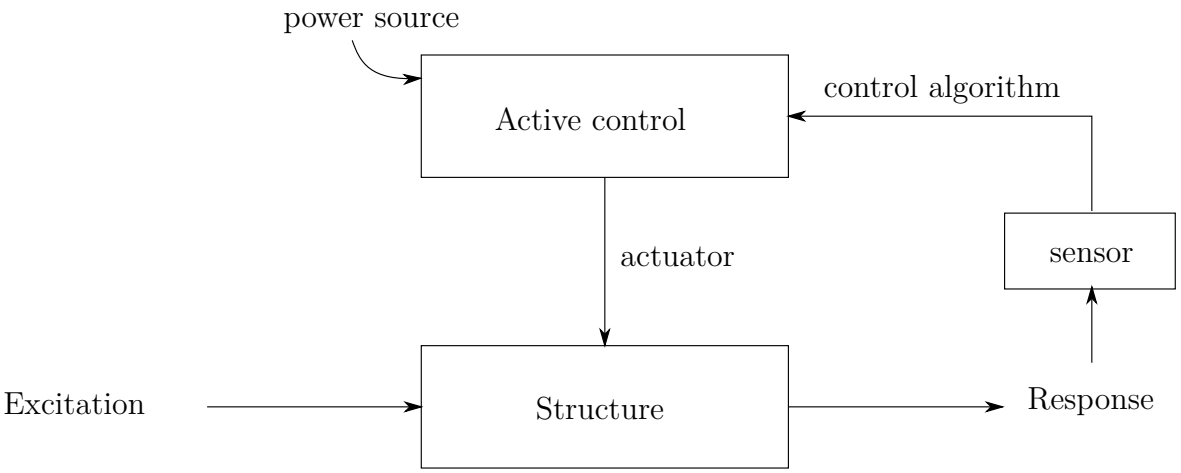

Figure 2.1 – Diagram of an active control system (Constantinou et al., 1998).

A hybrid control originates from passive controls that have undergone modification to allow adjustments in their mechanical properties. Hence, it implies the combination of an active and passive control in which it provides the reliability of passive devices, yet maintaining the versatility of fully active systems without requiring the large power source (Saaed et al., 2015). The mechanical properties of semi-active control systems can be represented similarly to the elements depicted in Figure 2.1. However, the control forces are developed through the movements of the attachment points of the semi-active device. Semi-active control systems require power source to adjust the mechanical properties of the system. In general, energy demand is low compared to active control systems. For instance, a system can be equipped with distributed viscoelastic damping and supplemented with an active mass damper near the top of the structure.

This work focus on passive control techniques. For this reason a more detail description of this approach, the reason why it was chosen and examples of application are given next.

2.2 Passive control

Passive structural control covers a range of materials and devices to increase damping and can be used for both natural disaster mitigation and rehabilitation of old or damaged structures. These devices are characterized by their ability to increase energy dissipation of the structure. This effect can be obtained by converting kinetic energy to heat, or by transferring energy between vibration modes (Soong & Dargush, 1997). Structural control includes equipment that operates based on the principles of friction,

yielding of metals, phase transformation, deformation of viscoelastic solids or fluids and fluid orificing that acts as an absorber or supplementary dynamic vibration absorber. Table 2.1 summarizes the classification of these devices.

Passive control is the simplest type of control system since it does not require any external power source or a control algorithm in form of actuators. The energy in passively controlled structural systems are developed in response to the displacement of the main structure in dynamic excitation as shown in Figure 2.2. They are optimally tuned to protect the structure from a specific dynamic loading, but their efficiency will not be the optimal for other types of dynamic loading. Next, we focus our discussion solely on dynamic vibration absorber, which are the main subject of this thesis.

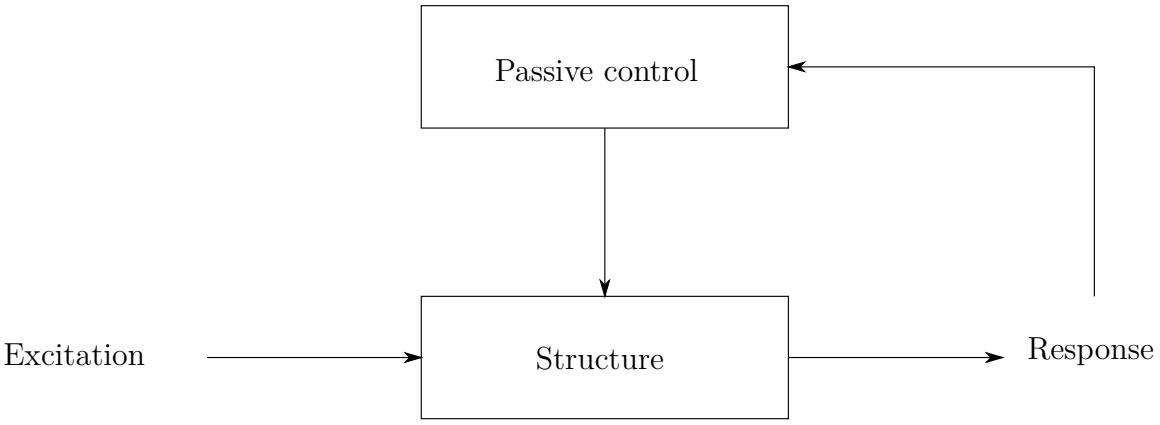

Figure 2.2 – Diagram of a passive control system (Constantinou et al., 1998).

2.2.1 Tuned mass damper (TMD)

Tuned mass damper had its first appearance in patents of Frahm (1911), and was extensively studied by Hartog (1985). The scheme shown in Figure 2.3 is known as Frahm's Absorber. The device consists of a small mass m and a spring with rigidity k fixed to the main mass M that has rigidity K. Considering the simplest case of harmonic loading it is possible to keep the main mass M completely stationary when the natural frequency of the absorber $\sqrt{k/m}$ is chosen (tuned) as the excitation frequency.

The first structures to use TMDs were aimed at absorbing wind-induced excitation. TMDs were installed at the Centerpoint Tower in Sydney, Australia, and at Citicorp in New York. The building can be represented by a simple modal mass of approximately 20 tons so that the TMD forms the system of two degrees of freedom. Tests performed on Citicorp showed that TMD produces 4 % more damping than the 1 % damping of the original structure which can reduce the acceleration levels of the structure by about 50 % (Soong & Dargush, 1997).

In recent years, numerical and experimental studies have been carried out to evaluate the efficiency of TMDs. It is worth noting that passive TMD can only be tuned

Table 2.1 – Summary of classification of passive control systems and common passive control devices

Passive control classification	**Description**	**Common devices**
Seismic isolation devices	Part of the energy is absorbed by the isolation system. Efficient against vibrations transmitted through ground, such as traffic and seismic vibration. It can be implemented at different locations within structures.	elastomeric-based systems: low-damping natural, synthetic rubber bearings (LDRBs), lead-plug bearings (LRBs), high-damping natural rubber (HDNR) systems; Isolation systems based on sliding: Teflon Articulated Stainless Steel (TASS) systems, friction pendulum systems (FPSs), and sleeved-pile isolation systems (SPISs).
Energy dissipation devices	Relatively small elements located between the main structure and the bracing system. The main role is to absorb or divert part of the input energy.	Hysteretic devices: Metallic dampers and friction dampers; Viscoelastic devices (VE): viscoelastic solid dampers, viscoelastic fluid dampers; Recentering devices: pressurized fluid dampers (PFD), preloaded spring-friction dampers (PSFD); Phase transformation dampers; Dynamic vibration absorber: tuned mass dampers (TMD), tuned liquid damper (TLD)

at a specific frequency. For cases of n-degrees of freedom structures that have TMD, the response to the first mode of vibration (first degree of freedom) can be reduced considerably, although the other responses show an increase in vibration. For seismic type excitations, considering a 12-story building, the response to the first mode of vibration corresponds to more than 80 % of the total motion. However, for larger structures the response to the other modes of vibration becomes more significant (Soong & Dargush, 1997).

2.2.2 Tuned liquid damper (TLD)

TLD is a class of TMD where the mass is replaced by a liquid (usually water) to act as a dynamic vibration absorber. Its basic principle involves installing a TLD to reduce the dynamic response of the structure in a similar way to a TMD. However, the system response is nonlinear due to the effect of sloshing (movement of irregular fluid in the reservoir near the surface) or the presence of reservoir interior holes that generate turbulent effects. Compared to TMDs, the advantages associated with TLDs include low

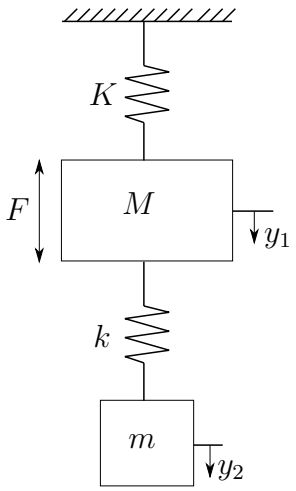

Figure 2.3 – Example of a TMD, undamped system with main mass subjected to harmonic excitation (Soong & Dargush, 1997).

cost, virtually zero maintenance and tuning depending only on the chosen geometry of the reservoir.

Applications of TLDs were first carried out in Japan, among them, Nagasaki Airport in 1987, Yokohoma Marine Tower also in 1987, Higashi-Kobe cable-stayed bridge constructed in 1992 and Tokyo International Airport in 1993. The TLD installed at Tokyo International Airport consist of 1400 water containers, where floating particles and preservatives that serve to optimize energy dissipation through an increase in surface area and through contact between the particles are included. The containers are stacked in six layers on metal shelves. The total mass of the TLD is approximately 3.5 % of the mass of the first generalized mode of the tower. The frequency of sloshing is optimized at 0.743 Hz. Other works have been proposed and are in the design phase such as the Millennium Tower in Tokyo, Japan and Shanghai Financial Trade Center in Shanghai, China. In all cases, efficiency, economicity, adaptability to fit in different physical spaces and the fact that they are against failures when well designed are proven. For winds with instantaneous velocity of 25 m/s, the observed results show that TLD reduces the response to 60 % crosswind acceleration from the value without the damper (Soong & Dargush, 1997).

The TLDs have several ramifications, among them are tuned oscillatory dampers (TOD), tuned liquid column dampers (TLCD), circular tuned liquid dampers (CTLD), among others. The functioning of the TODs is due to the “sloshing” phenomenon of the liquid present in the container. A small part of the liquid in the TODs participates in the sloshing motion and therefore, to increase the liquid’s share, the TLCDs are proposed (Min et al., 2014).

The TLCDs are the focus of this work because it is still a fairly new solution for application in wind turbines. They have its operation due to the movement of the liquid in the liquid column. The column can have several geometries, in this work, the type of TLCD chosen has the shape of tube in “U”. Unlike TCDs, damping is dependent on

the amplitude of the liquid, and therefore the TLCD dynamics is nonlinear. The main advantages of TLCDs are its low cost, low maintenance frequency and multi use of the device for e.g. water tank. Besides that, the TLCD does not require any bearings, special floor type for installation, activation of the mechanism, springs, and other mechanical elements that only increase the price of vibration absorber expenses. Consequently, their geometry varies according to design needs making them quite versatile devices. Some recent applications of TLCDs are stabilization of ships, satellites, buildings and towers.

TLCDs can be controlled through a hole located in a horizontal section tube. According to the opening of that orifice, it is possible to control the coefficient of head loss associated with turbulent dissipation of kinetic energy of the liquid in its passage through the orifice section, consequently, affecting the damping of the structure. Although this is a possible solution, the adopted solution does not involve active control, but passive. The size of the orifice opening is decided in the tuning phase of the design.

The use of TLCDs as a mechanism of vibration absorption is quite interesting because the mechanism naturally has low frequencies and is relatively easy to tune to the structure. There are basically two types of energy absorption involved in this configuration, the absorption due to the TLCDs and the sloshing damping type where there is oscillation in the free surface of the liquid. Sloshing type absorption, although simple to apply, requires some considerations to be made in the optimization scheme, because the frequency of the absorber increases with the amplitude of excitation.

2.3 Previous works

Structural control gained significant space in applications in wind turbines with the emergence of offshore harvest of wind energy. Offshore wind turbines are prone to fatigue-driven failure due to the nature of the environment, propitious to high stresses caused by loads such as sea waves and winds. These structures need to be very resilient to this harsh environment, which makes them more expensive in pricing and complex structurally. They possess challenges concerning the lack of easy access which also increase maintenance costs.

TMD are relative well established in the literature of vibration absorbers. The basic design concept of the TMD is quite simple, however, the parameters (mass, damping, and stiffness) of the TMD system must be obtained through optimal design procedures to attain a better control performance. The search for optimized parameters began in the classical work of Hartog (1985) on vibration absorber dynamics. In his work, Hartog derived optimized expressions for the damping ratio and natural frequencies ratio optimized for a non-damping system subject to harmonic excitations. It was observed that the parameters that minimize the response of the main system are only a function of the ratio of the masses.

McNamara (1977) published and developed TMDs in buildings taking into account experimental analysis and wind loads with successful implementation, for example, in the John Hancock tower in Boston and the Citicorp Building in New York City.

Several studies have investigated the behavior of the offshore wind turbine using TMD type vibration mitigation systems and TLCD. In the study of Stewart (2012), several models of turbines were analyzed in order to observe the behavior of the system affected by the use of absorbers using passive and active techniques. The models were tested by two methods, the first by initial disturbance where the tower is displaced and the second method where the system is subjected to wind and wave modeling. The TMD's parameters determined by the optimization were integrated into a series of wind turbine design code simulations using the FAST-SC suit. From his simulations, tower fatigue damage reductions of between 5 and 20% are achieved for the various TMD configurations. These load reductions for all of the platforms could have a beneficial effect on the cost of an offshore wind turbine as long as the TMD could be constructed at a reasonable cost.

The work of Guimaraes et al., (2014), analyzes the dynamic behavior of an offshore wind turbine with the use of an AMS pendulum type absorber attached to the main system in order to reduce the excessive vibrations. Numerical simulations were performed to define TMD parameters for two cases of wind load: harmonic and white noise. Guimaraes et al. concluded that passive devices work properly only for the designed frequency range. However, wind forces consist of random type of excitations. Hence, better results would be achieved if a different control were developed.

Initial applications of TLCD in building were proposed by Sakai et al. (1989) and describing the application of the absorbers in buildings and in cable-stayed bridges (Sakai et al., 1991) In Sakai et al. experiment, the relationship between the coefficient of liquid head loss (as well as its dependence on the orifice opening ratio) and the liquid damping were first defined. Hence, validating the proposed equation of motion describing liquid column relative motion under moderate excitation.

TLCDs were first studied for excitation of structures that underwent wind actions by Xu et al. (1992). The structure was modeled as a lumped mass multi-degree-of-freedom system taking into account both bending and shear and the wind turbulence is modeled as a stochastic process that is stationary in time and non-homogeneous in space. A random vibration analysis utilizing transfer matrix formulation is carried out to obtain response statistics. The nonlinear damping term in the fundamental equation of the tuned liquid damper is treated by an equivalent linearization technique. Xu et al. concluded that excess liquid motion in a tuned liquid column might reduce the effectiveness of this damper. Furthermore, the wind-induced force and acceleration responses of the structure with a damper, which is usually tuned to the fundamental frequency of the structure, should involve more than one vibration mode as higher-mode responses may become as large or even larger than the controlled-mode response

Since then, new research on the subject emerge out every year. Enevoldsen & Mørk (1996) investigated the performance of a wind turbine using structural optimization with and without mass absorber. In his article, the effects of the mass damper were determined using structural optimization of the tower, which allows the various damping contributions to be examined consistently. A sensitivity analysis of the optimal designs was presented and the structural response was determined from linear stochastic vibration analysis. The stochastic load consists of aerodynamic forces due to turbulence components of the wind. The comparison results of optimal designs showed that the mass damper was efficient for reducing the volume of the tower design, especially when the uncertain aerodynamic damping from the rotor motion was not taken into account. The sensitivity analysis and evaluation of the optimal designs showed that the sensitivity due to the damping contributions was significantly reduced when the mass damper was introduced.

Chang & Qu (1998) established unified formulas for five types of passive dynamic absorbers, among them, TMDs, TLCDs, and other geometric shapes for tuned liquid damper such as circular and rectangular. Optimal properties and the equivalent damping ratios for these five dynamic absorbers were derived analytically. His work was important because it provided a comparison for different types of absorbers.

More recently, Colwell & Basu (2009) took advantage of increased interest in offshore wind turbines and performed a realistic simulation of the TLCD-type absorber structure subject to wind and sea forces. Colwell & Basu used the Kaimal wind spectrum with the JONSWAP wave spectrum that combines the loading of wind and waves to excite the offshore wind turbine model as a multiple degrees of freedom system. Cases for turbine blades lumped at the nacelle and rotating blades were simulated, to investigate the effects of the rotation of blades. It was shown that implementing TLCDs decreased the structural costs, and prolong the life of the tower. The fatigue life calculation for the tower is carried out using the rain-flow counting technique for cases with and without TLCD.

Lackner & Rotea (2011) applied passive and active structural control techniques in floating offshore wind turbines. Lackner & Rotea determined by means of parametric investigation, optimized passive parameters. A model with limited degrees of freedom was identified and then time domain simulations were made. The results obtained were compared with the base system and a 10% passive fatigue reduction was observed and for the active control a 30% reduction was observed. Lackner & Rotea concluded that the active structural control model is an effective way to reduce structural load.

Farshidianfar (2011) investigated the application of a bi-directional TLCD-type vibration system with periodic adjustment equipment used to reduce the vibration of skyscrapers suffering from earthquake oscillations. The system consists of two TLCD in the form of a U and a pendulum. This study helped to gain a better understanding of TLCD for application in buildings and to lead the quest of designers to obtain absorbers that are more efficient.

Li et al. (2012) performed experiments on a 1/13 scale of a wind turbine using a ball vibration absorber (BVA). Li et al. examined the reduction of displacement, acceleration, stresses for different loads. Their results show an improvement of the structure with the spherical absorber compared to the base structure.

Altay et al. (2014) presented an optimization approach for a TLCD considering the mathematical description of the damper geometry within the tuning procedure. The TLCD was chosen because it has very low fundamental frequencies. In addition, it is not easy to find a suitable spring element, which can be tuned to the fundamental frequencies of wind turbines, as they are generally lower than 0.4 Hz. The numerical verification was demonstrated by means of a three-bladed 5 MW reference wind turbine, periodically and stochastically excited by non-uniform steady state and turbulent wind flow. Altay et al. results showed that TLCD can effectively mitigate wind induced resonant tower vibrations and improve the fatigue life of wind turbines. Figure 2.4 shows a wind turbine with a TLCD attached to the nacelle.

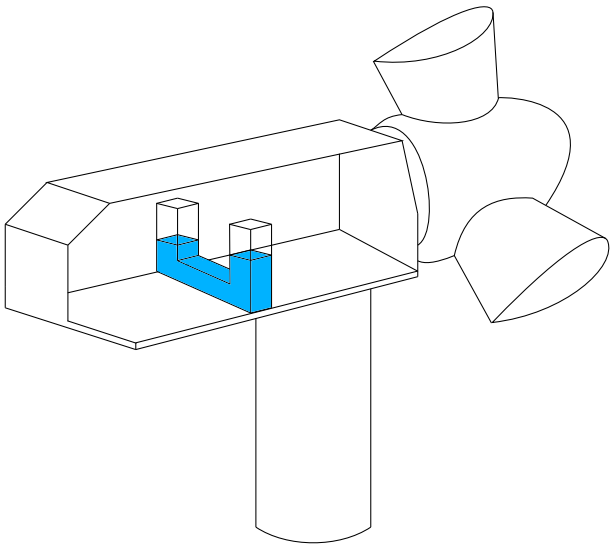

Figure 2.4 – Example of a TLCD in a wind turbine (Altay et al., 2014).

In the next chapter, fundamental concepts for random vibrations and probability theory are presented.

3 Fundamentals of random vibration

A system with nondeterministic motion is exposed to random vibrations. For instance, if we analyze the movement of a leaf floating on the wind, an unpredictable behavior in its trajectory can be seen. The leaf is subject to random excitations from constantly changing force and direction of the wind. However, the rate and amount of movement to which the sheet is subjected depends not only on the severity of the wind excitation, but also on its inherent mass, stiffness and damping (Newland, 2012). The concept of random vibrations is concerned with determining the characteristics of the movement of a randomly excited system, such as the leaf, which depend on the statistics of the excitation, in this case the wind, and the dynamic properties of the vibrating system, in this case the mass, the stiffness and damping of the sheet.

Cases in which the vibrational responses of a system are known for a given time t, are called deterministic vibrations. Deterministic vibration exists only when you have a perfect control of all the variables that influence the structure and loads of the system. There are several processes and phenomena that cannot be precisely determined, for any given moment, processes of this type are known by random variable or random processes. Examples of random vibrations can be found in simulations that deal with natural phenomena such as wind, fluid and seismic events.

This chapter consist of a first exposition of the fundamental concepts of random vibration and probability theory. The aim is to review the key principles of the probability theory and thus facilitate its application to solve problems in the random vibration. The reader interested in this theory is referred to (Newland, 2012) for a introduction and (Krée & Soize, 2012) for a mathematical exposition.

3.1 Random vibration

A deterministic system, usually a vibration structure, such as a machine, or a building, has input parameter $x(t)$, which constitute the excitation of the system, and output parameters $y(t)$, representing the system response. Two simplifications are proposed,

first, it is assumed that the systems are linear, so that each input excitation corresponds to an output response of the system, also taking into account the principle of superposition, and therefore, it is possible to treat each input and output parameter, which simplifies the analysis. The linearity hypothesis is accepted because the vibration in the system usually involves only small displacements. It is possible to represent the relationship between the input and output parameters of the system by means of a linear differential equation, however, more convenient alternative methods for the analysis of dynamic systems are used, such as frequency response and impulse response. The concepts of frequency response and impulse response are also important when it is desired to represent random vibration and will be briefly presented below.

The frequency response method requires an input parameter with constant amplitude and fixed frequency so that by the linearity relation the system response will have a fixed amplitude with the same frequency as the input but lagged by a phase. Thus, by knowing the relation between the input and output amplitudes and the phase angle for each frequency, it is possible to define the transmission characteristics of the system.

The impulse response method is another way of representing the dynamic characteristic of the system. From an initial impulse, the transient response is measured for all times until the static equilibrium is established.

It is possible to relate frequency response and impulse response using the concepts of Fourier analysis. The relation between the two methods by means of a Fourier transform that can be understood by the following argument, when the linear system is subjected to a permanent harmonic excitation at a frequency ω, it responds with an output harmonic response of the same frequency. It is therefore reasonable to expect that for an aperiodic signal, the frequency band of the input signal correspond to the same frequency band of the output signal. The following relationship is valid

$$Y(\omega) = H(\omega)X(\omega), \tag{3.1}$$

and the relation between the frequency response and the impulse response is given by,

$$H(\omega) = \int_{-\infty}^{\infty} h(t)e^{-j\omega t}dt. \tag{3.2}$$

A common way to analyze the behavior of a dynamical system is to investigate its responses to harmonic excitations at different frequencies. For linear systems, the information on responses to harmonic excitations, which is contained in frequency response functions, allows to identify the system and analyze it. The lack of such methods for nonlinear systems is one of the reasons why nonlinear systems and controllers are more challenging to tackle.

A signal is non-deterministic when it cannot be predicted exactly. Figure 3.1 shows a sample of a non-deterministic signal.

A random excitation can be generate digitally, or capture in an experiment. In the latter case, an analog-digital converter is used to convert analogical signal into digital.

Time (s)

Figure 3.1 – A sample of a non-deterministic signal

From the digital signal, a discrete temporal series is obtained and a variety of statistical analysis tools can be used to characterize the excitation. More commonly when dealing with random excitation, we can use the Fourier transform to extract the frequency components of the temporal series.

A method utilized to estimate the spectral components is to calculate the correlation function based on the temporal data and then apply the Fourier transform. This method was well known since the 1960 and it indeed followed the mathematical formalities although very time consuming. Since the rise of computation algorithms, a very popular algorithm called Fast Fourier Transform (FFT) manage to decrease the computation time in a very efficient manner to calculate a Fourier transform of a signal. A more detail explanation of FFT is given in sections 3.5.

In the following sections, the discrete Fourier transform is further explore to develop the fast Fourier transform algorithm. Nevertheless, the basic concepts of probability and power spectral density is introduced.

3.2 Probability density function

The probability density function of a random process is defined as a function representing the probability distribution of a random function.

Consider a random variable X that can assume any value $x_1, x_2, ..., x_n$ with probability $p_1, p_2, ..., p_n$

$$\bar{x} = \frac{1}{N} \sum_i p_i x_i. \tag{3.3}$$

In a continuous process we can obtain a probability distribution function $P(x)$. The probability distribution function is interpreted as the area on the probability density curve. That is,

$$P(x) = \int_{-\infty}^{x} p(x)dx, \tag{3.4}$$

in which the derivative of $P(x)$ with respect to x is called the probability density function. That is,

$$p(x) = \frac{dP(x)}{dx} = \lim_{\Delta x \to \infty} \frac{P(x + \Delta x) - P(x)}{\Delta x}, \tag{3.5}$$

we can interpret the expression $P(x + \Delta x) - P(x)$ as the probability of $x(t)$ to be between the interval $[x, x + \Delta x]$. The probability density function $p(x)$ can be interpreted with the distribution density of x. By definition,

$$Prob(-\infty \leqslant x \leqslant \infty) = P(x = \infty) = \int_{-\infty}^{\infty} p(x)dx = 1. \tag{3.6}$$

A commonly used probability density function is the Gaussian distribution shown in Figure 3.2 and expressed in Equation (3.7) where σ_x is the standard deviation and m an average. The Gaussian process, also called the normal process, has a bell-shaped format. Many natural processes of random vibration have a Gaussian-like form and, therefore, the importance of this probability density function.

$$p(x) = \frac{1}{\sqrt{2\pi}\sigma_x^2} e^{-(x-m)^2/2\sigma_x^2}. \tag{3.7}$$

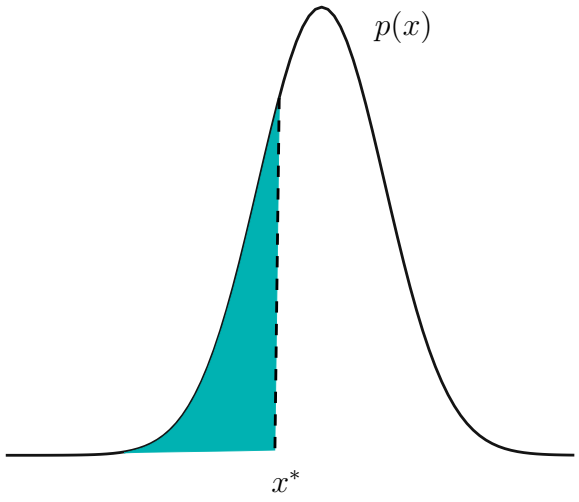

Figure 3.2 – Normal, or Gaussian probability density function

3.3 Stochastic process

In many cases, when dealing with random variables the results obtained for a sample are not sufficient. For example, the measurement of winds obtained would most likely not recur in the following year. The solution to this problem is to perform infinite measurements and thus analyze the sample set. It is obvious that it is not possible to carry out infinite measurements, but assuming a considerable value, the approximation becomes acceptable.

Figure 3.3 illustrates samples of a random process. Instead of calculating the probability distribution of only one sample, it is now possible to calculate the probability distribution of the sample set. With this, the stationary concept can be defined for the case of a random process in which the probability distribution of the sample set does not depend on the absolute time. A process is said to be stationary if when divided into time intervals the various sections of the process exhibit essentially the same statistical properties. Otherwise, it is said non-stationary. The term stationary refers to the probability distribution rather than the samples themselves. This implies that all means, squared means and standard deviation of the samples are independent of the absolute time.

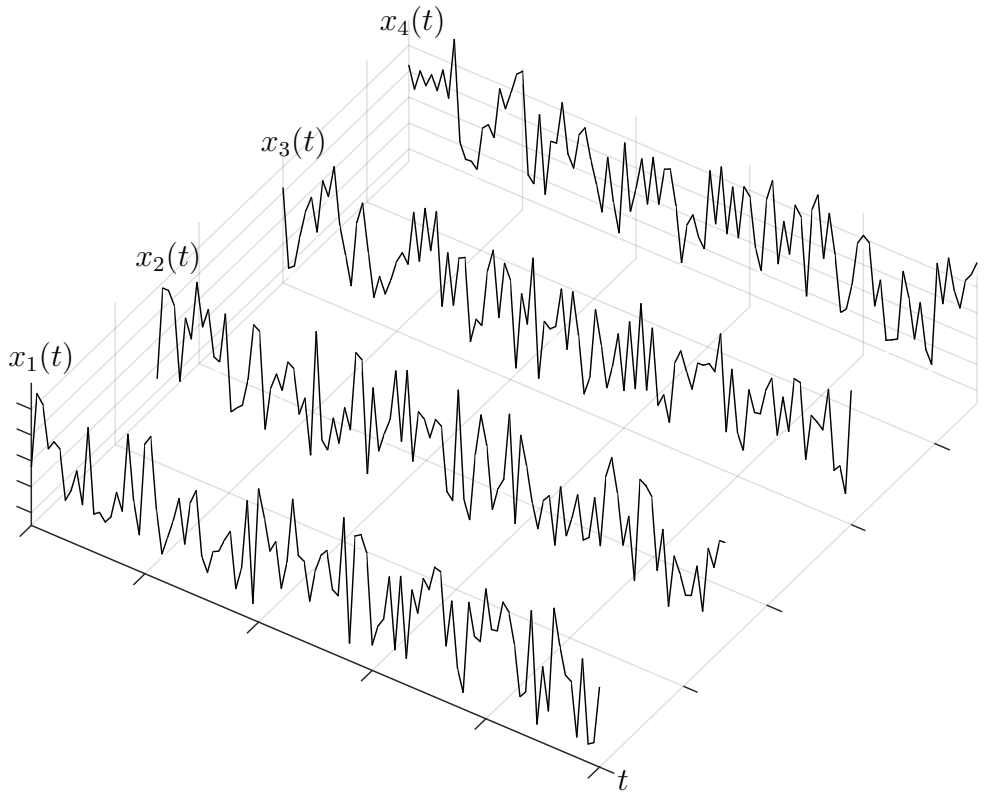

Figure 3.3 – Random samples of a process

A stationary process is ergodic if, in addition to the stationarity condition in absolute time, the average of each sample must be equal to the average of the set of samples. In practical terms, this implies that each sample is a complete representation of the set of samples representing the random process. Note that every ergodic process is stationary, but the reverse is not valid.

3.4 Correlation and autocorrelation

The definition of correlation and autocorrelation is based on the statistical concepts of expected value. The expected value is defined as the average of a random process as follows: for a function of a random process, $x(t)$ with period T and probability density

function $p(t)$,

$$E[x] = \int_0^T x(t)\frac{dt}{T} = \int_{-\infty}^{\infty} xp(t)dx, \tag{3.8}$$

hence, it is possible to determine the average of a random process when the probability density function is known.

From the definition of mean, it is possible to derive other relevant quantities such as the mean squared, $E[x^2]$, and the square of the standard deviation, $\sigma^2 = E[x^2] - (E[x])^2$, also known as variance. The concept of squared mean gives us the tool to compare (correlate) two functions or the same function at different intervals (autocorrelation).

The autocorrelation function of a random process, $x(t)$ is defined as the average of the product where τ is a time interval that separates the two samples. For stationary processes, the value of $E[x(t)x(t+\tau)]$ is determined independently of the absolute value of time t, so we can rewrite the product of the expected value $x(t)(t+\tau)$ as follows

$$E[x(t)x(t+\tau)] = R_x(\tau), \tag{3.9}$$

Where $R_x(\tau)$ is the autocorrelation function of $x(t)$ in the time interval τ.

3.5 Fourier series and the Fourier transform pair

Fourier analysis is a powerful tool used to express periodic signals by adding together sinusoidal functions of various amplitudes, frequencies and phases. Signals in time domain represent how the system behaves in real life. When we represent the signal in the frequency domain using Fourier analysis, we require very few information such as amplitude, frequencies and phases to characterize de signal. The reason for using sinusoidal functions is that they are a fundamental signal in nature. For instance, they might occur in electromagnetic waves and in oscillatory motion.

Consider a function $x(t)$ with period T_p, we can represent this function as

$$x(t) = \frac{a_0}{2} + \sum_{n=1}^{\infty}\left(a_n \cos\frac{2\pi nt}{T_p} + b_n \sin\frac{2\pi nt}{T_p}\right), \tag{3.10}$$

where a_0, $a_n k$ and b_n are constants terms given by

$$\frac{a_0}{2} = \frac{1}{T_p}\int_{-T/2}^{T/2} x(t)dt, \tag{3.11}$$

$$a_k = \frac{2}{T_p}\int_{-T_p/2}^{T_p/2} x(t)\cos\frac{2\pi nt}{T_p}dt, \quad n > 1, \tag{3.12}$$

$$b_k = \frac{2}{T_p}\int_{-T_p/2}^{T_p/2} x(t)\sin\frac{2\pi nt}{T_p}dt, \quad n > 1, \tag{3.13}$$

where T_p is the period and $\omega_n = 2\pi n/T_p$ is the n-th fundamental frequency.

The terms a_0, a_n and b_n are the Fourier coefficients which provide information on the frequency domain. The term a_0 represents the mean of the time history, while the therms a_n and b_n represents the amplitude of various cosine and sine waves which added together comprise the time history.

Figure 3.4 shows the Fourier expansion for a particular square wave time history. By the third summation, the expansion is seen to give a reasonable representation of the original time history although the corners never reach full convergence due to Gibbs' phenomenon as seen by the twentieths terms summation.

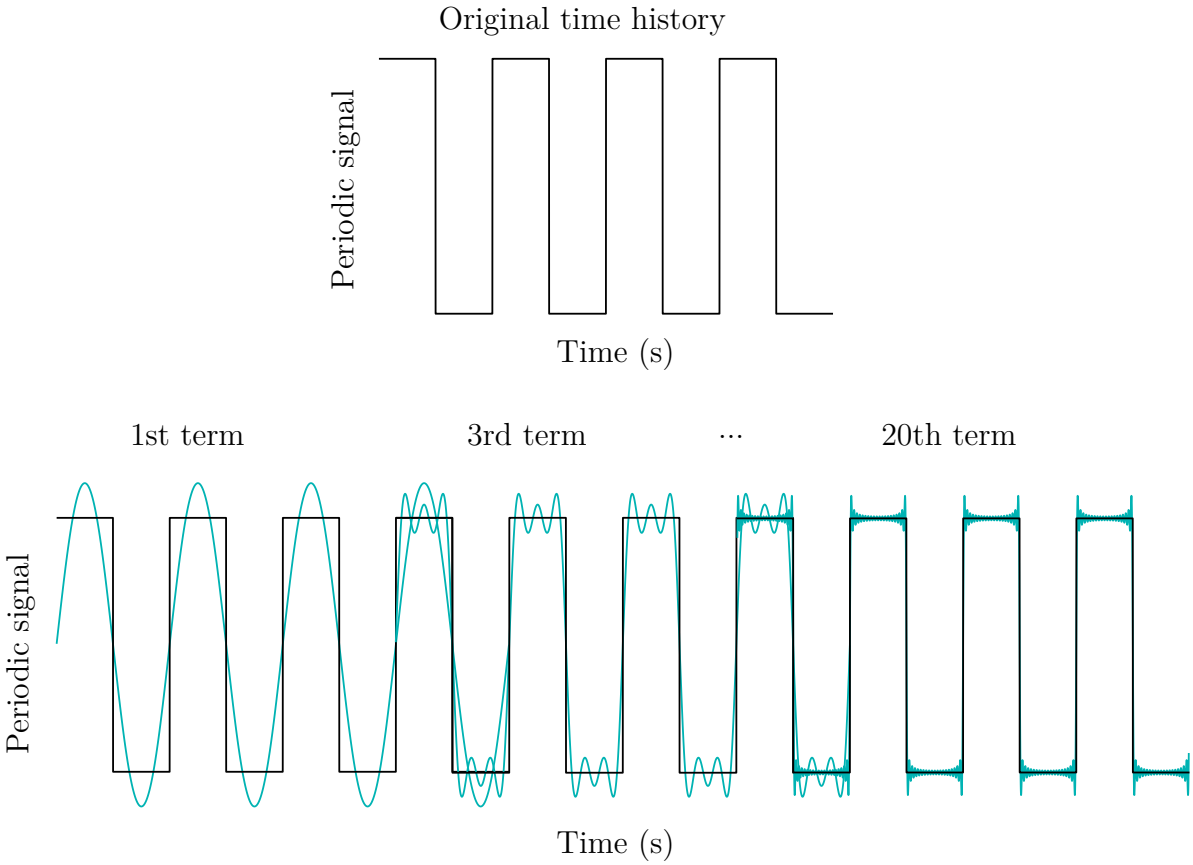

Figure 3.4 – Fourier expansion of a square wave periodic signal with partial sums of the $n = 1$, $n = 3$ and $n = 20$ terms of the expansion.

3.5.1 The complex form of the Fourier series

In practice, the Fourier coefficients can be cumbersome to manipulate algebraically. An alternative approach is to represent the Fourier series using its complex form by noting that $e^{j\theta} = \cos\theta + j\sin\theta$ and

$$\cos\theta = \frac{1}{2}(e^{j\theta} + e^{-j\theta}), \tag{3.14}$$

$$\sin\theta = \frac{1}{2j}(e^{j\theta} + e^{-j\theta}), \tag{3.15}$$

which gives, after some manipulations of Equation (3.10)

$$x(t) = \sum_{n=-\infty}^{\infty} c_n e^{j2\pi nt/T_p}, \tag{3.16}$$

$$c_n = \frac{1}{T_p} \int_{-T_p/2}^{T_p/2} x(t) e^{-j2\pi nt/T_p}, \tag{3.17}$$

where we can notice the component c_n now contain both amplitude and phase information of the Fourier decomposition.

3.5.2 Fourier integrals

In general, random vibrations are not periodic. Hence, the concepts of signal representation by Fourier analysis can be extended to non-periodic signal using Fourier integrals. The basic difference in the representation is that the discrete summation of the Fourier series becomes a continuous summation, i.e. an integral form.

Consider the Fourier representation of a periodic signal from Equations (3.16) and (3.17). By letting T_p become larger $T_p \to \infty$, the fundamental frequency $f_1 = 1/T_p$ becomes smaller, consequently, the multiples of the fundamental frequency ($f_n = nf_1$) becomes densely packed on the frequency axis. We define the separation of frequencies as $\Delta f = 1/T_p$. Hence, Equation (3.17) becomes

$$c_n = \lim_{\substack{T_p \to \infty \\ (\Delta f \to 0)}} \Delta f \int_{-T_p/2}^{T_p/2} x(t) e^{-j2\pi f_n t} dt, \tag{3.18}$$

where each Fourier coefficient c_n is obtained for a frequency n/T_p Hz. The frequency interval between each coefficient Δf is therefore $1/T_p$ Hz. This cause problems as the frequency at which the coefficients are calculated is dependent on the period T_p chosen. It is common practice to normalize the coefficients to eliminate de dependence on T_p. Hence, the ratio $c_n/\Delta f$ is desirable in order to avoid $c_n \to 0$ as $\Delta f \to 0$. Equation (3.18) can be rewritten as

$$\lim_{\Delta f \to 0} \frac{c_n}{\Delta f} = \lim_{T_p \to \infty} \int_{-T_p/2}^{T_p/2} x(t) e^{-j2\pi f_n t} dt, \tag{3.19}$$

assuming the limits exist, we get

$$X(f_n) = \int_{-\infty}^{\infty} x(t) e^{-j2\pi f_n t} dt, \tag{3.20}$$

since $\Delta f \to 0$, the frequencies f_n become a continuum and we can write f instead as follows

$$X(f) = \int_{-\infty}^{\infty} x(t) e^{-j2\pi ft} dt. \tag{3.21}$$

Now, with analogous arguments, we can represent the continuous form of Equations (3.16) as

$$x(t) = \int_{-\infty}^{\infty} X(f) e^{j2\pi ft} df. \tag{3.22}$$

Equations (3.21) and (3.22) are known as Fourier integral pair. The function $X(f)$ is the complex Fourier transform of $x(t)$. These results are relevant for random vibration since it can relate a temporal series with its frequency components in a random process. The Fourier pair can be written using $\omega = 2\pi f$ as an alternative form

$$X(\omega) = \int_{-\infty}^{\infty} x(t)e^{-j\omega t}dt, \tag{3.23}$$

$$x(t) = \frac{1}{2\pi}\int_{-\infty}^{\infty} X(f)e^{j\omega t}df. \tag{3.24}$$

The sufficient condition for existence of a Fourier integral is

$$\int_{-\infty}^{\infty} |x(t)|dt < \infty \tag{3.25}$$

where a function can be written as a Fourier integral if, and only if, the function decay to zero $t \to 0$. Usually this condition can be avoided using the Dirac delta function properties.

3.5.3 Discrete Fourier transform

When dealing with digital signal, the function defining the signal is discrete. The discrete signal can occur naturally such as stock exchange market or occur due to sampling such as collecting data at Δ seconds interval. A sequence is denoted as $x[n]$, where n is a finite number of elements in the sequence.

The discrete Fourier transform (DFT) is a Fourier representation of a finite length sequence and in fact, the DFT itself is a sequence rather than a continuous function of frequency.

Consider first the Fourier transform of a sample sequence $x(n\Delta)$ given by

$$X(e^{j2\pi f\Delta}) = \sum_{n=0}^{N-1} x(n\Delta)e^{-j2\pi fn\Delta} \tag{3.26}$$

this result can be obtained from discretized a signal using delta functions. Besides that, this representation is still continuous in frequency. If we want to evaluate this at frequencies $f = k/N\Delta$, then the right side of Equation (3.26) becomes

$$X(k) = \sum_{n=0}^{N-1} x(n\Delta)e^{-j(2\pi/N)nk} \tag{3.27}$$

where we can simplify the notation $X(k) \equiv X_k$ and $x(n\Delta) \equiv x_n$. Equation (3.27) has an inverse relationship called the inverse discrete Fourier transform (IDFT)

$$x_n = \frac{1}{N}\sum_{k=0}^{N-1} X_k e^{j(2\pi/N)nk}. \tag{3.28}$$

While the values of the continuous time series $x(t)$ cannot be obtained from X_k, it does permit to regain exactly the values of the discrete time series x_n. Both X_k and x_n are periodic with period N.

The Fourier representation depends on the type of signal. They can be continuous or discrete time signal and periodic or non-periodic. Signals that are continuous in time end up being non-periodic in frequency, and signals, which are discrete in time, become periodic in frequency. Similarly, signals non-periodic in time become continuous in frequency, and signals periodic in time become discrete in frequency. These conditions are summarized in Figure 3.5.

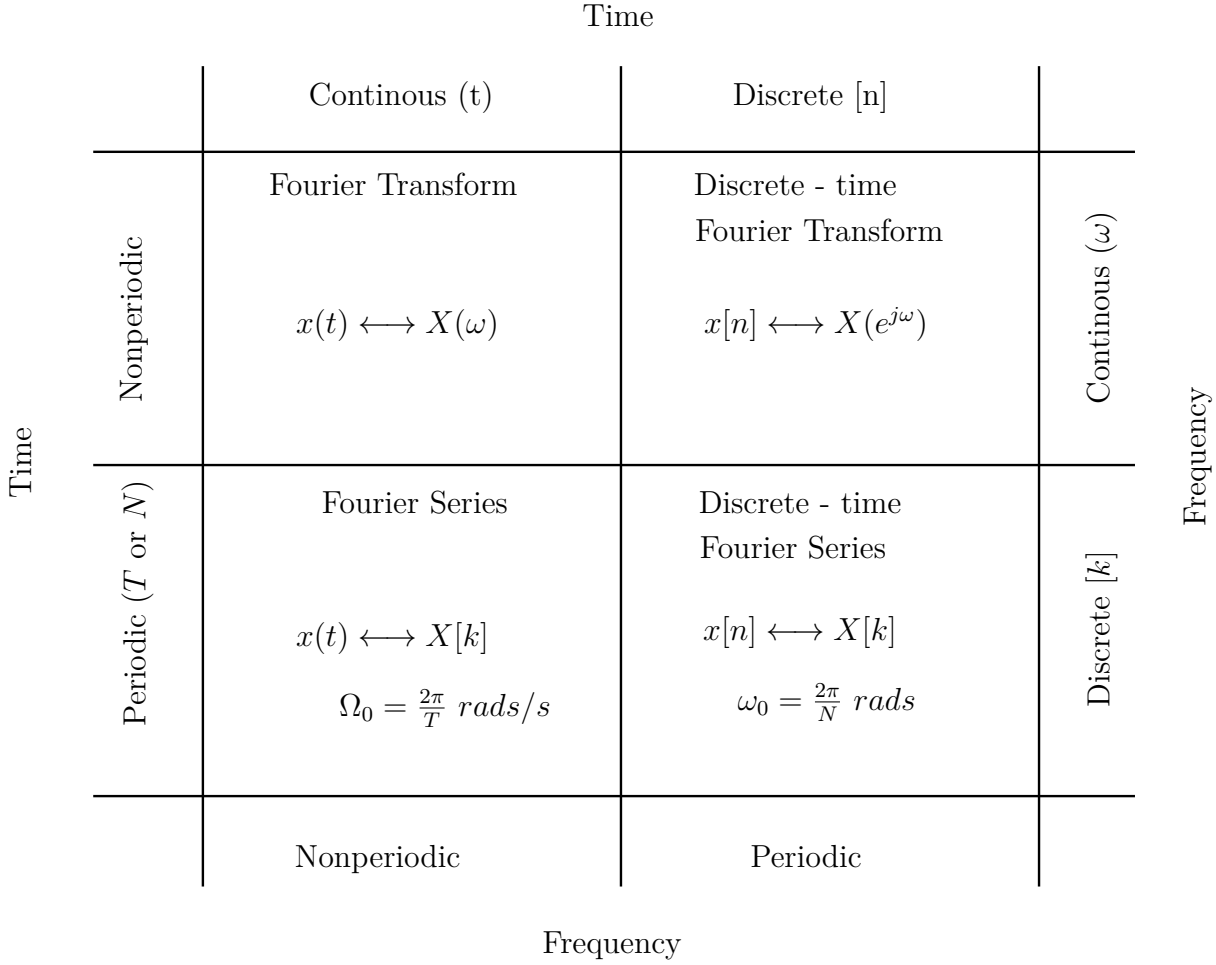

Figure 3.5 – Four Fourier representation of signals

3.5.4 Fast Fourier transform

As discussed, the concepts of discrete Fourier transform can be used to estimate the power spectral density of a random process and consequently to develop an algorithm that allows us to obtain the time series from the spectral density and vice versa with low computational cost.

Starting from the definition of correlation and spectral density of the discrete time

series x_r and y_r

$$R_r = \frac{1}{N}\sum_{s=0}^{N-1} x_s y_{s+r} \qquad r = 0, 1, 2, \ldots, (N-1) \tag{3.29}$$

$$S_k = \frac{1}{N}\sum_{r=0}^{N-1} R_r e^{-i(2\pi kr/N)} \tag{3.30}$$

combining Equations (3.29) and (3.30), we have

$$S_k = \frac{1}{N}\sum_{r=0}^{N-1}\left\{\frac{1}{N}\sum_{s=0}^{N-1} x_s y_{s+r}\right\} e^{-i(2\pi kr/N)} \tag{3.31}$$

rearranging the terms,

$$S_k = \frac{1}{N^2}\sum_{r=0}^{N-1}\sum_{s=0}^{N-1} x_s e^{-i(2\pi ks/N)} y_{s+r} e^{-i(2\pi k(s+r)/N)} \tag{3.32}$$

the terms with the variable r can be grouped together

$$S_k = \frac{1}{N}\sum_{s=0}^{N-1} x_s e^{-i(2\pi ks/N)}\left\{\frac{1}{N}\sum_{r=0}^{N-1} y_{s+r} e^{-i(2\pi k(s+r)/N)}\right\} \tag{3.33}$$

defining a new variable $t = (s + r)$, we have

$$\frac{1}{N}\sum_{t=s}^{(N-1)+s} y_t e^{-i(2\pi kt/N)} \tag{3.34}$$

comparing both side of Equation (3.33) with Equation (3.26), it follows

$$S_k = X_k^* Y_k \tag{3.35}$$

This result is important because it is the basis of the FFT algorithm. An estimate of the spectrum only by knowing the discrete time series and vice versa without requiring the correlation calculation can be found. By knowing the value of the discretized spectral density S_k, one can obtain its real value.

The FFT works by partitioning the sequence x_r into a number of small sequences. Instead of calculating the DFT of the original sequence, only the DFT of the minor sequences are calculated. The FFT then combines these results to generate the total PDT of x_r.

Consider a sequence x_r with N numbers of events that is partitioned into two sequences y_r and z_r

$$y_r = x_{2r}; \qquad z_r = x_{2r+1} \tag{3.36}$$

the DFT of these two sequences are given by Y_k e Z_k

$$Y_k = \frac{1}{N/2}\sum_{r=0}^{N/2-1} y_r e^{-i\frac{2\pi kr}{(N/2)}}, \quad k = 0, 1, 2, \ldots, (N/2-1) \tag{3.37}$$

$$Z_k = \frac{1}{N/2}\sum_{r=0}^{N/2-1} z_r e^{-i\frac{2\pi kr}{(N/2)}} \tag{3.38}$$

returning to the DFT of the original sequence x_r and rearranging the sum into two sums, even and odd

$$X_k = \frac{1}{N}\sum_{r=0}^{N-1} x_r e^{-i\frac{2\pi kr}{(N)}} \tag{3.39}$$

$$X_k = \frac{1}{N}\left\{\sum_{r=0}^{N/2-1} x_{2r} e^{-i\frac{2\pi k(2r)}{N}} + \sum_{r=0}^{N/2-1} x_{2r+1} e^{-i\frac{2\pi k(2r+1)}{N}}\right\} \tag{3.40}$$

using the sequences of Equation (3.36) into Equation (3.40), we obtain

$$X_k = \frac{1}{N}\left\{\sum_{r=0}^{N/2-1} y_r e^{-i\frac{2\pi kr}{(N/2)}} + e^{-i\frac{2\pi k}{N}}\sum_{r=0}^{N/2-1} z_r e^{-i\frac{2\pi kr}{(N/2)}}\right\} \tag{3.41}$$

otherwise

$$X_k = \frac{1}{2}\{Y_k + e^{-i\frac{2\pi k}{N}} Z_k\} \tag{3.42}$$

for $k = 0, 1, 2, \ldots, (N/2-1)$.

The DFT of the original sequence can be obtained directly from the DFT of the two sequences Y_k and Z_k according to Equation (3.42). This equation is the basis of the FFT method. For the case of number of samples N of the sequence x_r the computational cost and of the order of N^2. If you use the FFT method, the computational cost decreases to the order of $N \log_2 N$ which represents a considerable reduction, as N increases.

We now introduce the basic concepts of power spectral density.

3.6 Spectral analysis

The use of frequency spectra to view periodic functions is a very useful method to understanding the behavior of the process by analyzing the frequency domain. A spectrum-shaped graph is described by a amplitude for each harmonic component as a function of frequency.

In this cases, the frequency composition in a random process $x(t)$ is not periodic and therefore cannot be expressed by the Fourier series since we do not know for sure the behavior of the function that can change from sample to sample. This difficulty in describing the process can be solved by looking at the autocorrelation function $R_x(\tau)$ instead of the random function. The reason is that the autocorrelation function provides information about the frequency in a random process, that is, in a correlation analysis it is possible to obtain the frequencies present in a random sample.

The power spectral density function of a random stationary process remains invariant when under time variation. Hence, it can be defined by the Fourier transform of the autocorrelation function as follows

$$S_{xx}(\omega) = \frac{1}{2\pi}\int_{-\infty}^{\infty} R_{xx}(\tau) e^{-i\omega\tau} d\tau, \tag{3.43}$$

so that

$$R_{xx}(\tau) = \int_{-\infty}^{\infty} S_{xx}(\omega) e^{i\omega\tau} d\omega, \tag{3.44}$$

the autocorrelation function $R_{xx}(\tau)$ makes statistical connections between values of the variable function $x(t)$ in different time intervals τ, but does not depend on the instant t. Stochastic processes with this characteristic are called ergodic. Equations (3.43) and (3.44) are known by Wiener-Khintchine expressions (Ghanem & Spanos, 2003).

One of the most important properties of $S_{xx}(\omega)$ becomes apparent when $\tau = 0$ in Equation (3.44), in this case,

$$E[x^2] = R_{xx}(\tau = 0) = \int_{-\infty}^{\infty} S_{xx}(\omega) d\omega \tag{3.45}$$

this result can be interpreted graphically where the squared mean of the random process is equal to the area of the spectral density graph.

The relation between the spectral density function of the response and the excitation can be extracted from the input and output ratios of a deterministic linear system. Let the elements $x(t)$ and $y(t)$ be the input and output of the system. Now consider these functions in the frequency domain, $X(\omega)$ and $Y(\omega)$, the relation between them can be obtained as

$$y(t) = \int_{0}^{\infty} h(\nu) x(t-\nu) d\nu, \tag{3.46}$$

$$Y(\omega) = H(\omega) X(\omega). \tag{3.47}$$

Now, consider that $x(t)$ e $y(t)$ represent stochastic processes. The relations between input and output are still valid, but now they have a stochastic nature and need to be interpreted considering probabilistic theory.

The output correlation function relates to the input correlation function as

$$R_{yy}(t_1, t_2) = \int_{-\infty}^{\infty} \int_{-\infty}^{\infty} h(t_1 - \nu_1) R_{xx}(\nu_1, \nu_2) h^T(t_2 - \nu_2) d\nu_1 d\nu_2 \tag{3.48}$$

where the variables ν_1 and ν_2 can be interpreted as a time delay. For the case where $x(t)$ is stationary, $R_{xx}(t_1, t_2)$ depends only on the difference $\tau = t_2 - t_1$, and therefore $R_{yy}(t_1, t_2)$ also depends only on τ. Thus, by rewriting Equation (3.48), with a change of variables

$$R_{yy}(\tau) = \int_{-\infty}^{\infty} \int_{-\infty}^{\infty} h(\nu_1) R_{xx}(\tau + \nu_1 - \nu_2) h^T(\nu) d\nu_1 d\nu_2 \tag{3.49}$$

The Fourier transform of Equation (3.49) is performed using the concepts of power spectral density, we have

$$S_{yy}(\omega) = \frac{1}{2\pi} \int_{-\infty}^{\infty} d\tau e^{i\omega t} \left\{ \int_{-\infty}^{\infty} d\nu_1 \int_{-\infty}^{\infty} d\nu_2 h(\nu_1) h^T(\nu_2) R_{xx}(\tau + \nu_1 - \nu_2) \right\}, \tag{3.50}$$

$$S_{yy}(\omega) = \frac{1}{2\pi} \int_{-\infty}^{\infty} d\nu_1 h(\nu_1) \int_{-\infty}^{\infty} d\nu_2 h^T(\nu_2) \int_{-\infty}^{\infty} d\tau e^{i\omega t} R_{xx}(\tau + \nu_1 - \nu_2), \tag{3.51}$$

we can show that $\int_{-\infty}^{\infty} e^{i\omega t} R_{xx}(\tau + \nu_1 - \nu_2) d\tau = 2\pi S_{xx}(\omega) e^{i\omega(\nu_1 - \nu_2)}$. Hence,

$$S_{yy}(\omega) = S_{xx}(\omega) \int_{-\infty}^{\infty} h(\nu_1) e^{i\omega\nu_1} d\nu_1 \int_{-\infty}^{\infty} h^T(\nu_2) e^{-i\omega\nu_2} d\nu_2, \tag{3.52}$$

by the definition of the impulse function,

$$S_{yy}(\omega) = H^*(\omega) H(\omega) S_{xx}(\omega), \tag{3.53}$$

in which $H^*(\omega)$ is the conjugate transfer function. Since the complex product of a number by its conjugate equals its square magnitude, we conclude that

$$S_{yy}(\omega) = |H(\omega)|^2 S_{xx}(\omega). \tag{3.54}$$

Equation 3.54 Is the most important random vibration equation since it provides a direct and simple relation between the input and output power spectral density.

4 Probabilist description of wind loads

This chapter deals with the effects of the probabilistic aspect of wind in low atmospheric layers on flexible structures. The problems is confined to along-wind response of structures. Moreover, cross-wind response or aero-elastic coupled problems are left out of discussion. The idea is discuss some general notions, which should cast some light on the complexity of the phenomenon.

4.1 The wind behavior near ground

The wind flow near a body is perturbed because it should bypass the body. This perturbation generate the aerodynamic forces acting on the body. The aerodynamic forces exerted on the body are the sum of the pressure field acting on the body and the forces of friction. For structures situated in the atmospheric turbulent boundary layer, the flow around it separates and cannot adhere back. This leads to high difference of pressure between downstream and upstream and generates in this way a pressure drag, which is considerably larger than viscous drag.

Air is a viscous fluid and in high altitudes, the ideal fluid approximation is valid. The velocity of wind results from a balance between the Coriolis force produced by Earth rotation and the force exerted by the atmospheric pressure field. The wind direction is approximately parallel to the isobar. At low altitudes, near Earth's surface, turbulent boundary layer is form due to forces of friction from its roughness. Consequently, the Coriolis forces are negligible with respect to the forces of friction and the direction of the mean wind varies only with altitude.

The wind velocity fluctuates with time near the ground. In fact, the spectral analysis of this velocity over a long time interval revels several scales of fluctuation. Figure 4.1 shows a typical power spectrum of the horizontal velocity of wind at 100 meters above ground. Furthermore, Figure 4.1 shows that the low frequency energy is concentrated over a period of four days, which is associated to geostrophic motions (Krée & Soize, 2012). Another peak is commonly placed at 12 or 24 hours and is due thermal phenomena of

night and day alternation. For last, part of the energy is concentrated over a period of one minute and correspond to the time scale of turbulent motion. This micro-meteorological effects can be attribute to turbulent gust caused by eddies in the wind load over obstacles in the vicinity of the turbine i.e. towns, trees, hills and valleys. If the surface is relatively flat such as in the sea, there will be less turbulence then in the field.

The average wind velocity varies along the structure; hence, the wind load is non-homogeneous in space. Although the wind load depends on the response of the structure, such an interaction effect can usually be neglected, and the wind load can be computed from the wind velocity. Consequently, the wind load consists of a static load due to the average wind velocity and a dynamic load due to wind fluctuations. For the reduction of acceleration responses in structural control, only the fluctuating wind load should be considered. Due to the uncoupled motion of the structure, the wind loads in both directions the along-wind and across-wind (Wu & Yang, 1998).

Wind turbulence is an important consideration if the first natural period of a structure is around 0.5 seconds and it is mostly likely the cause of fatigue damage in lattice towers (Halfpenny, 1998). The power spectrum from Figure 4.1 also shows that there is an energy hole for periods between 10 minutes and 2 hours. Therefore, if an average wind velocity is desirable over a period T corresponding to the energy hole, i.e. in the 10 minutes up to 2 hours range, the mean velocity will be almost stable (Krée & Soize, 2012) and over a time T the wind velocity can be modeled by a locally stationary stochastic process.

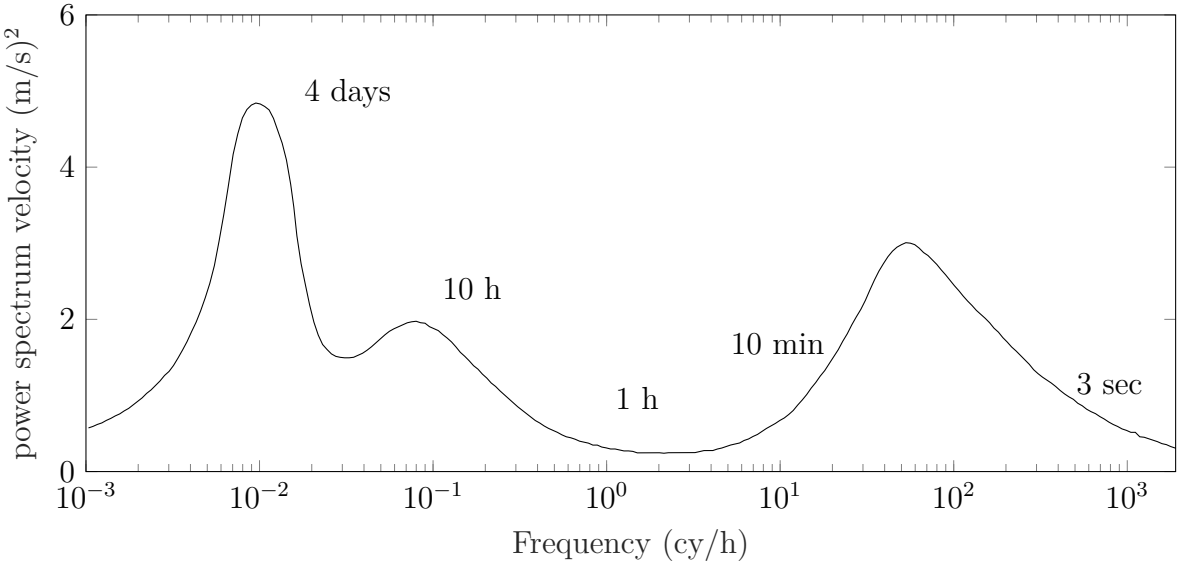

Figure 4.1 – Typical power spectrum of the horizontal velocity of wind at 100 m above the ground.

Two approaches can follow, a short-term and a long-term modeling. The short-term

modeling describes the fast fluctuations due to turbulence and is modeled by a stochastic process. If we take into account the slow variations of the mean velocity over a long period, we obtain a long-term modeling. However, due to lack of meteorological deterministic forecast over a long period, one has to resorts to probabilistic modeling. Hence, the mean velocity and other parameters are modeled by random variables where the probabilistic models are the outcome of statistical processing of meteorological measurements.

The following analysis focus on short-term model of the wind flow.

4.2 Short-term wind model

We are interested in discuss the short-term modeling of wind, which permits a description of the fast fluctuations caused by turbulence in the 0-300 meters layer. The short-term parameters are the mean wind velocity $\mathbf{v}$, containing its magnitude and direction, and a global roughness parameter $\mathbf{r}$. We set

$$q = (\mathbf{v}, \mathbf{r}) \in R^3. \tag{4.1}$$

The mean velocity is defined as the absolute magnitude of the mean velocity of the horizontal component of the wind velocity over a time period measure at a reference altitude (say, 10 meters). The mean velocity is completely specified by its direction and its absolute magnitude. The short-term modeling aim is to be able to describe for a fixed position, the profile of the mean velocity $\mathbf{v}(\mathbf{x})$ at a certain point $\mathbf{x}$ and the fluctuation $\mathbf{v}'(\mathbf{x}, t)$ modeled by a stochastic field. Hence,

$$\mathbf{v}(\mathbf{x}, t) = \mathbf{v}(\mathbf{x}) + \mathbf{v}'(\mathbf{x}, t). \tag{4.2}$$

Considering the orthonormal frame $Oxyz$ such as the origin is at ground level, Oz is the positive vertical axis and Ox is the axis parallel to the direction of the reference mean wind. Assuming the following notation

$$\mathbf{v}(\mathbf{x}) = (v_1(\mathbf{x}), v_2(\mathbf{x}), v_3(\mathbf{x})), \tag{4.3}$$

assuming $(v_1(\mathbf{x}), 0, 0)$, the mean longitudinal component velocity $v_1(\mathbf{x})$ with respect to height is known as wind shear. The law governing the variation of $v_1(\mathbf{x})$ at a point $\mathbf{x}$ with respect to the z-axis is a purely empirical power law worked out by Davenport (1961)

$$v_1(\mathbf{x}) = v_1(z_0) \left(\frac{z}{z_0} \right)^{\beta}, \tag{4.4}$$

where $v_1(z_0)$ is the friction velocity at the site, z_0 is the hub height and β is the coefficient of roughness due the viscosity stress. The viscosity stress decelerate the airflow near earths boundary layer up to the gradient height which is imposed by the terrain roughness. Considering that the roughness classes are assumed to be homogeneous over a sufficiently large distance, they can be classify into five types of site according to Table 4.1.

Table 4.1 – Roughness class of different site types

Site type	Roughness class **r**
Sea and large water surface	I
Flat terrain with some isolated obstacles	II
Rural areas with low builds and trees	III
Urban, industrial, or forest areas	IV
Center of large cities	V

Once the complete description of the wind velocity field have been established, the resulting aerodynamic forces acting on the structure can be derived. Considering a dimensionless aerodynamic drag coefficient C_D and neglecting the relative velocity of the structure, the force is given by

$$dF(z,t) = \frac{1}{2}\rho_{air} C_D dA[v_1(z) + v_1'(z,t)]^2 \tag{4.5}$$

since the only variable not constant is the wind velocity we can use it as our measure of force.

The short-term probabilistic model of the fluctuation $\mathbf{v}'(\mathbf{x},t)$ is defined by a stochastic process, in R^3, time-stationary, second-order, mean square continuous and Gaussian. It follows from our assumptions that $\mathbf{v}'(\mathbf{x},t) = v_1'(\mathbf{x},t)$. The process $v_1'(\mathbf{x},t)$ can be described by its transverse auto-correlation function

$$R(\tau) = E[v_1'(\mathbf{x},t)v_1'(\mathbf{x},t+\tau)]. \tag{4.6}$$

the mean speed also varies with time. In a storm, for instance, it is expected a higher mean wind speed than during a calm weather. This variation can be expressed using probability density function. Many distributions have been proposed. Davenport considered the wind speed as a resultant of two independent Gaussian variable assuming that wind is isotropic and uniformly distributed which approximate to a Rayleigh distribution.

Mayne (1979) proposed a Weibull distribution described as

$$p(u) = \frac{k}{c}\left(\frac{v_1}{c}\right)^{k-1} e^{-(v_1/c)^t} \tag{4.7}$$

where k is the Weibull slop parameter and c is the Weibull mode parameter.

The Weibull distribution tends to the Rayleigh as $k = 2$. The Weibull parameters can be found in different meteorological station and in standard references. They can also be estimated from the annual mean wind speed record.

From an engineering standpoint, the structure design must withstand the most severe wind loads. Although the statistics may be obtained from a Weibull distribution, this practice can lead to erroneous results because the tail of the distribution does not provide a good fit for extreme events.

Turbulence is responsible for the fluctuations in the velocity. This phenomena is best described stochastically as a process with zero mean velocity value and its standard deviation σ_v. The standard deviation of the turbulence is defined as

$$\sigma_{v_1} = \psi v_{hub} \tag{4.8}$$

where ψ is the wind speed coefficient of variation, also called turbulence intensity, and $v_{hub} = v_1(z_0)$ is the short term mean value of the hub height velocity.

The velocity variance spectra of the turbulence wind field is defined as

$$\sigma_{v_1} = \int_0^\infty S_{v_1}(f)df \tag{4.9}$$

where $S_{v_1}(f)$ is the power spectral density.

Next, different wind profile power spectral density models are discussed and compared. It will be shown that lower frequency band proves most important when considering wind turbine dynamics.

4.3 Wind profile power spectral density

Wind excitations are highly dynamic, irregular external loads. Therefore, they are better represented by mean of the power spectral density (PSD). This section discusses how these could be simulated through the different PSDs models such as white noise, Kanai-Tajime, Kaimal and Davenport.

White noise is a signal idealization where its PSD covers all frequency band with a constant value. Other PSD models can be physically more meaningful to represent wind profiles by taking into account aspects of relevance to the real problem such as roughness, heights, wind forces and general changes in dynamic properties. Kaimal and Davenport spectrum models are first order filter that can be used to approximate wind-induced positive pressures along wind loading. Kanai-Tajimi is a representation of a second order filter, which is typically used in earthquake profiles, but will be used in this work for sake of comparison. Table 4.2 summarizes each respective power spectral density function expressions.

For Kaimal PSD, $L_k = 340.2\ m$ is a scale parameter that involves the wind turbine height and $v_{hub} = 16\ m/s$ is the mean wind velocity. According to Burton et al. (2001), Kaimal spectrum provides a good fit to empirical observation of atmospheric turbulence. For Davenport PSD, κ is the drag coefficient referred to the mean velocity and L in the hub height (Davenport, 1961). For Kanai-Tajimi PSD, $\omega_g = 10.5\ rad/s$ and $\xi_g = 0.317$ can be interpreted as characteristic frequency and characteristic damping ratio respectively (Kareem, 1984). Kanai-Tajimi spectrum amplifies the frequency around ω_g and it attenuates high frequencies (Thráinsson et al., 2000).

Table 4.2 – Common power spectral density functions models.

Filter	Power Spectral Density Functions
White Noise	$S_{WN}(\omega) = S_0$
Kanai-Tajimi	$S_{KT}(\omega) = \frac{(1+4\xi_g^2(\omega/\omega_g)S_0)}{1+(\omega/\omega_g)^2+4\xi_g^2(\omega/\omega_g)^2}$
Kaimal	$S_{Kai}(\omega) = \left[\frac{4S_0^2[L_k/v_{hub}))}{1+(6\omega(L_k/v_{hub}))}\right]^{5/3}$
Davenport	$S_{Dav}(\omega) = \frac{4\kappa L v_{hub}^2 \chi}{(1+\chi^2)^{4/3}}, \quad \chi = \omega L/v_{hub}$

Figure 4.2 shows the spectral and time history characteristics of different wind models with added Gaussian noise.

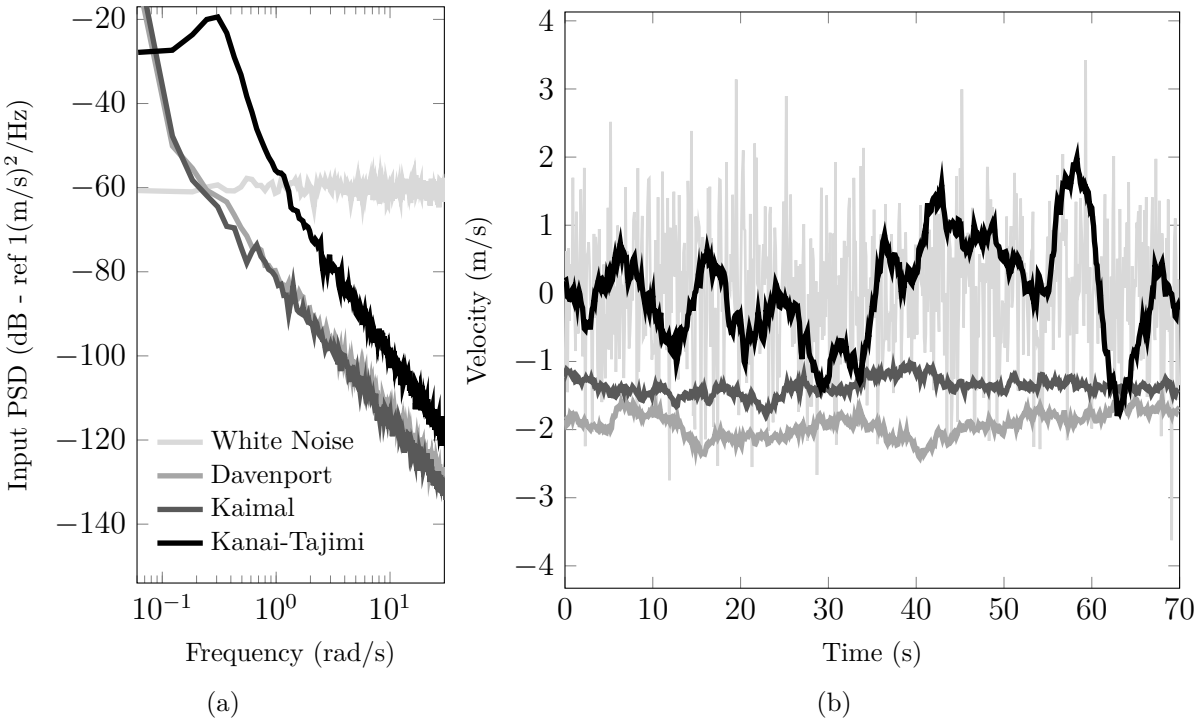

Figure 4.2 – (a) Power spectral density and (b) zero mean time history wind velocity for white noise, Davenport, Kaimal and Kanai-Tajimi models.

From Figure 4.2(a), it can be noticed that both Kaimal and Davenport spectra show more dominant low frequency components. Since Kanai-Tajimi is a second order filter, the formation of a peak near its characteristic frequency can be clearly noticed. In addition, Figure 4.2(b) shows the velocity of the wind in the time domain. This time history is numerically generated by a FFT based algorithm. Taking the inverse discrete Fourier transform (IDFT) of the discretized signal in the frequency domain where its amplitude is estimated as the square root of the discretized PSD, $\sqrt{S_k}$. Then, the random phase is generated from a uniform distribution within the interval $[0, 2\pi]$ (Newland, 2012).

It can be noticed that the white noise velocity profile is the least smooth of all, because the velocity at one point in time is independent from the velocity at any other instant. Moreover, it has the largest dispersion around the mean, which is proportional to the area under the PSD curve. This spectrum is not physically meaningful, but it is usually applied because it is easier to manipulate analytically than other model. The Kanai-Tajimi spectrum also shows a large dispersion, due to its large area under the PSD curve, but it presents smoother time domain history than the white noise spectrum. Finally, Kaimal and Davenport spectra present a more physically meaningful wind velocity profile with good autocorrelation (Murtagh et al., 2004).

5 Mathematical description of dynamic system

In this chapter, how the wind excitation influence the dynamic behavior of the structure is considered. First, some comments on why a simplified model of wind turbine is used are presented.

A complete model of wind turbine needs to consider the structural model, the aerodynamics (i.e. lift, drag, momentum) and the interface effects. In the structural model, both the blades and the tower have an impact in the overall performance. Figure 5.1 shows a diagram of a complete model of forces and their interaction acting on a wind turbine. Moreover, nonlinearities and coupling effects can affect the structure response. Time domain simulations provide a reasonable assessment of this response. However, such analysis is computationally expensive, in particular when fatigue analysis is desired. FEA is more computationally complex and not recommended for a preliminary stage. Besides that, performance analysis such as optimization techniques can be carried out using the simplified model.

From previous works (Baumgart et al., 2002) it is known that an efficient, systematic stability analysis cannot be performed for large systems of differential equations (i.e. the order of differential equations higher than 100) because some numerical effects in the solution of the equations of motion as initial value problem or eigenvalue problem become predominant. It is therefore of interest study how a simplified dynamic model could estimate the structural response. The simplified model is reduced to the elementary coordinates but still needs to describe the relevant physical process under consideration with good accuracy. Such a simplified model can be used as an early design of new wind turbines.

This work focus on the structural dynamic aspect of wind turbines considering a lattice towers with concentrated mass at the top, hence, the model does not include the gyroscopic effects due to turbine blade rotation. In flexible tower structures, more than 90% of the total energy dissipation usually occurs due to the fundamental mode in flexure (Murtagh et al., 2004). However, the vibrating frequency and shape mode of the tower are indeed effected by not only the shear force but also the moment force, generated by the motion of the additional mass attached at the free end. Auciello (1996) developed an exact analysis of free vibration of tapered cantilever beams with tip mass.

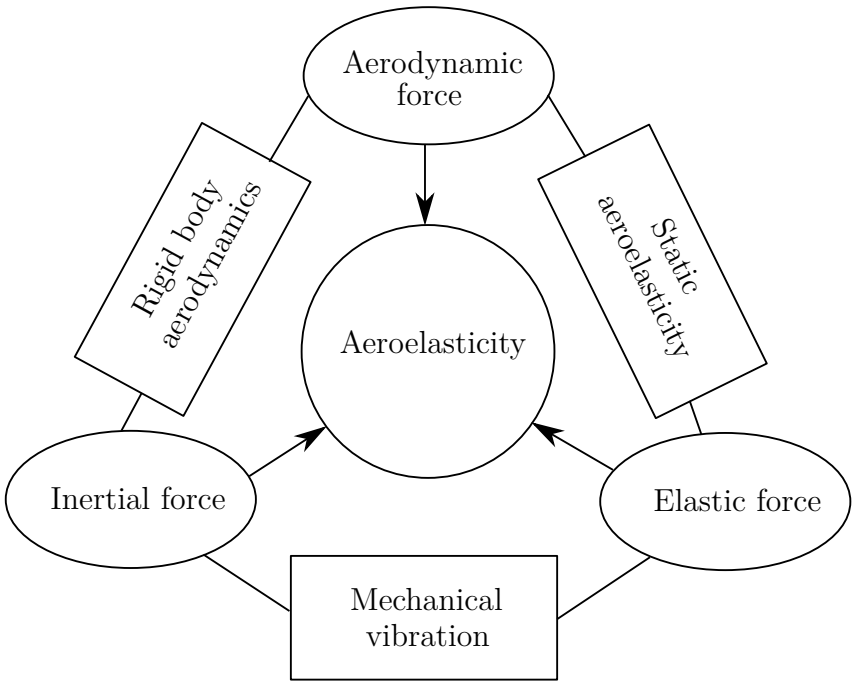

Figure 5.1 – Diagram of a completed model of forces acting on a wind turbine (Ageze et al., 2017).

Auciello considered the rotary inertia of the concentrated mass with its eccentricity. The solutions were given in terms of Bessel Functions and his model was proven a good alternative to the classical Rayleigh-Ritz approach. Murtagh et al. (2004) demonstrated two simple approximate methods for obtaining the natural frequencies. This simplification is acceptable for low frequency analysis (Kang et al., 2016). The first method employs the lumped mass technique, which reduces the order of the model, ultimately discretizing the tower-top mass system into several convenient degrees-of-freedom. The second method involves approximating the tower and utility by a cantilever beam with a concentrated mass at its free end. Then, the generic form of the fundamental mode shape is assumed, and the exponent, which is the unknown parameter of the mode shape expression, is determined. This method, which is more simplified compared to the former, concentrates on the fundamental mode of a structural system along with the corresponding mode shapes.

The mathematical model of the structure using a similar methodology of the Murtagh et al.'s second method is considered. The aim of this chapter is to discuss in what conditions the structural system consisting of distributed mass and elasticity can be modeled as a one-degree of freedom system using the principle of virtual work. Next, a brief introduction to the governing equation of a TLCD the coupled system equation in matrix form.

5.1 Equivalent parameters of a cantilever beam

The wind turbine structure is modeled as a cantilever beam with a mass at the free end. Gyroscopic effects due the turbine blade rotation are not considered. A simplification to a one degree of freedom equivalent system is considered. The usually employed equivalent stiffness, $k_{eq} = 3EI/L^3$, which is obtained for a concentrated tip mass with negligible distributed mass, does not always seem reasonable. An alternative approach consist of applying the principle of virtual work, which has been widely used in studies of elastic structural analysis. The principle of virtual work is perhaps one of the most fundamental principles in mechanics, and it can be stated as follow (Paz, 2012):

"For a system that is in equilibrium, the work done by all the forces during an assumed displacement (virtual displacement) that is compatible with the system constraints is equal to zero."

In other words, the principle of virtual work can be use to describe an equivalent systems where the kinetic and potential energies are the same as the original system. A system with multiple degree of freedom can be analyzed using the virtual work principle provided that only a single mode shape can be developed during motion, that is, if prior knowledge of the displacement of a single point in the system is known, the displacement of the entire system can be determined.

First, a description of the general model for a distributed mass cantilever beam with tip mass. Then, the required assumptions to describe the system as a single degree of freedom equivalent system are considered.

The wind turbine can be modeled as a cantilever beam with tip mass because the majority of its weight is concentrated at the top. Consider an elastic Euler-Bernoulli beam, viscously damped and fixed at the bottom as shown in Figure (5.2). The tower has a concentrated mass at the tip and the tip is subjected to a load per unit length $F(z,t)$ (not shown).

The motion of a Euler-Bernoulli beam is describe as

$$\frac{\partial^2}{\partial z^2}\left(EI\frac{\partial^2 w(z,t)}{\partial z^2}\right) + m\frac{\partial^2 w(z,t)}{\partial t^2} = F(z,t) \tag{5.1}$$

where $w(z,t)$ is the transverse displacement response, E is the elastic modulus, I is the moment of inertia averaged over the tower length L. The solution of a homogeneous ($F(z,t) = 0$) fourth order differential equation has an infinite number of natural frequencies (eigenvalues) and associated modes (eigenvectors). Considering the variable separation method where displacement can be described as $w(z,t) = \phi(z)Y(t)$, the equation of motion solely in the spatial variable is given by

$$\frac{d^2}{dz^2}\left(EI\frac{d^2\phi(z)}{dz^2}\right) + m\frac{d^2\phi(z)}{dt^2} = 0. \tag{5.2}$$

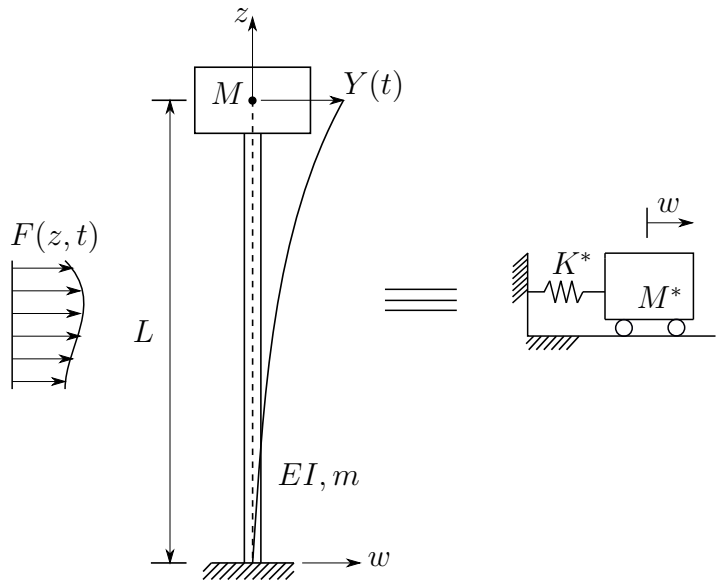

Figure 5.2 – Schematic model of the structure and equivalent simplified model.

To solve Equation (5.2), the four spatial form of the boundary conditions need to be satisfied:

fixed end at $z = 0$

$$\phi(0) = 0, \quad \frac{d\phi(0)}{dz} = 0, \tag{5.3}$$

free end with tip mass M at $z = L$

$$EI\frac{d^2\phi(L)}{dz^2} = \omega_n^2 \frac{d\phi(L)}{dz} J, \tag{5.4}$$

$$EI\frac{d^3\phi(L)}{dz^3} = \omega_n^2 \phi(L) M, \tag{5.5}$$

where J is the rotary mass moment of inertia, M is the tip mass and ω_n the natural frequencies of vibration. The solution of Equation (5.2) has the following form

$$\phi(z) = A_1 \cos(\lambda z) + A_2 \sin(\lambda z) + A_3 \cosh(\lambda z) + A_4 \sinh(\lambda z), \tag{5.6}$$

where A_i, $i = 1, 2, 3, 4$ are the four constants to be found using the boundary conditions, and λ is the root of the eigenvalue problem given by

$$\lambda = \left(\frac{\omega_n^2 M}{EI}\right)^{1/4}, \tag{5.7}$$

the spatial form of the boundary condition can be combined with Equation (5.6) to find the values of λ which give non-trivial values for the modal shapes $\phi(z)$. By writing the system of equations in matrix form, we notice that

$$A_1 + A_3 = 0 \tag{5.8}$$

$$A_2 + A_4 = 0 \tag{5.9}$$

hence,

$$\begin{bmatrix} \lambda^2(\cos\lambda L + \mathrm{ch}\lambda L) + \frac{\omega_n^2 J}{EI}\lambda(\sin\lambda L + \mathrm{sh}\lambda L) & \lambda^2(\sin\lambda L + \mathrm{sh}\lambda L) \\ \lambda^3(\sin\lambda L - \mathrm{sh}\lambda L) + \frac{\omega_n^2 M}{EI}(\cos\lambda L - \mathrm{ch}\lambda L) & -\lambda^3(\cos\lambda L - \mathrm{ch}\lambda L) \\ -\frac{\omega_n^2 J}{EI}\lambda(\cos\lambda L - \mathrm{ch}\lambda L) \\ +\frac{\omega_n^2 M}{EI}(\sin\lambda L - \mathrm{sh}\lambda L) \end{bmatrix} \begin{Bmatrix} A_1 \\ A_3 \end{Bmatrix} = \begin{Bmatrix} 0 \\ 0 \end{Bmatrix}. \tag{5.10}$$

The coefficients of Equation (5.10) have to be singular in order to obtain non-trivial values of A_1 and A_3. Setting the determinant of the square matrix equals to zero to obtain

$$1 + \cos\lambda L\mathrm{ch}\lambda L + \lambda\frac{\omega_n^2 M}{EI}(\cos\lambda L\mathrm{sh}\lambda L - \sin\lambda L\mathrm{ch}\lambda L) - \frac{\omega_n^2 J}{EI}\lambda^3(\mathrm{ch}\lambda L\sin\lambda L + \mathrm{sh}\lambda L\cos\lambda L) + \frac{\omega_n^4 MJ}{(EI)^2}(1 - \cos\lambda L\mathrm{ch}\lambda L) = 0 \tag{5.11}$$

The roots of Equation (5.11) give the eigenvalues of the system. Since the boundary-value problem is positive definite, the system has infinitely many positives eigenvalues for infinitely many natural modes of vibration. Hence, the eigenvalue of the rth vibration mode is λ_r, and it is associated with the rth eigenfunction (Erturk & Inman, 2011)

$$\phi_r(z) = A_r\left[\sin\lambda_r z - \mathrm{sh}\lambda_r z + \left(\frac{\sin\lambda z + \mathrm{sh}\lambda z}{\cos\lambda z + \mathrm{ch}\lambda z}\right)(-\cos\lambda_r z + \mathrm{ch}\lambda_r z)\right], \tag{5.12}$$

where A_r is the rth eigenfunction. Figure 5.3 shows the two first mode shapes of a cantilever beam with tip mass.

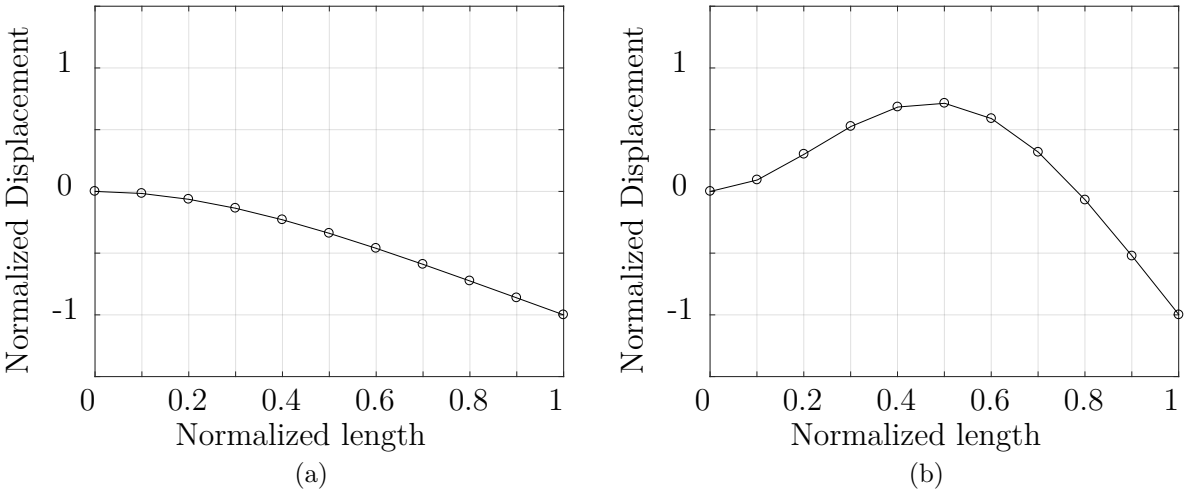

Figure 5.3 – The (a) first and (b) second modes of vibration of a cantilever beam with tip mass (Hatch, 2000).

Most commonly, tower vibration is approximated to the first term of Equation (5.12) which produces the first mode response of the tower. Kim (2017) proposed an equivalent mass and stiffness of a beam. The first bending mode was proposed by combining

polynomials representing the respective deflection shapes of a beam under a concentrated force at the tip and a uniformly distributed force.

An alternative approach was proposed by Avila et al. (2016) where for the first modal shape of a cantilever beam with tip mass was given by assuming the following modal shape (Paz, 2012)

$$\phi(z) = 1 - \frac{\cos \pi z}{2L} \tag{5.13}$$

this form is the one utilize thought out the rest of the analysis.

From the virtual work principle, assuming the modal shape ϕ given by Equation (5.13), the generalized mass and kinetic energy T are given by

$$T = \int_0^L \frac{1}{2} m(z) w^2(z,t) dz = \frac{1}{2} M^* Y^2(t), \tag{5.14}$$

$$T = \int_0^L \frac{1}{2} m(z) \{\phi(z) Y(t)\}^2 dz = \frac{1}{2} M^* Y^2(t), \tag{5.15}$$

hence,

$$M^* = \int_0^L m(z) \phi^2(z) dz, \tag{5.16}$$

and for the generalized stiffness, using the potential (strain) energy V, we obtain

$$V = \int_0^L \frac{1}{2} EI \left(\frac{d^2 w}{dz^2} \right)^2 dz = \frac{1}{2} K^* Y^2(t), \tag{5.17}$$

$$V = \int_0^L \frac{1}{2} EI \{\phi''(z) Y(t)\}^2 dz = \frac{1}{2} K^* Y^2(t), \tag{5.18}$$

hence,

$$K^* = \int_0^L EI \phi''(z) dz. \tag{5.19}$$

substituting the modal shape of Equation 5.13 in Equations (5.16) and (5.19), the generalized mass ans stiffness can be computed as

$$K^* = \frac{\pi^4}{32 L^3} EI, \tag{5.20}$$

$$M^* = \frac{mL}{2\pi} \left[\pi \left(3 + 2 \frac{L_e}{L} \right) - 8 \right], \tag{5.21}$$

where m is the mass for unit length of the beam, M is the tip mass, L_e is the equivalent length defined as $L_e = M/m$.

5.2 TLCD model and system equation of motion

TLCDs were originally created to mitigate rolling motion of ships and became popular through patents applications by Sakai et al., (1989). The oscillating liquid works as

a damping device transferring energy from the primary structure to the liquid. Furthermore, the energy of the oscillating liquid can be dissipated through friction and turbulence effects. Considering the TLCD rigidly connected on the primary structure as sketched in Figure 5.4. The TLCD consist of a "U" shaped reservoir filled with a Newtonian fluid such as water. From the previous section, the primary structure is a tower structure modeled as a one degree of freedom system with equivalent mass, stiffness and viscously damping.

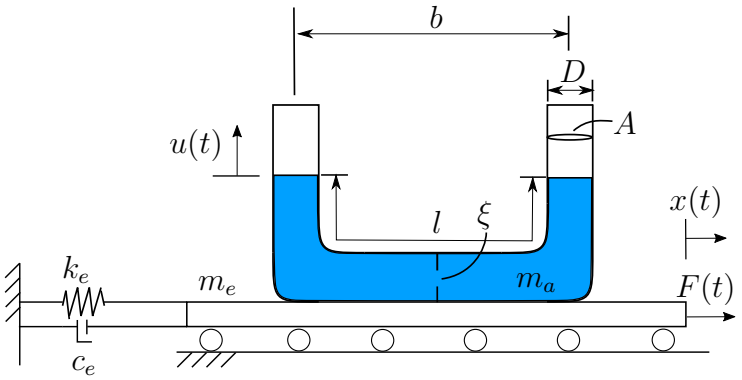

Figure 5.4 – Schematic model of the TLCD.

The liquid motion and oscillation can be derive from the Bernoulli equation. A more detail description of the TLCD mathematical model can be found in Streeter et al., (1998). The equation describing the motion of the fluid is given by

$$\rho A l\ddot{u}(t) + \frac{1}{2}\rho A\xi|\dot{u}(t)|\dot{u}(t) + 2\rho A g u(t) = -\rho A b\ddot{x}(t), \tag{5.22}$$

where $u(t)$ is the displacement of fluid, $x(t)$ is the displacement of the primary system, ρ is the fluid density, ξ is the head loss coefficient, A is the cross section area of the column, b and l are the horizontal and total length of the column respectively and g is the gravity constant. The TLCD equivalent mass, damping and stiffness are given respectively by $m_a = \rho A l$, $c_a = \frac{1}{2}\rho A\xi|\dot{u}(t)|$ and $k_a = 2\rho A g$. Therefore, the linearized column's natural frequency is given by $\omega_a = \sqrt{2g/l}$. The term on the right side of the Eq. (5.22) is the coupling term with the primary structure.

The equation of motion of the primary structure can be written as

$$(m_e + m_a)\ddot{x}(t) + \rho A b\ddot{u}(t) + c_e\dot{x}(t) + k_e x(t) = F(t), \tag{5.23}$$

where the parameter m_e is the structure mass, k_e the structure stiffness, c_e the structure damping and $F(t)$ the excitation force. From the previous section, we have $m_e = M^*$ and $k_e = K^*$ from now on. The term $\rho A b\ddot{u}(t)$ is a reaction force that occurs due to the motion of the liquid column induced by the structure. Thus, combining Equations (5.22) and (5.23), the equation of motion in matrix form is given by

$$\begin{bmatrix} m_e + m_a & \alpha m_a \\ \alpha m_a & m_a \end{bmatrix} \begin{Bmatrix} \ddot{x} \\ \ddot{u} \end{Bmatrix} + \begin{bmatrix} c_e & 0 \\ 0 & c_a \end{bmatrix} \begin{Bmatrix} \dot{x} \\ \dot{u} \end{Bmatrix} + \begin{bmatrix} k_e & 0 \\ 0 & k_a \end{bmatrix} \begin{Bmatrix} x \\ u \end{Bmatrix} = \begin{Bmatrix} F(t) \\ 0 \end{Bmatrix}, \tag{5.24}$$

$$|u| \leqslant \frac{l-b}{2}, \tag{5.25}$$

where $\alpha = b/l$ is the dimensionless length ratio. The condition presented by Equation (5.25) is needed to ensure the liquid in the column do not spill water and consequently change its mass and damping characteristics. Equation (5.24) can also be written with the mass matrix in its dimensionless form

$$\begin{bmatrix} 1+\mu & \alpha\mu \\ \alpha & 1 \end{bmatrix} \begin{Bmatrix} \ddot{x} \\ \ddot{u} \end{Bmatrix} + \begin{bmatrix} 2\omega_e\zeta_e & 0 \\ 0 & \frac{\xi|\dot{u}|}{2l} \end{bmatrix} \begin{Bmatrix} \dot{x} \\ \dot{u} \end{Bmatrix} + \begin{bmatrix} \omega_e^2 & 0 \\ 0 & \omega_a^2 \end{bmatrix} \begin{Bmatrix} x \\ u \end{Bmatrix} = \begin{Bmatrix} \frac{F(t)}{m_e} \\ 0 \end{Bmatrix}, \tag{5.26}$$

where

$$\zeta_e = \frac{c}{2m_e\omega_e} \tag{5.27}$$

$$\omega_e = \sqrt{\frac{k_e}{m_e}} \tag{5.28}$$

are the damping ratio and natural frequency of the linearized structure alone, respectively. The dimensionless parameters mass ratio μ and tuning ratio γ are defined as $\mu = m_a/m_e$ and $\gamma = \omega_a/\omega_e$. It can be noted that the nonlinear term is included in the TLCD damping matrix.

In the next chapter, two numerical analysis are considered, a parameter optimization and a sensitivity analysis.

6 Optimization

This Chapter proposes a global direct search optimization algorithm for the TLCD's parameters subjected to an arbitrary wind spectrum, given by its power spectral density (PSD). A simple verification is made considering the analytical solution of undamped primary structure under white noise excitation. Finally, a numerical example with a simplified wind turbine model is given to illustrate the efficacy of TLCD. Time and frequency domain results from the random vibration analysis are also shown.

To avoid solving nonlinear equations simultaneously, solutions such as statistical linearization (Roberts & Spanos, 2003) and parameter optimization (Vanderplaats, 1984) have been proposed in previous works. Yalla & Kareem (2000) derived a closed-form solution for optimized TLCD damping ratio and head loss coefficient. Although the method does not rely on an iterative procedure, in order to solve the minimum variance integrals, a formula is derived indirectly considering some properties of the spectrum of the stationary output of a linear time-invariant system to white noise input. Altay et al. (2014) presented an expanded optimization approach which considers the geometric layout of the damper. Numerical verification was carried out by stochastic inflow turbulence simulator TurbSim and the aero-elastic dynamic horizontal axis wind turbine simulator FAST which are well known wind turbine simulation tools.

Optimization procedures have also been proposed for structures with mounted TLCD under harmonic load. By maximizing the reduction of peak structural response under harmonic excitation, Gao et al. (1997) designed the optimum tuning parameters for a TLCD for a wide frequency range. Shum (2009) proposed a close-form optimal solution by optimizing the response of primary structure at two invariant points using the fixed-point method with a perturbation technique.

Some interesting optimization approaches can also be found for tuned mass damper (TMD). To avoid the limitations of the close-form optimal solutions, Lee et al. (2006) proposed an optimal design theory with a systematic and efficient procedure for searching optimal design parameters of a TMD. Zuo & Nayfeh (2004) proposed a numerical approach based on the descent subgradient method to maximize the minimal damping of modes in a prescribed frequency range for general multi-degree-of-freedom TMD, then followed by a performance comparison between the minmax, H_2 and H_∞ methods.

This Chapter objective is to propose an optimization approach, based on a global

direct search optimization algorithm, in order to find the optimum TLCD parameters for reducing vibration levels in slender structures such as wind turbines, when subject to an arbitrary stationary random wind excitation. The mathematical description of the slender structure and TLCD were discussed in Chapter 5. Four different wind models are investigated given by a power spectral density (PSD) profile and their effects on the optimum parameters are discussed. The wind profile model used were discussed in Chapter 4. Then, a numerical example with a simplified wind turbine model is used to illustrate the efficacy of TLCD.

This Chapter is organized as follow. Section 6.1 presents the optimization approach as well as a numerical verification. Section 6.2 presents a random vibration analysis through a numerical example using a simplified wind turbine model. Finally, Section 6.3 presents some concluding remarks.

6.1 Parameter optimization criteria

The nonlinear nature of TLCD damping in Equation (5.26) requires the determination of its equivalent form in order to perform random vibration analysis. Statistical linearization is the classical approach but other methods can also be used. In this section, the linearization is firstly introduced followed by the parameter optimization.

Roberts & Spanos (2003) proposed a procedure to estimate the linearized equivalent damping using statistical linearization. From this approach, the error between the nonlinear term with its equivalent linearized can be expressed as $\epsilon = \xi|\dot{u}|/2l - c_{eq}\dot{u}$, where the value of the equivalent damping c_{eq} can be obtained by minimizing the standard deviation of the error value, namely $E\{\epsilon^2\}$. Assuming a probability density function with Gaussian form, it is possible to obtain an expression for the equivalent linearized damping as a function of the standard deviation of the fluid velocity $\sigma_{\dot{u}}$ and the head loss coefficient ξ. An iterative method is then carried out to find the optimized head loss coefficient.

Another linearization strategy is described in Yalla & Kareem (2000). By writing the TLCD's nonlinear damping in its linear form, $2\omega_a\zeta_a$, where ω_a and ζ_a are the TLCD's natural frequency and damping ratio respectively, Yalla & Kareem minimized the primary structure variance response with respect to the damping ratio and the tuning ratio to find their optimal conditions when both equations were solved simultaneously. Although this method does not rely on iterative procedure, it involves a rather large computation (Roberts & Spanos, 2003). Furthermore, the minimization solution changes if different wind models are used.

In this work, the proposed method considers the linearization as described in Yalla & Kareem (2000) but instead of solving the optimization problem analytically, a numerical approach is considered, extending the methodology to an arbitrary spectrum. We can

write Equation (5.26) in its linearized form as follows

$$\begin{bmatrix} 1+\mu & \alpha\mu \\ \alpha & 1 \end{bmatrix} \begin{Bmatrix} \ddot{x} \\ \ddot{u} \end{Bmatrix} + \begin{bmatrix} 2\omega_e\zeta_e & 0 \\ 0 & 2\omega_a\zeta_a \end{bmatrix} \begin{Bmatrix} \dot{x} \\ \dot{u} \end{Bmatrix} + \begin{bmatrix} \omega_e^2 & 0 \\ 0 & \omega_a^2 \end{bmatrix} \begin{Bmatrix} x \\ u \end{Bmatrix} = \begin{Bmatrix} \frac{F(t)}{m_e} \\ 0 \end{Bmatrix}. \tag{6.1}$$

From the linearized system, a frequency response function (FRF) is defined which will be used in the random vibration analysis. The frequency response functions are obtained by assuming the system in Equation (6.1) oscillates under harmonic motion. The system response vector is then given by

$$\begin{aligned} \mathbf{X}(\omega) &= [-\omega^2\mathbf{M} + j\omega\mathbf{C} + \mathbf{K}]^{-1}\mathbf{F}(\omega) \\ &= \mathbf{H}(j\omega)\mathbf{F}(\omega) \end{aligned} \tag{6.2}$$

where ω stands for the driving frequency, $\mathbf{F}(\omega)$ is the vector of the exciting force, $\mathbf{H}(j\omega) = [-\omega^2\mathbf{M} + j\omega\mathbf{C} + \mathbf{K}]^{-1}$ is the frequency response function, j is the imaginary unit, and $\mathbf{M}$, $\mathbf{C}$ and $\mathbf{K}$ are the mass, damping and stiffness matrix respectively. For both degrees of freedom, the explicit expressions of the diagonal terms of the FRF matrix are given by

$$H_{11} = \frac{(j\omega)^2 + \zeta_a\omega_a(j\omega) + \omega_a^2}{[(j\omega)^2(1+\mu) + 2\zeta_e\omega_e(j\omega) + \omega_e^2][(j\omega)^2 + 2\zeta_a\omega_a(j\omega) + \omega_a]^2 - (j\omega)^4\alpha^2\mu}, \tag{6.3}$$

$$H_{22} = \frac{-\alpha(j\omega)^2}{[(j\omega)^2(1+\mu) + 2\zeta_e\omega_e(j\omega) + \omega_e^2][(j\omega)^2 + 2\zeta_a\omega_a(j\omega) + \omega_a)^2] - (j\omega)^4\alpha^2\mu}. \tag{6.4}$$

Equation (6.3) and (6.4) depend on the system parameters such as the absorber damping ratio and the natural frequencies.

If the excitation force $\mathbf{F}(t)$ is a stationary random signal with power spectral density (PSD) $S_{ff}(\omega)$, the structural response is also random and with PSD given by $S_{yy} = \mathbf{H}S_{ff}\mathbf{H}^T$, where the superscript T denotes the matrix transpose. Note that $S_{ff}(\omega)$ is proportional to the power spectral density of the wind velocity and it can assume different models depending on the wind profile.

The desired performance index (cost function) Ξ will be defined by the mean square response. If the exciting force is zero mean then the response also has zero mean, therefore the mean square response equals the variance, thus

$$\begin{aligned} \Xi(\zeta_a, \gamma) &= \int_{-\infty}^{\infty} S_{yy}(\omega)d\omega \\ &= \int_{-\infty}^{\infty} \mathbf{H}(j\omega)S_{ff}(\omega)\mathbf{H}(j\omega)^T d\omega \end{aligned} \tag{6.5}$$

where the response PSD $S_{yy}(\omega)$ is real positive and, therefore, the sufficient and necessary conditions for the optimization are met (Lee et al., 2006). For the prescribed frequency range $[\omega_l, \omega_u]$ the optimization problem consists of looking for the parameters that minimize

the variance of response PSD, i.e.

$$\begin{aligned} &\min_{\zeta_a,\gamma\in\Omega} \Xi_i(\zeta_a,\gamma) \\ s.t. \quad &\zeta_a,\gamma \geq 0 \\ &I = \{i \mid \omega_l \leq \omega_i \leq \omega_u\} \end{aligned} \tag{6.6}$$

where Ω is the set of design parameters ζ_a and γ satisfying the constraint. To solve the optimization problem we introduce the optimization algorithm in the next subsection.

6.1.1 Generalized patter search

The Generalized Patter Search (GPS) is a class of direct search methods, originally proposed for unconstrained minimization problems (Hooke & Jeeves, 1961), and then extended in its generalized form for problems with bound and linear constraints (Torczon, 1997). GPS is a non-gradient-based algorithm therefore, it is not as strongly affected by random noise in the cost function. However, it requires more function evaluations than gradient-based algorithms to find the true minimum. A more detailed description of the method can be found in Kolda et al. (2003). The MATLAB environment is used to perform the GPS algorithm with its included solver *patternsearch* as showing in Algorithm 1 bellow.

Algorithm 1 *patternsearch* algorithm

```
X0 = [zeta gamma];          # Starting point
LB = [0 0];                 # Lower bound
UB = [inf inf];             # Upper bound
Objfcn = @objfun;
PSoptions = optimoptions('patternsearch',...
                         'ConstraintTolerance',1e-14,
                         'FunctionTolerance',1e-14,
                         'StepTolerance',1e-14);
[xopt,Fps] = patternsearch(Objfcn,X0,[ ],[ ],[ ],[ ],LB,UB,PSoptions);
```

6.1.2 Verification procedure

In order to verify if the algorithm and cost function are adequate for solving the optimization problem, a simple case where the closed-form solution is available is investigated.

Considering the case of undamped primary structure ($\zeta_e = 0$) and white noise excitation, Yalla & Kareem (2000) solved the mean variance problem to obtain the following

expression for optimal parameters

$$\zeta_{opt} = \frac{\alpha}{2}\sqrt{\frac{2\mu\left(\alpha^2\frac{\mu}{4} - \mu - 1\right)}{(\alpha^2\mu^2 + \alpha^2\mu - 4\mu - 2\mu^2 - 2)}}, \tag{6.7}$$

$$\gamma_{opt} = \frac{\sqrt{1 + \mu(1 - \frac{\alpha^2}{2})}}{1 + \mu}, \tag{6.8}$$

which are function of the length ratio α and mass ratio μ.

Figure 6.1 shows the optimized parameters from Yalla & Kareem (2000) and the proposed algorithm as a function of the mass ratio for different length ratio α. It can be noticed a very good agreement in Figure 6.1(a) for the tuning ratio. A slight difference in Figure 6.1(b) can be seen between the two methods in the optimum damping ratio for large values of mass ratio which can be attributed to tolerance error in the optimization algorithm and the chosen cost function's interval of integration that, in this case, were chosen between 2 and 5 rad/s with resolution of 0.01 rad/s. An increase in the interval or resolution would result in a small change in the optimized values but increase considerably the computation time. Additionally, the optimized damping ratio sensibility does not seems to influence the characteristics of the system.

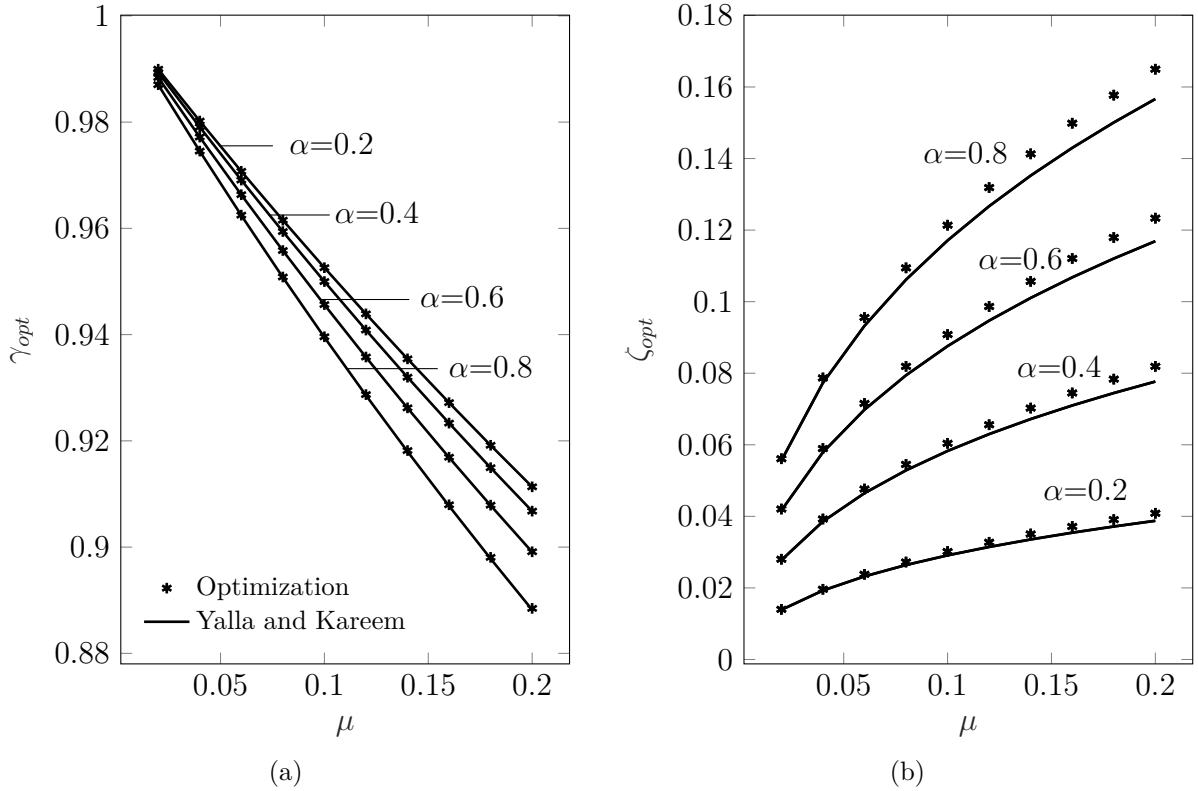

Figure 6.1 – Comparing optimized (a) tunning ratio and (b) damping ratio subject to White Noise spectrum as a function of the mass ratio μ for different length ratio α.

The wind excitation PSDs considered are detailed in Chapter 4. The next section describes a numerical example of a simplified wind turbine using random vibration analysis, wind profiles and the optimized parameters.

6.2 Random vibration analysis

In this section, the random vibration analysis to find the system response in the frequency domain is introduced. Statistics of the response, e.g. mean value, standard deviation and autocorrelation, of a linear systems under random stationary excitation can be calculated straightforwardly. However, non-linear systems require the direct time domain solution of the differential equations in order to calculate the response statistics or some linearization approach. These difference can be summarized in the diagram shown in Figure 6.2.

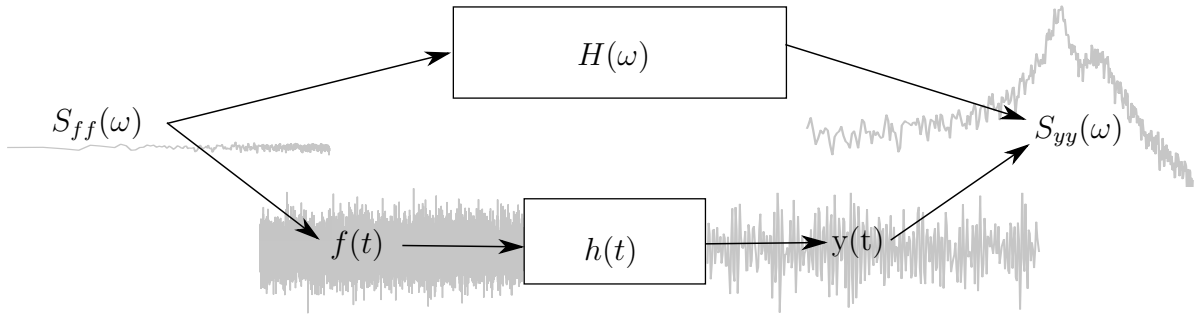

Figure 6.2 – Response PSD $S_{yy}(\omega)$ obtained from frequency response function for the linearized case (upper path), and from numerical integration for the nonlinear case (lower path).

The upper path of the diagram indicates the first approach. In this case, to obtain the frequency response function we first apply the proposed linearization procedure to the system and then calculate the optimized parameters. From the excitation PSD S_{ff}, the response PSD S_{yy} can be calculated directly by (Newland, 2012)

$$S_{yy}(\omega) = \mathbf{H}(\omega) S_{ff}(\omega) \mathbf{H}(\omega)^T. \tag{6.9}$$

where this expression is equivalent to the expression presented in Equation 3.54. Moreover, Equation 6.9 is computationally cheaper than the direct integration approach. The later, typically requires the use a 4^{th} order Runge Kutta Felberg ($ode45$) solver. The wind profile time history can be calculated from the procedure described in Section 4.3. Finally, the response PSD $S_{yy}(\omega)$ can be estimated via a periodogram approach (Newland, 2012). This approach can lead to the solution of the structure response. However, it would still be necessary to find the optimized parameters that would require several evaluations of this nonlinear system, which could be computationally prohibitive.

A comparison between the two approaches was carried out in Alkmim et al. (2016). The main result is presented in Figure 6.3, which illustrates the response PSD of the two

cases and the system without the TLCD using a first order filter PSD excitation. A good approximation between the two methods is shown as well as a good vibration dissipation comparing to the case without TLCD. In addition, there is a slightly difference between equivalent and nonlinear models near the resonance peak where the nonlinear case shows a slightly smaller amplitude PSD compared to the linearized case. This difference might be attributed by the numerical approximations such as the frequency range chosen for the optimization.

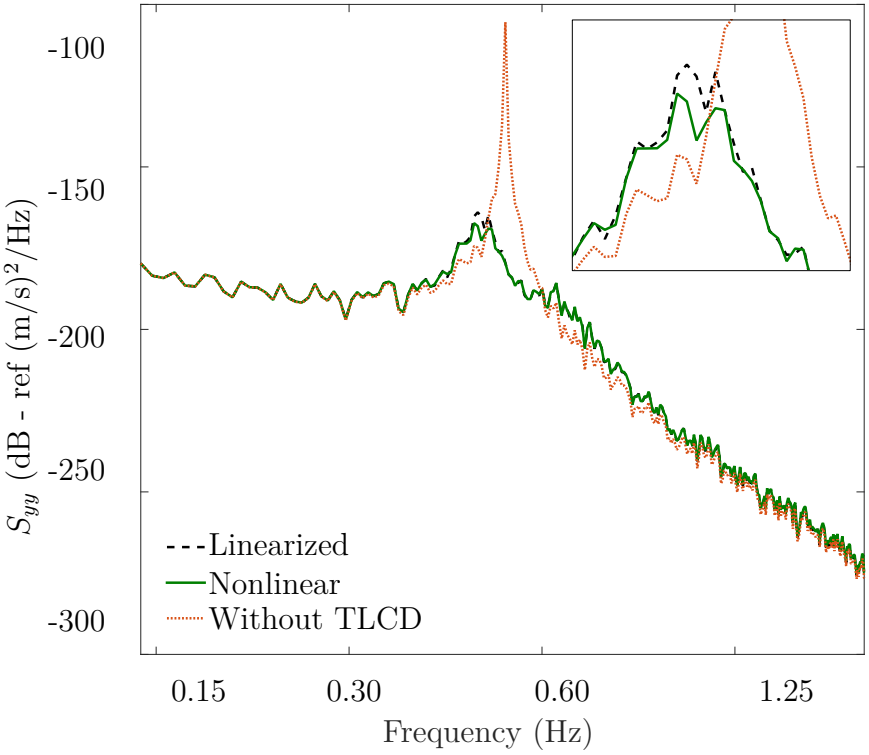

Figure 6.3 – PSD response of main system to a first order filter random excitation without and with TLCD, obtained via statistical linearization and via numerical integration of nonlinear system

6.2.1 Numerical example

In this section a numerical example is carried out using the wind turbine parameters, summarized in Table 6.1, same as proposed by Murtagh et al., (2005). First, optimized parameters are obtained for a fixed length ratio and different mass ratios and wind spectra cases. Then, comparisons of the system response PSD with and without TLCD are shown.

Table 6.2 presents the obtained optimized TLCD damping ratio ζ_{opt} and tunning ratio γ_{opt} for a fixed length ratio $\alpha = 0.8$ and different mass ratio and wind spectra. Fixed length ratio configuration is chosen because both mass and length ratios are inversely proportional and related to the physical constraint horizontal length of the liquid column, b, as follows

$$\mu = \left(\frac{\rho A}{m_e}\right)\frac{b}{\alpha}. \tag{6.10}$$

Table 6.1 – Wind turbine parameters

Parameter	Symbol	Equation	Value	Unit
Modulus of elasticity	E		2.1×10^{11}	Pa
Width	D		3	m
Thickness	t_h		0.015	m
Cross section area	A_h	$\pi D t_h$	0.14	m^2
Steel density	ρ_s		7850	kg/m^3
Tip mass	M		19876	kg
Beam mass per length	m	$\rho_s A$	1110	kg/L
Total length	L		60	m
Equivalent length	L_e	M/m	17.91	
Second moment of area	I	$\pi t D^3/8$	0.16	m^4
Structure stiffness	k_e	Eq.(5.20)	470685	N/m
Structure mass	m_e	Eq.(5.21)	34975	kg
Structure natural frequency	ω_e	$\sqrt{k_e/m_e}$	3.67	rad/s
Structure damping ratio	ζ_e	$c_e/2m_e\omega_e$	1.83	%

where a fixed length ratio can have different horizontal lengths for each mass ratio.

From Table 6.2, it can be seen that the optimum TLCD damping ratio ζ_{opt} increases when increasing mass ratio μ, and it is only slightly affected by the choice of wind spectrum. This can be clearly noticed from Figure 6.4(b). On the other hand, the optimum tunning ratio γ_{opt} decreases for increasing mass ratio μ and it is significantly affected by the choice of wind spectrum, as can be clearly seen from Figure 6.4(a). Kaimal and Davenport spectra present almost the same values of tunning ratio, which are overall increasingly smaller for increasing mass ratio μ, when compared to the white noise spectrum. This is expected, since both Kaimal and Davenport spectra are very similar to each other and with significantly more energy content in lower frequencies, when compared to the white noise spectrum. Moreover, Kanai-Tajimi spectrum shows overall larger values of optimized tunning ratio. Furthermore, the choice of wind spectrum can influence the response magnitude and therefore it is relevant for the appropriate choice of optimum TLCD parameters. One suitable strategy one might take is to use white noise spectrum as an initial dynamic analysis. If we consider the system is undergoing magnitude higher than it would be expected of other spectrums such as Kaimal and Davenport were utilized, it means we are in favor of safety. The opposite can be said for Kanai-Tajimi spectrum.

Figure 6.5 shows the system response in frequency and time domain, under Kaimal spectrum excitation and optimized parameters for $\mu = 0.06$. A significant reduction of the response is obtained in both PSD S_{yy} and time domain response, when compared to the case without TLCD, as expected. Moreover, results are shown for two other cases in which non-optimum parameters are chosen for $\mu = 0.02$ and $\mu = 0.15$, to illustrate the effect of optimized parameters. While the optimized response PSD shows two peaks with same magnitude, the latter presents two peaks, one slightly bigger than the other and the former has only one peak, which is bigger than the optimized one.

Table 6.2 – Optimized LCD damping ratio ζ_{opt} and tunning ratio γ_{opt} for a fixed length ratio $\alpha = 0.8$ and 1% primary structural damping

	White Noise		Davenport		Kaimal		Kanai-Tajimi	
μ	ζ_{opt}	γ_{opt}	ζ_{opt}	γ_{opt}	ζ_{opt}	γ_{opt}	ζ_{opt}	γ_{opt}
0.02	0.0561	0.9861	0.0559	0.9815	0.0559	0.9815	0.0563	0.9874
0.04	0.0787	0.9732	0.0783	0.9655	0.0783	0.9656	0.0790	0.9754
0.06	0.0955	0.9609	0.0950	0.9504	0.0950	0.9505	0.0961	0.9638
0.08	0.1094	0.9491	0.1086	0.9360	0.1086	0.9360	0.1102	0.9527
0.10	0.1213	0.9377	0.1203	0.9222	0.1203	0.9222	0.1224	0.9419
0.12	0.1317	0.9267	0.1305	0.9088	0.1305	0.9089	0.1331	0.9315
0.14	0.1411	0.9161	0.1396	0.8960	0.1396	0.8961	0.1427	0.9213
0.16	0.1497	0.9058	0.1479	0.8836	0.1479	0.8837	0.1515	0.9115
0.18	0.1575	0.8959	0.1555	0.8717	0.1555	0.8717	0.1595	0.9019
0.20	0.1647	0.8862	0.1625	0.8601	0.1625	0.8602	0.1669	0.8927

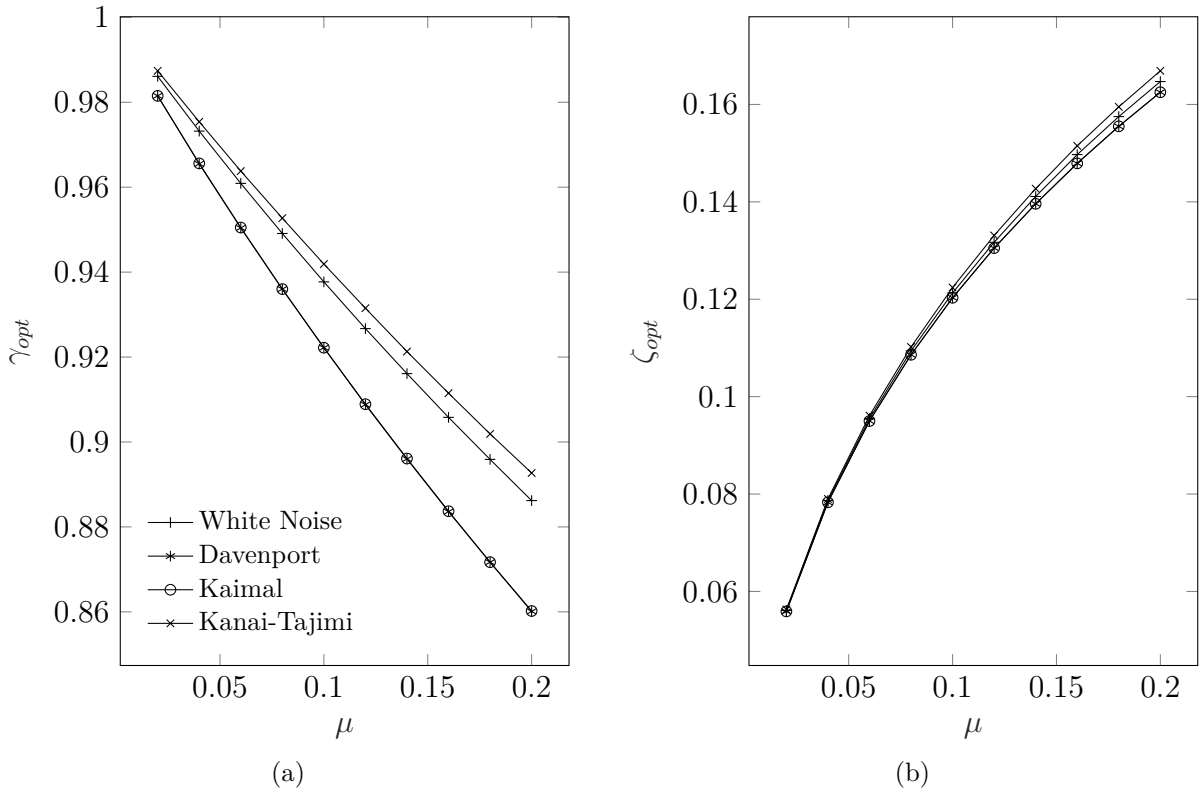

(a) (b)

Figure 6.4 – Optimum (a) tunning ratio γ_{opt} and (b) damping ratio ζ_{opt} subject to different wind spectra as a function of the mass ratio μ for a fixed length ratio $\alpha = 0.8$ and 1% primary structural damping.

6.3 Concluding remarks

In this Chapter, it was proposed an optimization approach to find the optimum TLCD parameters for reducing vibration levels in slender structures such as wind turbines, when subject to an arbitrary stationary random wind excitation.

The TLCD model presented a nonlinear damping term, which is then approximated

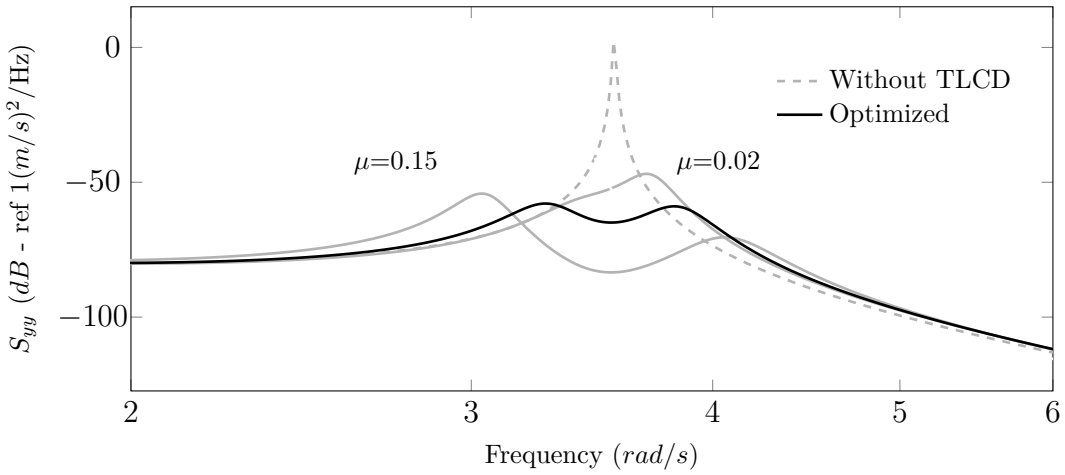

(a)

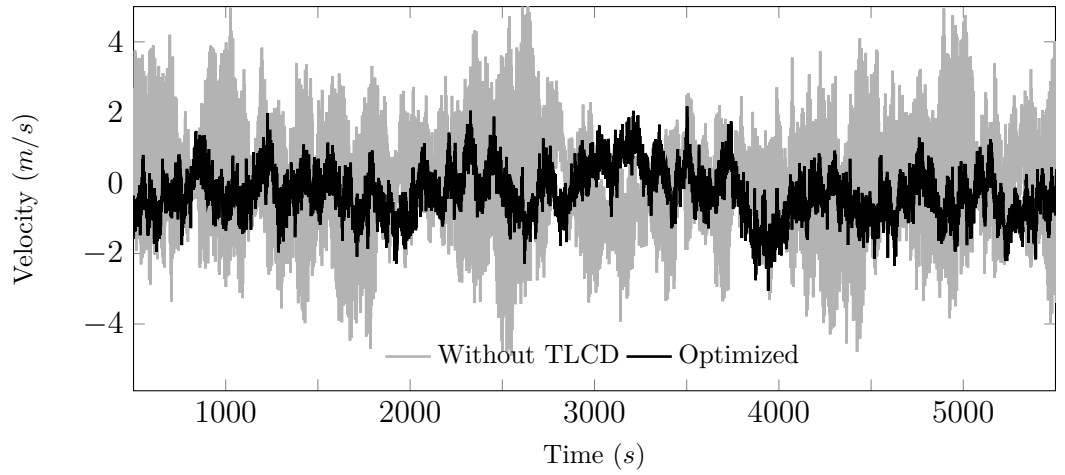

(b)

Figure 6.5 – Response of main system under Kaimal spectrum for $\mu = 0.06$ and $\alpha = 0.8$ (a) without TLCD (dashed), optimized (solid black) and two different mass ratio (solid grey scale) in the frequency domain and (b) without TLCD (solid grey scale) and optimized (solid black) in the time domain.

by a linear coefficient utilizing a statistical linearization approach. Then an optimization criteria was chosen such that it minimizes the area under the response PSD S_{yy} and a global direct search optimization algorithm was used to find optimum TLCD parameters as it can provide the optimized parameters for a more general case and for any wind spectral model. Four different wind models, given by a PSD profile, were investigated, namely Davenport, Kaimal, Kanai-Tajimi and a white noise, and it was shown that they can significantly affect the choice of the optimum parameters. White noise is commonly used in the literature, hence care should be taken since it might give misleading results.

A verification of the proposed approach is made considering the case of undamped primary structure under white noise excitation, which has an analytical solution available. The TLCD design parameters are obtained from damping ratio ζ and tunning ratio γ. It is shown that the optimum TLCD damping ratio ζ_{opt} increases for increasing mass ratio μ, and it is only slightly affected by the choice of wind spectrum. Besides, the optimum

tunning ratio γ_{opt} decreases for increasing mass ratio μ and it is significantly affected by the choice of wind spectrum.

A numerical example considering a simplified 1 DoF wind turbine as a slender structure and results in time and frequency domain showed better vibration attenuation performance when compared non-optimum parameters.

7 Uncertainty analysis

The aim of this Chapter is to investigate the behavior of the structure response and TLCD considering parameter variability. Computational models have proven to be a reliable source of information of the behavior of physical problems. However, every finite element analysis contains some degree of uncertainty. As simulation analysis increases over complex problems, uncertainty can play bigger roles since it can grows with size and complexity.

To the casual eye, uncertainty quantification seems a contradictory statement. Nevertheless, uncertainty quantification has become a scientific and engineer approach with a structured methodology much like the verification and validation method (V&V).

Uncertainties can arise from many sources. For instance, inadequate modeling of boundary conditions, fabrication process, effect of nonstructural elements, degradation due to aging and temperature, fluctuations in structural mass, member capacities, yield strength, inertial moment, elasticity module, etc (Marano et al., 2010).

Another major limitation of the deterministic approach is that uncertainties in the performance cannot be included in the damper parameter optimization since the damper efficiency can drastically reduce if the parameters are off-tuned to the vibration mode (Chakraborty & Roy, 2011). For this reason, the probabilistic approach offers a rational basis of accounting for both load and structural uncertainties in the design process.

In order to increase the credibility of the model, these uncertainties need to be modeled appropriately. The study of randomness associated with mechanical systems was introduced in the early 20th century. However, only the external loading was considered random leaving uncertainties related to the model unconsidered (Newland, 2012).

To quantify uncertainties in dynamic structures, random variables need to be associated with the system parameters along with their probability density function. Building the probability density function that best represents the physical problem is not trivial and requires experimental data to assist in its construction (Soize, 2001). One way around this problem is to associate to the random variable a Gaussian probability density function. However, this procedure is not always advisable as it may lead to physically incoherent results.

Many strategies can be used to construct the probability density function such as

the hypothesis test, a Bayesian approach and the Maximum Entropy Principle (MEP). In the hypothesis test, the probabilistic model is propose as the null hypothesis and then confronted with observed data. The Bayesian approach is utilized by supposing a initial probabilistic model. The model is then update using new information from experimental or numerical data.

Alternatively, the Maximum Entropy Principle can be used to construct the probability density function of the random variable uncertainties of the model. The principle consist of using only the information available to build possible probability density functions (PDF) and from there, search for the function with maximum entropy (or uncertainty). This method avoids using misinformation in the construction of model ranging from the physics of the problem (Sampaio & Ritto, 2008). After defining the proper PDF's, a Monte Carlo simulation is made to describe the implications of this variability in the system.

Two paths can be followed in modeling uncertainties: random scalar variable, when scalar parameters are modeled with uncertainty and random matrix variable when model uncertainty is included by random matrices. The first case is indicated for uncertain data model while the latter is suitable for uncertainties in the model also known as nonparametric approach (Soize, 2005). The scope of this Chapter will be limited to the random scalar variable method.

The outline of the Chapter is as follows. After a brief description of the proposed uncertainty model, Section 7.2 describes how the structural uncertainties are modeled using Monte Carlo simulation. Section 7.3 presents the case study and the results of the application of the proposed procedure. Finally, some concluding remarks are given in Section 7.3.

7.1 Uncertainty model

Uncertainty analysis is taken into account in order to describe how the system parameters may impact the device performance and improve design reliability considering the optimum damping developed in previous sections and its inherent variability. Hence, for this analysis, the probabilistic parameters are assumed to be the viscous damping coefficient ζ_a and the stiffness of the structure k_e. The masses and the other parameters are assumed deterministic.

First, the probability distribution function (PDF) will be constructed using the Maximum Entropy principle (Soize, 2005). By relying only on the information available, it is possible to obtain the optimum probabilistic model using the one with maximum entropy (uncertainty).

The equation of motion can be written in the frequency domain using the Fourier

transform. One can obtain the the frequency response function (FRF) for the two degree of freedom

$$H_{11}(i\omega) = \frac{\hat{x}}{\hat{F}}; \tag{7.1}$$

$$H_{22}(i\omega) = \frac{\hat{u}}{\hat{F}}, \tag{7.2}$$

Equations (7.1) and (7.2) are functions of frequency and they depends on the parameters of the system such as the absorber damping ratio ζ_a and the structure natural frequency, hence the structure stiffness k_e. The parameters considered as uncertain are the TLCD damping ratio ζ_a and the structure stiffness k_e. The random variable Z is associated to the damping ratio and K for the structure stiffness. A underline bar is used to represent the mean value of these parameters. The procedure to find the PDF is similar for both parameters, for this reason, the following analysis will show only the PDF construction of the Z parameter.

The basic available information are the mean reduced model, the positive-definiteness of the random variable and the existence of second-order moments, in other words:

(1) the support of the probability density function is $]0, +\infty[$,

(2) the mean value is assumed to be known, $E\{Z\} = \underline{Z}$ and

(3) the condition $E\{\ln(Z)\} < +\infty$, which implies that zero is a repulsive value (Cataldo et al., 2010).

The probability density function p_Z has to verify the following constraint equations (Kapur & Kesavan, 1992)

$$\int_{-\infty}^{+\infty} p_Z(z)dz = 1, \tag{7.3}$$

$$\int_{-\infty}^{+\infty} z p_Z(z)dz = \underline{Z}, \tag{7.4}$$

$$\int_{-\infty}^{+\infty} \ln(Z) p_Z(z)dz < +\infty, \tag{7.5}$$

applying the Maximum Entropy Principle yields the probability density function given by the gamma distribution (Cataldo et al., 2010)

$$p_Z(z) = \mathbf{1}_{]0,+\infty[}(z) \frac{1}{\underline{Z}} \left(\frac{1}{\delta_Z^2}\right)^{\frac{1}{\delta_Z^2}} \frac{1}{\Gamma(1/\delta_Z^2)} \left(\frac{1}{\underline{Z}}\right)^{\frac{1}{\delta_Z^2}-1} e^{\frac{-z}{\delta_Z^2 \underline{Z}}}, \tag{7.6}$$

where $\delta_Z = \sigma_Z/\underline{Z}$ is the coefficient of dispersion of the random variable Z and σ_Z is the standard deviation of Z such that $0 \leq \delta_Z \leq 1/\sqrt{2}$. It can be verified that Z is a second-order random variable and that $E\{1/Z^2\} < +\infty$ (Soize, 2001). The gamma function Γ is defined as

$$\Gamma(1/\delta_Z^2) = \int_0^{+\infty} t^{1/\delta_Z^2 - 1} e^{-t} dt, \qquad 1/\delta_Z^2 > 0. \tag{7.7}$$

The PDF for the structural stiffness follow the same procedure and is given by

$$p_K(k) = \mathbf{1}_{]0,+\infty[}(k)\frac{1}{\underline{K}}\left(\frac{1}{\delta_K^2}\right)^{\frac{1}{\delta_K^2}}\frac{1}{\Gamma(1/\delta_K^2)}\left(\frac{1}{\underline{K}}\right)^{\frac{1}{\delta_K^2}-1}e^{\frac{-k}{\delta_K^2\underline{K}}}, \tag{7.8}$$

since the values of coefficient of dispersion are not known for both parameters, the following sections will show results for a variation of this parameter. From the constructed PDF's, we can now perform a Monte Carlo simulation.

7.2 Monte Carlo sampling

The Monte Carlo method is a class of computational techniques based on synthetic generation of random (pseudo-random) variables in order to deduce the implications for the probability distribution (Rubinstein & Kroese, 2016). In other words, since only one sample would not be a good representation of a uncertain variable, we need a significant amount of samples to be able to calculate the relevant statics of the variable. The samples are generated from the PDF previously found using the inverse transform method. As already stated, in probabilistic simulations, we must ensure that the probability density function of the random variable has significant physical meaning.

The simulation convergence criterion is given by (Sampaio & Ritto, 2008)

$$conv(n_s) = \frac{1}{n_s}\sum_{j=1}^{n_s}\int_B \|H_j(\theta,\omega) - \underline{\hat{H}}(\omega)\|^2 d\omega, \tag{7.9}$$

where $\|H_j(\theta,\omega)\|$ is the stochastic system response in the frequency domain calculated for the θ realization, $\|\underline{\hat{H}}(\omega)\|$ is the mean stochastic system response.

The deterministic model is obtained by using the mean value of damping ratio $\underline{Z}$. The value of $\underline{Z}$ is determined by a optimization method developed by Yalla & Kareem which, for a white-noise excitation and considering undamped primary system, it can be expressed as

$$\underline{Z} = \frac{\alpha}{2}\sqrt{\frac{2\mu\left(\alpha^2\frac{\mu}{4} - \mu - 1\right)}{(\alpha^2\mu^2 + \alpha^2\mu - 4\mu - 2\mu^2 - 2)}}, \tag{7.10}$$

where for $\alpha = 0.9$ and $\mu = 0.05$ it follows that $\underline{Z} = 0.0965$.

The mean values of the structure stiffness $\underline{K}$ is obtained by a simplified model of cantilever beam from Chapter 7.

$$\underline{K} = \frac{\pi^4}{32L}EI \tag{7.11}$$

where L is the beam length and EI is the flexural stiffness. Using $L = 60\ m$, $3\ m$ width and $0.015\ m$ thickness, $E = 2.1$ x $10^{11}\ N/m^2$, density of the steel $\rho = 7,850\ kg/m^3$ one can find $\underline{K} = 463,671\ N/m$. The rotor mass is $M = 19,876\ kg$. Using the dimensionless parameter length ratio $\alpha = 0.9$ and $\nu = 0.1$, it follows that $\omega_e = 3.6450\ rad/s$ and $\zeta_e = 0.0018$.

7.3 Results for parameter uncertainty

Two cases are studied in this section, in the first case, uncertainties are considered only in the TLCD damping ratio parameter. In the second case, uncertainties are included in both the TLCD damping ratio and the structural stiffness. In both cases, we are interested in construct the frequency response function of structure $H_{11}(\omega)$ from Equation (7.1) for different coefficients of dispersion using Monte Carlo (MC) simulation.

Figure 7.1 shows, for different values of coefficient of dispersion δ_Z, the mean model, the mean response of the stochastic model and the boundary lines representing the confidence region of 95%, which means that the response is inside the envelope with probability 95%. The statistics of the response were calculated using 3,000 MC samples.

It can be noticed from Figure 7.1 that the mean value of all realizations does not coincide with the deterministic value except for the first case, $\delta_Z = .2$, in Figure 7.1 (a), in which they are very similar. The uncertainty is only predominant near the resonance and anti-resonance region. As the value of δ_Z increases, the uncertainty also increases in the two peaks and in the region in between the peaks. This shows that the uncertainty in the damping parameter interfere in the amplitude of displacement of the primary structure not changing the resonance frequencies, as expected, significantly affecting the performance of the damper, by changing the amplitude values at design frequency.

Another interesting aspect of Figure 7.1 is the presence of invariant points. It is known that for undamped TMD's, there are two invariant points where the response is independent of the attached absorber's damping value (Hartog, 1985). For a TMD, the invariant points are used to find the optimal vibration absorber parameters. For the case of light damping levels as seen in TLCD's, the invariant point method gives nearly optimal values.

The convergence rate for all dispersion coefficients is shown in Fig. 7.3(a), occurring way bellow the 3,000 Monte Carlo samples.

For the second case, the uncertainty in the structure stiffness parameter is included in the model. The values of coefficients of dispersion have a small variation, which means that the random variable associated to the structural stiffness has a small standard deviation since the mean value is fixed.

Figure 7.2 shows, for different values of δ_Z and δ_K, the mean model, the mean response of the stochastic model and the boundary lines representing the confidence region of 95%. The statistics of the response were calculated using 3,000 MC samples.

From Figure 7.2, it is clear that uncertainty in the primary-system stiffness is much more significant than uncertainty in the damping ratio parameter, since the damping ratio uncertainty only changes the FRF amplitudes around the resonance frequencies and in this case we have uncertainties occurring in all frequencies. The uncertainties in the

primary-system stiffness comes from, generally, the reduction in model to a 1 degree of freedom model. When the value of the coefficients of dispersion increases, the response limits becomes too wide to give any satisfactory insight in the dynamic of the system. Furthermore, since the magnitude of the structural stiffness is big, a large variation would result in unsatisfactory results and the simulation would not converge. For this reason, it is important to keep the dispersion of this parameter as small as possible.

The convergence rate for all dispersion coefficients is shown in Figure 7.3(b), occurring way below the 3,000 Monte Carlo samples.

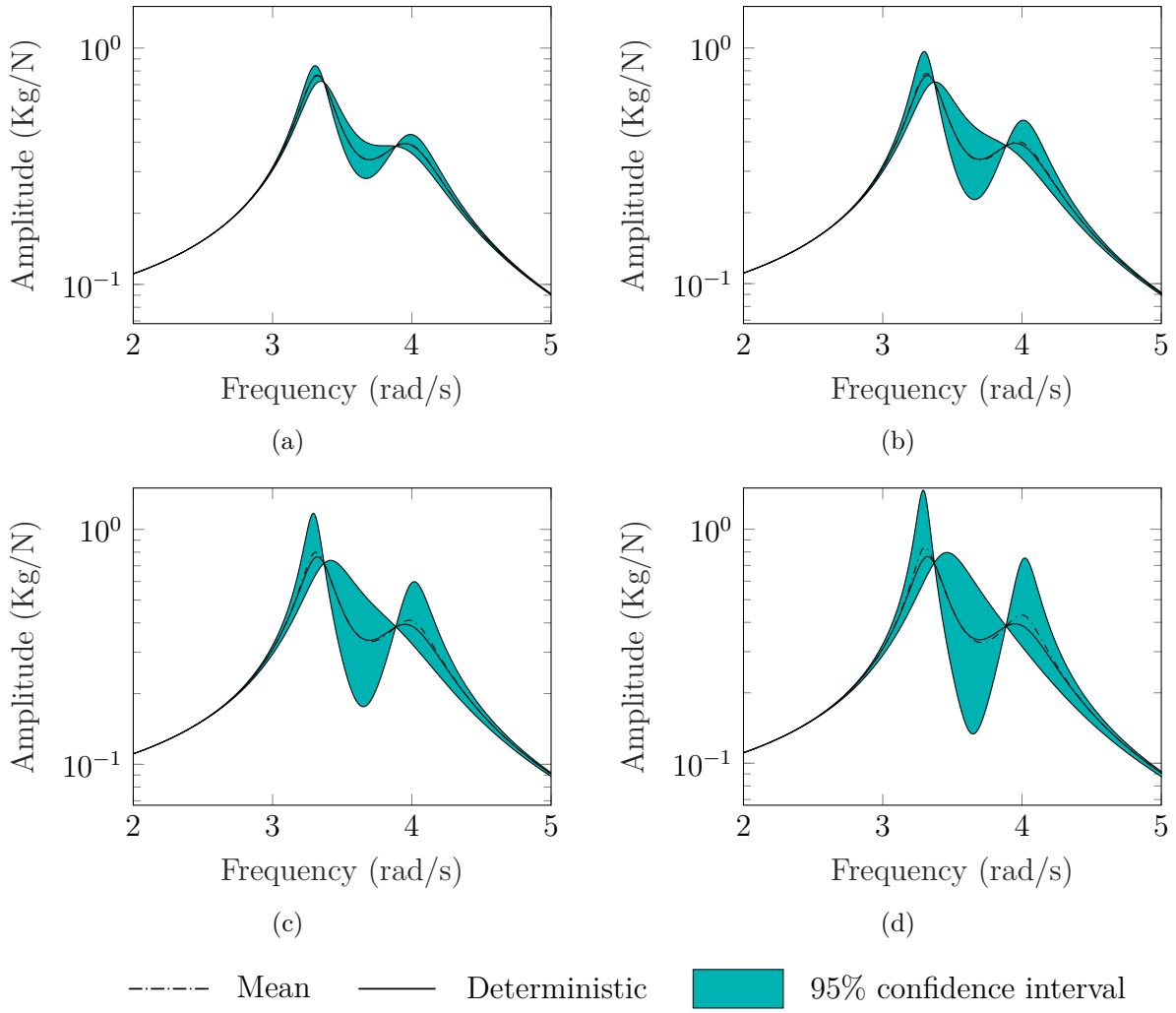

Figure 7.1 – FRFs amplitude with TLCD damping ratio uncertainties showing the deterministic model response, mean response of the stochastic model, and 95% confidence region for different values of δ_Z's: (a) .2 (b) .4 (c) .6 (d) .7.

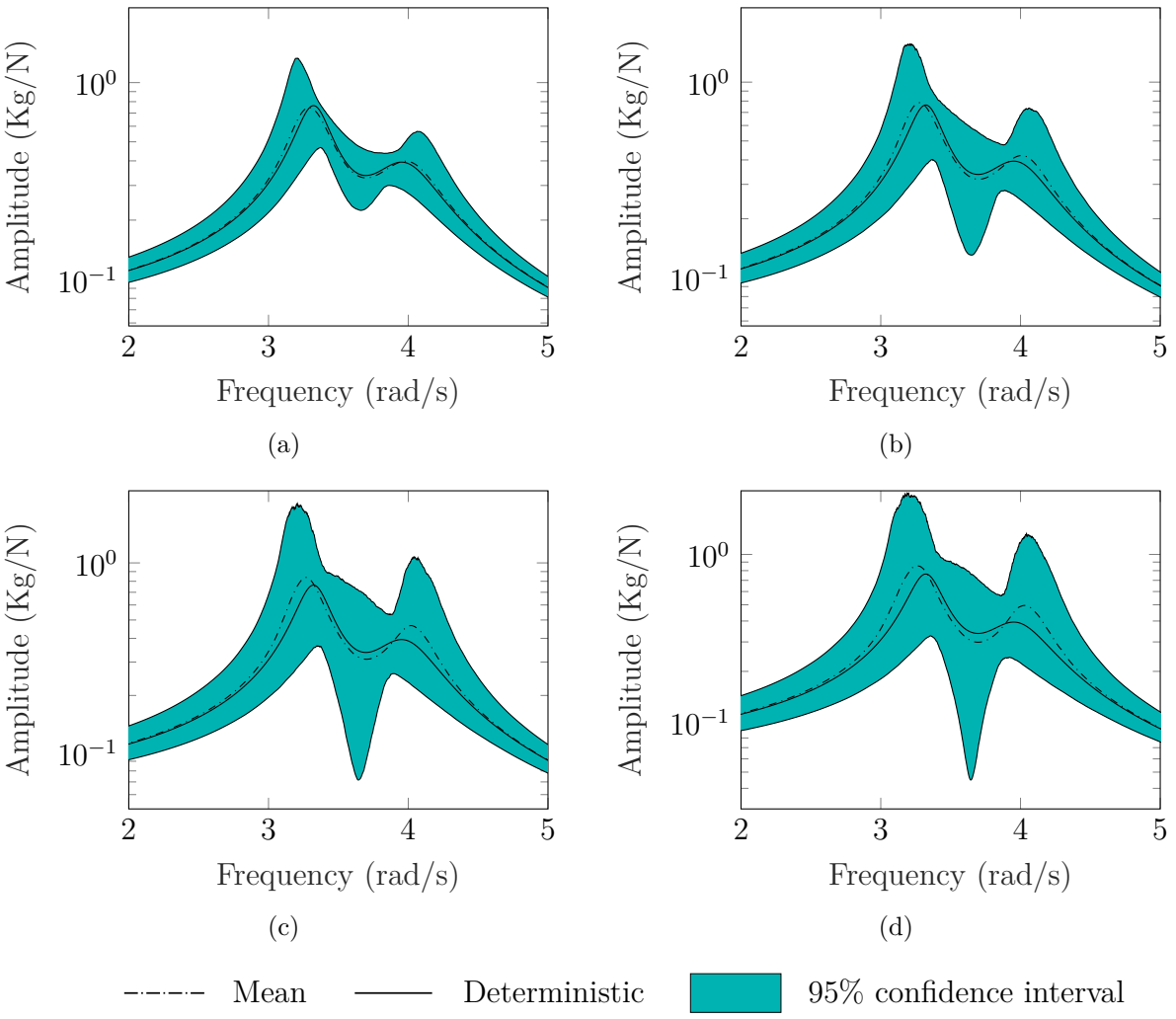

Figure 7.2 – FRFs amplitude with TLCD damping ratio and structure stiffness uncertainties showing the deterministic model response, mean response of the stochastic model, and 95% confidence region for different values of δ_Z and δ_K: (a) .2 & .05 (b) .4 & .15 (c) .6 & .25 (d) .7 & .35.

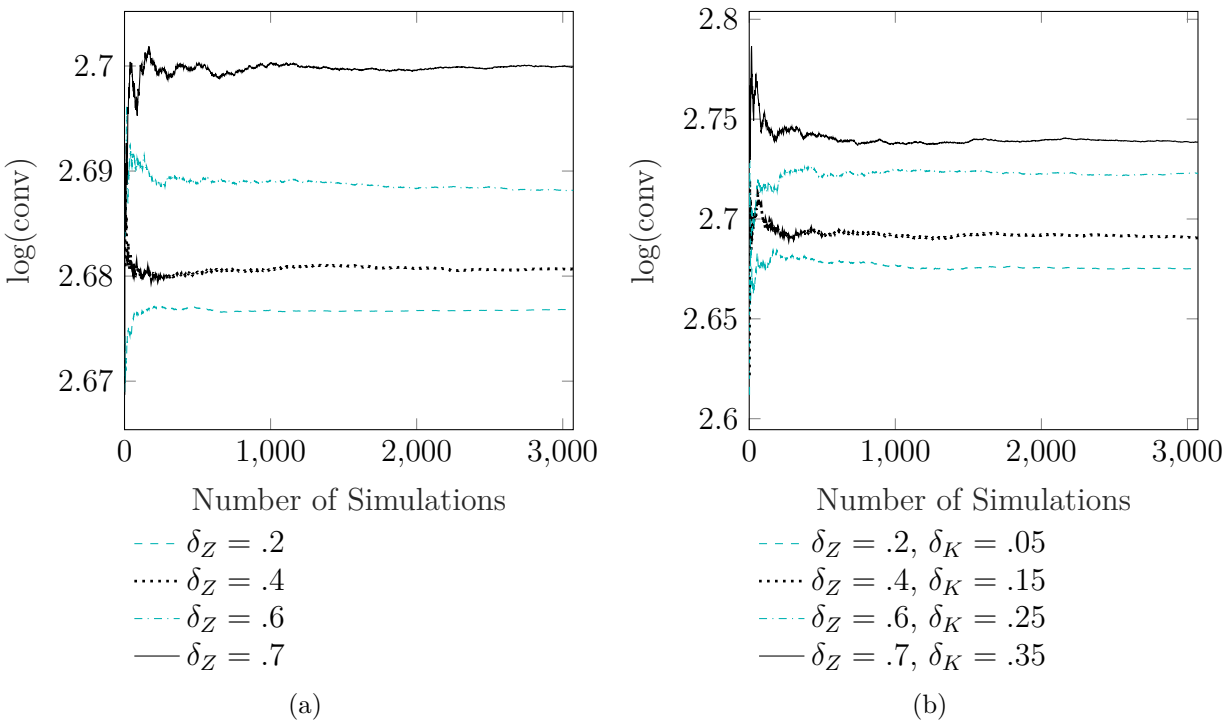

Figure 7.3 – Mean square convergence for (a) variability in δ_Z and (b) variability in both δ_Z and δ_K.

7.4 Concluding remarks

In this Chapter, we investigated parameters uncertainties in a TLCD applied in wind turbines. The assumption that uncertainties in structures have negligible response can be unacceptable in real situations and beside that, the uncertainties in the performance-related cannot be included in the damper parameter optimization. For this reason, to increase the credibility of the model, these uncertainties were included to help describe the range of potential outputs of the system at some probability level and estimating the relative impacts of input variable uncertainties.

The method consisted of considering the uncertainties in the absorber damping ratio and the structural stiffness element, constructed the probabilistic model from the Maximum Entropy principle and then, performed a Monte Carlo simulation. Two cases were studied in this thesis, the first only considering uncertainties in the absorber damping ratio and the second case considering both uncertainties in the absorber damping ratio and the structural stiffness. The results showed that the uncertainties can indeed interfere in the TLCD performance since it changes the FRF amplitude considerably in both cases and that uncertainty in the primary-system stiffness is relatively more significant than uncertainty in the damping ratio parameter although the last one interferes in the design performance.

Next chapter presents an experimental validation of the model.

8 Experimental Analysis

In this Chapter, the vibration phenomena through experimental observation.is investigated. Two major objectives are initially drawn: determining the nature and extent of vibration response levels and verifying theoretical models. The technique evolved on the advances made in digital signal processing, commonly called Modal test, provides the means for studying real structural vibration problems (Ewins, 1984).

Modal test is the combination of three components, the theoretical basis of vibration, accurate measurements of vibration and realistic data analysis. Free vibration analysis yields the system's FRF from an impact hammer test while a particular force response analysis, assuming harmonic motion, leads to the modal parameters such as natural frequency and damping factor.

Our great interest is to know how the structure vibrates under a given excitation. This depends not only upon the structure's inherent properties but also on the nature and magnitude of the imposed excitation. It is, however, convenient to present an analysis with a standard excitation from which the solution for any particular case can be constructed. The standard excitation chosen consist of a sinusoidal force applied at several points of the structure individually at every frequency.

The frequency range can be covered either by stepping from one frequency to another, or by slowly sweeping the frequency continuously. Pseudo-random or random excitation signals can replace the sine-wave approach by the existence of complex signal processing analyses capable of resolving the frequency content using Fourier analysis. Further extension can be apply to impulsive or transient excitation.

Efforts involving the matching or curve-fitting an expression and thereby finding the appropriate modal parameters are discussed next.

8.1 Identification of modal data

This section provides the basis of fundamental analysis technique. The analysis process of finding by curve fitting a set of modal properties which best match the response characteristics of the tested structure is called modal analysis. A general curve fitting approach is possible but inefficient. More details about different identification analysis can

be found in Ewins (1984).

A general form of the frequency response function for a single degree-of-freedom (SDoF) can take the form

$$H(\omega) = \sum_{r=1}^{N} \frac{A_r}{\lambda_r^2 - \omega^2} \tag{8.1}$$

and for a multi degree-of-freedom (MDoF)

$$\mathbf{H} = H_{jk}(\omega) = \sum_{r=1}^{N} \frac{\Phi_{jr}\Phi_{kr}}{\lambda_r^2 - \omega^2} \tag{8.2}$$

where A_r are the modal constants, ϕ_{jr} is the j^{th} element of the r^{th} eigenvector Φ_r, λ_r is the eigenvalues of the r^{th} mode and N is the number of degree of freedom (or modes).

A general curve-fitting approach is possible by considering a set of measured values $H_m(\omega_r)$, $r = 1, 2, \ldots$, in order to obtain estimates for the coefficients A_r, and λ_r^2, $r = 1, 2, \ldots$. The result found for theses coefficients are closely related to the modal properties of the system. However, such approach can be made, it is inefficient in a sense that it neither exploits the particular properties of resonant systems nor takes due account of the unequal quality of the various measured points in the data set $H_m(\omega_r)$, $r = 1, 2, \ldots$, both of which can have a significant influence on the solution. A variety of modal analysis method can be found in the literature and can be selected based on the appropriate condition the system impose.

A well established method is known as single-degree-of-freedom curve fitting or, more often, circle-fit procedure. The method, in essence, is based on the fact that at frequencies close to natural frequency, the mobility can often be approximated to that of a single degree-of-freedom system plus a constant offset term which accounts for the other modes. The procedure works by curve-fitting a circle to few measured data points and approximate the system's phase polar plot of the frequency response function which has a circular nature (Nyquist plot).

The circle-fit method has proven to be adequate in many practical cases, but care should be taken when the structure has close modes which can be seen when the Nyquist plot shows a lack of circular section (Ewins, 1984).

Turning to a response analysis, consider the case where a MDoF structure is excited harmonically by a set of forces in the same frequency, ω, with different amplitudes and phases. The equation of motion becomes

$$(\mathbf{K} - \omega^2\mathbf{M})\mathbf{x}e^{i\omega t} = \mathbf{f}e^{i\omega t} \tag{8.3}$$

rearranging to solve for the response

$$\mathbf{x} = (\mathbf{K} - \omega^2\mathbf{M})^{-1}\mathbf{f} \tag{8.4}$$

where the value $(\mathbf{K} - \omega^2\mathbf{M})^{-1}$ is the response model also called receptance matrix.

The mass normalization eigenvectors are written as Φ and have the following properties

$$\Phi^T \mathbf{M} \Phi = \mathbf{I}, \tag{8.5}$$

$$\Phi^T \mathbf{K} \Phi = diag(\omega_r^2), \tag{8.6}$$

the relation between the mass normalized mode shape and the general normalization is simply

$$\Phi = \frac{1}{\sqrt{m_r}} \Psi. \tag{8.7}$$

The general element of the receptance FRF can be written

$$\mathbf{x} = H_{jk}(\omega)\mathbf{f} \tag{8.8}$$

where

$$H_{jk}(\omega) = \frac{x_j}{f_k} \tag{8.9}$$

from this result, it is possible to determine the value of $H_{jk}(\omega)$ at any frequency of interest, although a matrix inversion is required at each frequency. An alternative way of derive the various FRF parameters is using the modal properties. Writing the FRF as follow

$$(\mathbf{K} - \omega^2 \mathbf{M}) = H_{jk}^{-1} \tag{8.10}$$

premultiply both side by Φ^T and post multiply both sides by Φ to obtain

$$\Phi^T (\mathbf{K} - \omega^2 \mathbf{M}) \Phi = \Phi^T H_{jk}^{-1} \Phi \tag{8.11}$$

or, using the normalization properties

$$diag(\omega_r^2) - \omega^2 \mathbf{I} = \Phi^T H_{jk}^{-1} \Phi \tag{8.12}$$

which gives

$$H_{jk} = \Phi (diag(\omega_r^2) - \omega^2 \mathbf{I})^{-1} \Phi^T \tag{8.13}$$

which is symmetric and can be used to compute any individual FRF parameter as follows

$$H_{jk}(\omega) = \sum_{r=1}^{N} \frac{\Phi_{jr} \Phi_{kr}}{(\omega_r^2 - \omega^2)} = \sum_{r=1}^{N} \frac{\Psi_{jr} \Psi_{kr}}{m_r (\omega_r^2 - \omega^2)} \tag{8.14}$$

which is the same expression found in Equation (8.1) if $A_r = \Phi_{jr} \Phi_{jr}^T$. This representation is easier to solve than Equation (8.9).

The same analysis can be done for a system with structural damping. The proportional damping has an advantage in the structure analysis because the mode shapes of such structure are identical to those of the undamped version and the natural frequencies

are very similar. The model properties of a proportionally damped system can be derive by analyzing the full undamped version and then making a correction for the presence of damping.

A more realistic and general damping can be considered called hysteretic damping. A general equation of motion for harmonic excitation and therefore harmonic solution takes the form

$$\mathbf{M}\ddot{\mathbf{x}} + \mathbf{K}\mathbf{x} + i\mathbf{D}\mathbf{x} = \mathbf{f}e^{j\omega t} \tag{8.15}$$

where $\mathbf{D}$ is the hysteretic damping matrix. A direct solution is obtained as

$$\mathbf{x} = (\mathbf{K} + i\mathbf{D} - \omega^2\mathbf{M})^{-1}\mathbf{f} = H_{jk}(\omega)\mathbf{f} \tag{8.16}$$

applying the same procedure of pre and post multiply by the eigenvector, it follows that

$$H_{jk}(\omega) = \sum_{r=1}^{N} \frac{\Phi_{jr}\P hi_{kr}}{(\omega_r^2 - \omega^2 + i\eta_r\omega_r^2} \tag{8.17}$$

where ω_r is the natural frequency and η_r is the damping loss factor for the r mode. From Equation 8.17, the FRF at any frequency can be found. Since, an system with hysteretic damping is considered, the natural frequency ω_r is not necessarily equal to the natural frequency of the undamped system (Ewins, 1984).

It assumed that at the vicinity of resonance the FRF is dominated by the contribution of that vibration mode and the contributions of other vibration modes are negligible (Fu & He, 2001). If this assumptions holds, then the FRF from a MDoF system can be treated as the FRF from a SDoF system at a certain bandwidth. The simplicity of the mathematical model for an SDoF system can then be used in the curve fitting to derive the modal parameters.

Circle fit method is based on the circularity of the Nyquist plot. Considering structural damping, the receptance $\alpha(\omega)$ FRF traces a perfect circle on the Nyquist plot

$$[Re(\alpha)]^2 + \left(Im(\alpha) + \frac{1}{2h}\right)^2 = \left(\frac{1}{2h}\right)^2 \tag{8.18}$$

where h is the structural (or hysteretic) damping.

We can assume that at the vicinity of a mode, the contribution of all other modes are negligible. This can be difficult to meet in reality. However, circle fit can rely on a more relaxed assumption. The receptance FRF of a N-Dof system with structural damping in modal form is given as

$$H_{jk}(\omega) = \sum_{r=1}^{N} \frac{\Phi_{jr}\Phi_{kr}}{(\omega_r^2 - \omega^2 + j\eta_r\omega_r^2)}. \tag{8.19}$$

If the rth mode is to be analyzed, we can single it out from the summation

$$H_{jk}(\omega) = \frac{\Phi_{jr}\Phi_{kr}}{(\omega_r^2 - \omega^2 + j\eta_r\omega_r^2)} + \sum_{\substack{s=1 \\ s\neq r}}^{N} \frac{\Phi_{js}\Phi_{ks}}{(\omega_s^2 - \omega^2 + j\eta_s\omega_s^2)}. \tag{8.20}$$

The summation term can be approximated by a complex constant, such that

$$H_{jk}(\omega) = \frac{\Phi_{jr}\Phi_{kr}}{\omega_r^2 - \omega^2 + j\eta_r\omega_r^2} + B_{jk} \tag{8.21}$$

thus, the circularity of the Nyquist plot shall not change except that the circle is shifted a distance away from the origin of the complex plane by the complex constant B_{jk}.

The procedure consists of first find the natural frequency then derive the damping loss factor and finally the modal constant. The accuracy of this method is significantly improved comparing to the peak-picking method (Fu & He, 2001). After the selection of FRF points at the vicinity of the resonance peak, the natural frequency can be found at the location where maximum arc change occurs on the Nyquist circle. Figure 8.1 shows the a representations of a Nyquist circle.

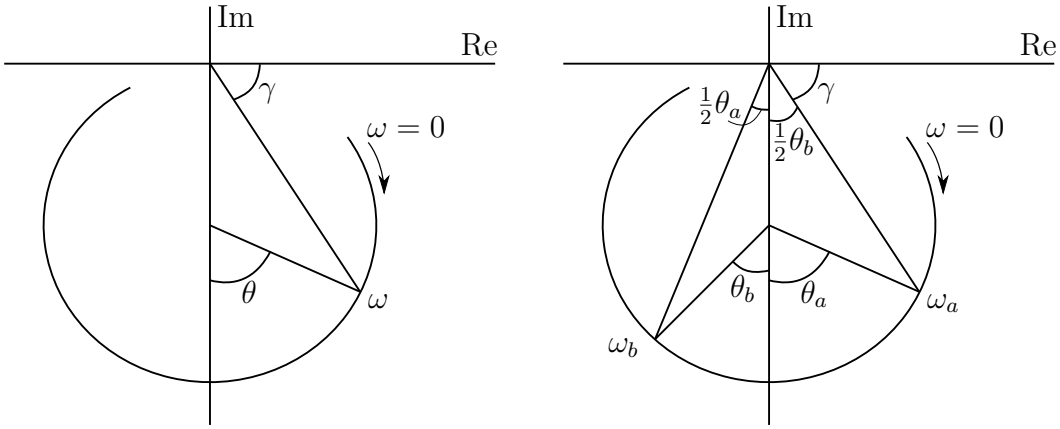

Figure 8.1 – Nyquist circle showing relevant angles for modal analysis.

From the relevant angles showing in Figure 8.1 and knowing that $\tan(\Im/\Re)$, hence

$$\tan\left(\frac{\theta}{2}\right) = \tan(90^o - \gamma) = \frac{\Re(\alpha)}{\Im(\alpha)} = \frac{\omega_r^2 - \omega^2}{\omega_r^2\eta_r}, \tag{8.22}$$

from which we obtain

$$\omega^2 = \omega_r^2\left(1 - \eta_r \tan\frac{\theta}{2}\right). \tag{8.23}$$

Differentiate Equation (8.23) with respect to θ we obtain a measure of the rate at which the locus sweeps around the circular arc, i.e.

$$\frac{d\omega^2}{d\theta} = -\frac{\omega_r^2\eta_r}{2}\left[1 + \left(\frac{1 - (\omega/\omega_r)^2}{\eta_r}\right)^2\right], \tag{8.24}$$

and it reaches a maximum value when $\omega = \omega_r$, which can be shown by further differentiating with respect to the frequency and equaling to zero

$$\frac{d}{d\omega}\left(\frac{d\omega^2}{d\theta}\right) = 0, \quad when \quad (\omega_r^2 - \omega^2) = 0. \tag{8.25}$$

Other than natural frequency, the damping loss factor can also be estimated from FRF data point (e.g. point a) using Equation (8.22)

$$\eta_r = \frac{\omega_r^2 - \omega_a^2}{\omega_r^2} \frac{1}{\tan(\theta_a/2)}. \tag{8.26}$$

Theoretically, the damping loss factor should be constant. However, due to measurement noise, nonlinearity and errors, the estimated damping loss factor varies for different data points. This variation can be useful to indicate the accuracy of the analysis.

The last quantity that can be extract from Nyquist plot is the modal constant which can be expressed using the mode shapes

$$A_{r_{jk}} = \Phi_{jr}\Phi_{kr} \tag{8.27}$$

the modal constant can be obtained from the diameter $D_{r_{jk}}$ which is conveniently quantified at the location of natural frequency

$$D_{r_{jk}} = \frac{A_{r_{jk}}}{\omega_r^2 \eta_r} \tag{8.28}$$

or

$$A_{r_{jk}} = D_{r_{jk}} \omega_r^2 \eta_r \tag{8.29}$$

the phase angle of the modal constant $A_{r_{jk}}$ is given by the location of the natural frequency.

8.2 Experimental setup

In this section, the experimental setup built in the Dynamic Systems Group (GDS) Vibration Laboratory is proposed. An experimental procedure is carried out to characterize the system and a comparison with the numerical analysis is performed. First, we discuss the methodology used to collect data of the two components of the systems, the structure and the TLCD.

In the literature, some previous experimental setups have been proposed. Lee et al. (2007) used a real-time hybrid testing method. The interacting or control force generated by a TLCD, which is observed from a load-cell is feedbacked to the control computer. With the feedback interacting force, the structural response of the story, where a TLCD is incorporated, is calculated from the numerical part. The shaking table excites the upper TLCD with this calculated response. While this methodology seems promising, it may defy the purpose of knowing a priori the optimized tuning values. Matteo et al. (2012) investigated the feasibility of a shear frame using a TLCD and a TMD for vibration mitigation. However, Matteo et al. did not study the optimized configuration. Besides that, he used sinusoidal waves as base excitation. In both works, base shaking excitation is utilized. The proposed approach uses an alternative method where the excitation happens at the top of the shear frame.

8.2.1 Structure characterization

The wind turbine tower can be simplified by a shear frame as showing in Figure 8.2. The structure construction is made of 4 steel beams and a plate whose masses are described in Table 8.1. Besides the element mass, an additional mass can be added on top of the plate. The added mass purpose is to increase the overall mass of the system since the plate mass is considerably small. The Beams and plate are connected by small aluminum plates with four screws which allows easy modification of height in the vertical axis.

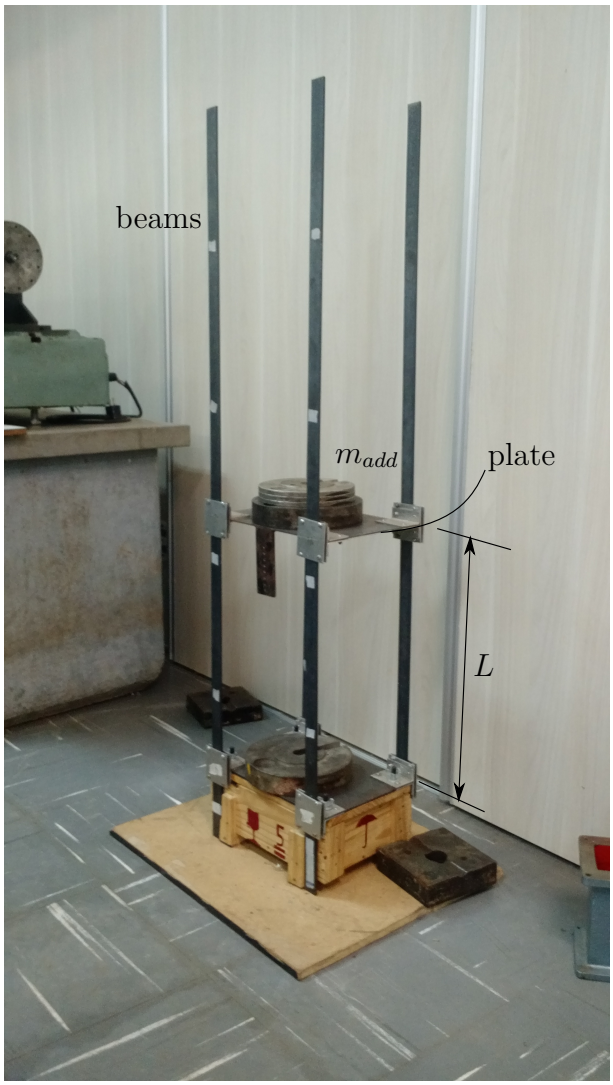

Figure 8.2 – Experimental structure assembly showing the main structural components.

The equipments used for modal testing are:

- Modally tuned impulse hammer with force sensor: Model PCB 086C01 with sensitivity 11.2 mV/N
- Accelerometer: Model PCB 353B03 with sensitivity 1.02 $mV/(m/s^2)$
- Data Acquisition Software: Polytec VibSoft

Table 8.1 – Structure masses and moment of inertia

	Symbol	Value	Quantity	total
Beam mass [kg]	m_{beam}	1.00	4	4.00
Plate mass [kg]	m_{plate}	1.17	1	1.17
			$\sum$ total m_e	4.17
Moment of inertia				
Beams cross section width	c_1 [m]	0.0055		
Beams cross section height	c_2 [m]	0.0256		
Moment of inertia	I [m^4]	0.35×10^{-9}	$(c_1 c_2^3/12)$	
Modulus of elasticity	E [Pa]	210×10^9		

The experimental characterization follows the procedure summarized in Figure 8.3. First, an impulse is applied to the structure near where the accelerometer is placed using the impact hammer. The impact should be as close to a perfect impulse as possible with infinitely short duration that results in a constant amplitude in the frequency domain. But since such an impulse is not possible, we need to know the contact time which is linked to the frequency band of the applied force.

The data from the sensor (accelerometer) is acquired using a data acquisition (DAQ) hardware from Polytec (Model VIB-E-220). The function of a DAQ is to measure an electrical of physical signal such as voltage, current, temperature or pressure from a sensor and then convert the signal through an analog-to-digital converter (ADC). Finally, the converted signal is conditioned and transferred to a computer with a programmable software. VibSoft is the chosen software for the application. The transferred data is treated and can be processed for visualization and for the FRF estimation.

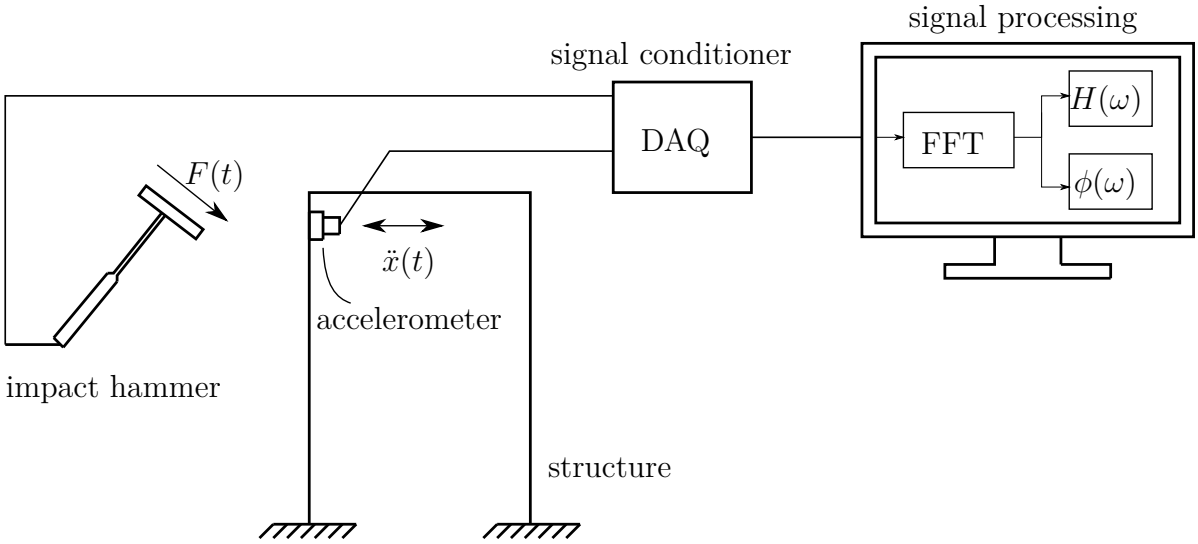

Figure 8.3 – Schematic representation of experimental procedure to characterize the structure.

Figure 8.4 shows the FRF of the structure for a specific height and for different masses. As the added mass increases, the first natural frequency decreases which is expected.

The first resonance peak occurs at about 3 to 4 Hz, the second one exhibit a similar amplitude and it occurs at around 23 Hz. The first two peaks of resonance can be attributed to translational modes of vibration. A third small peak that occur at frequencies around 47 Hz may be attributed to rotational mode of vibration. Even though the second mode amplitude is reasonably high, the structure is designed for low frequency applications and only the first mode is considered.

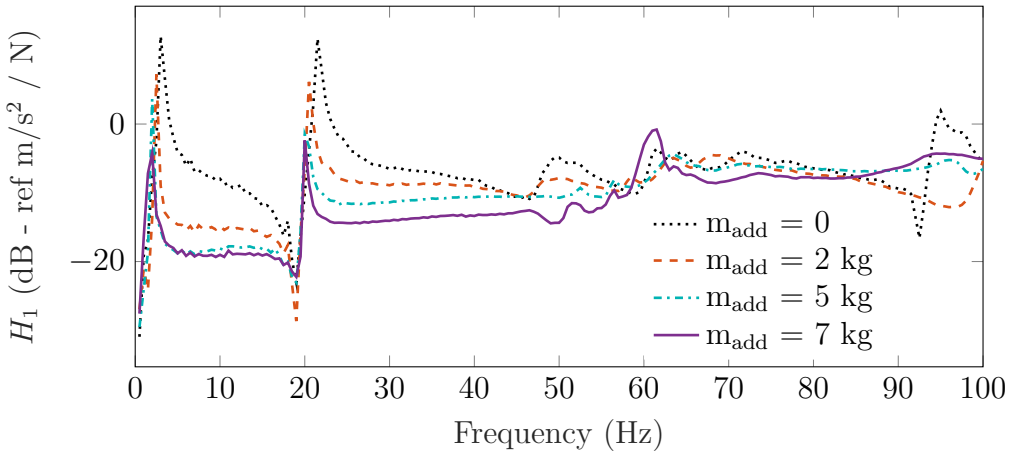

(a)

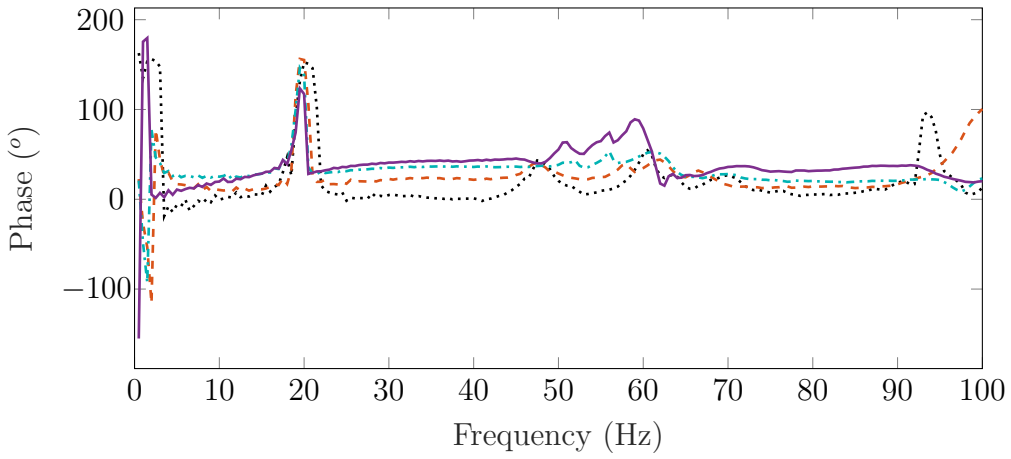

(b)

Figure 8.4 – Estimated FRF H_1 for different masses (black: $m = 0$ kg, red: $m = 2$ kg, blue: $m = 5$ kg, purple: $m = 7$ kg).

Figure 8.5 shows the experimental and theoretical structure's first mode natural frequency $f_{n,e}$ with respect to tower length L for different masses. The natural frequencies are estimated using the circle-fit method. The relation between the two parameter is not linear and an increase in height, results in a decrease of the natural frequency as expected. An increase in mass decreases the natural frequency for all heights shifting the curve in a downward direction. Moreover, we notice a good agreement between the theoretical values and the experimental values for the natural frequency. Some of the difference may be attributed to the structure construction and the circle-fit identification.

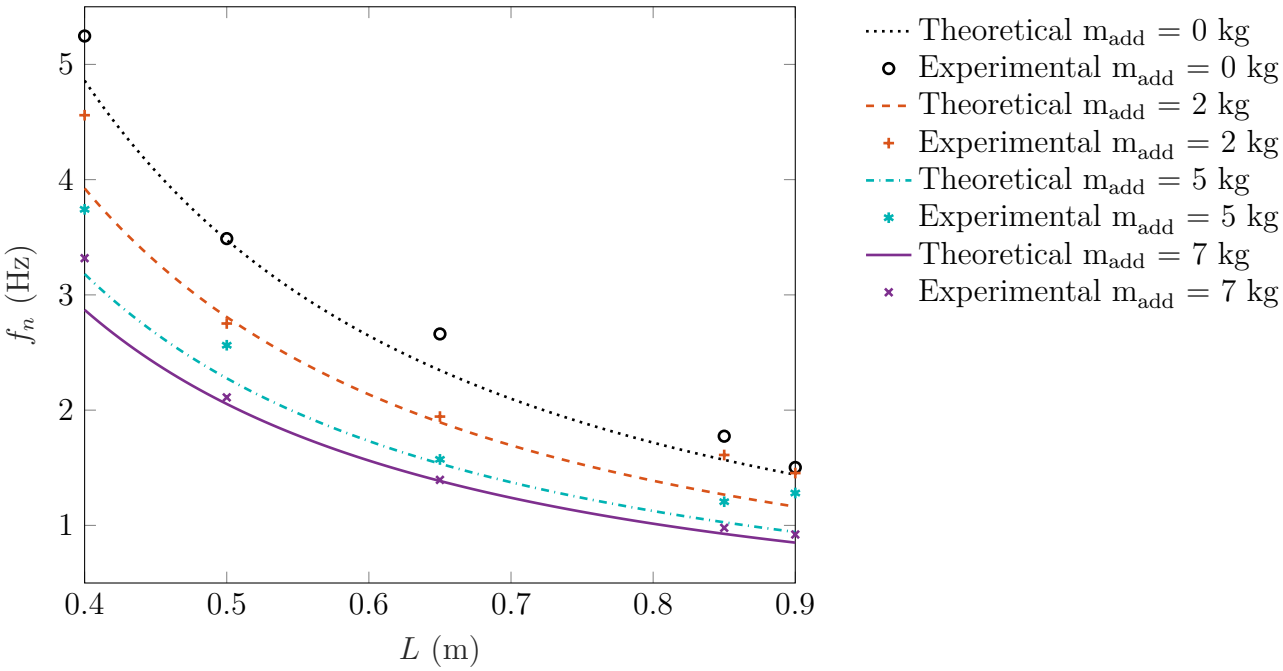

Figure 8.5 – Experimental and theoretical first mode natural frequency $f_{n,e}$ with respect to tower length L for different masses.

8.2.2 TLCD characterization

The TLCD was constructed as a straight edges reservoir. Transparent acrylic sheets with 2 mm thickness are used to build the reservoir and the chosen working fluid is water. The technical drawing in the Appendix shows the TLCD dimensions.

The experimental procedure follow the schematic showing in Figure 8.6. A recording camera was used to capture the liquid vertical displacement. In order to capture the displacement movement of the liquid column, a floating fish bait showing in Figure 8.7 is used as a reference point. After the initial disturbance, the displacement is captured and it results in a plot showing at Figure 8.8 where a curve is fitted to the displacement data and the modal parameter can be estimated. The displacement is fitted considering the general expression for the solution of a damped system given by

$$x(t) = Ae^{-\zeta\omega_n t}\sin(\omega_d t + \phi) + c \tag{8.30}$$

where A and c are constants. The algorithm uses a Levenberg-Marquardt nonlinear Least Squares method. The same procedure was repeated for different liquid column heights h_a from 35 cm to 105 mm which consequently changes the TLCD aspect(length) ratio α. The results are showing in Table 8.2 where the natural frequency can be found using the relation $\omega_d = \omega_n\sqrt{1-\zeta^2}$.

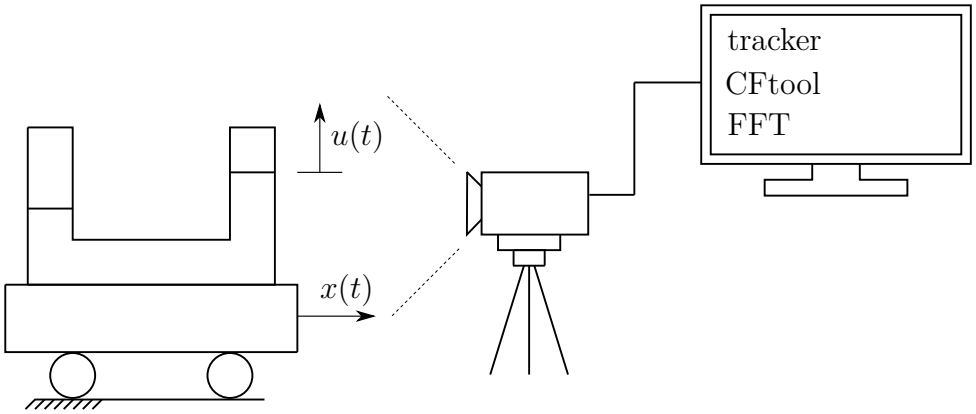

Figure 8.6 – Schematic representation of TLCD experimental procedure.

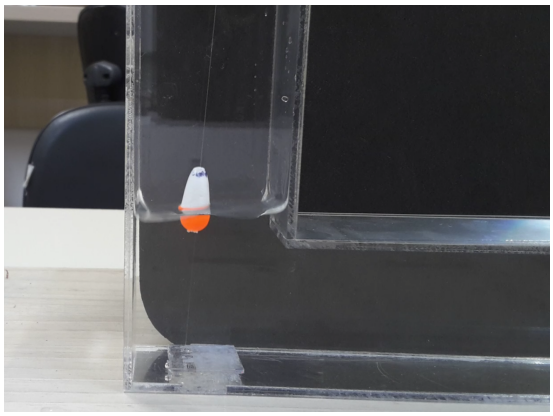

Figure 8.7 – Float fish bait used for capture the vertical displacement of the liquid column.

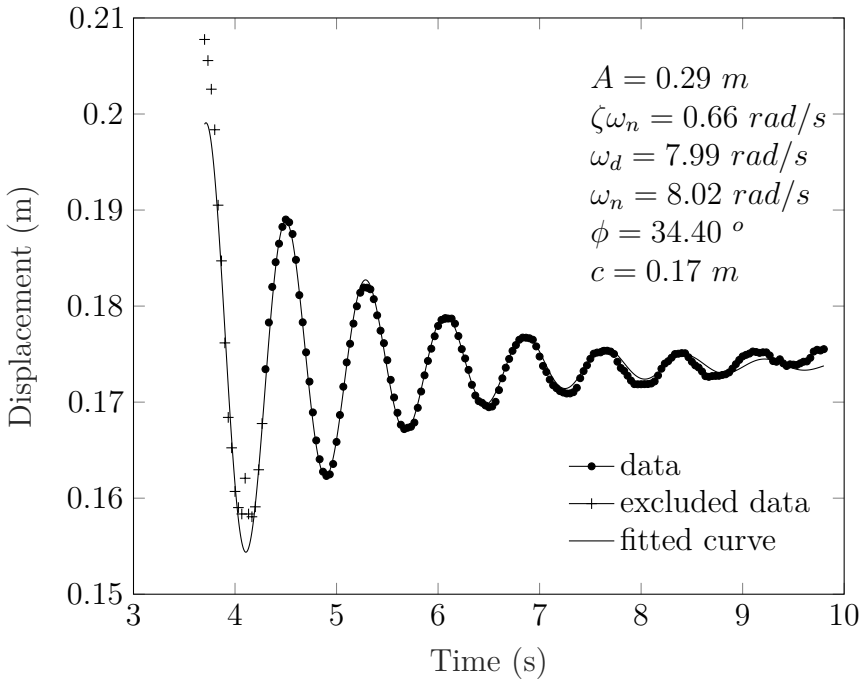

Figure 8.8 – Fitted curve of rectangular tlcd vertical displacement with respect to time and fitted coefficients.

Table 8.2 – TLCD experimental characterization parameters

Column height h_a [mm]	Aspect ratio α	TLCD mass m_a [kg]	Natural frequency $\omega_{n,a}$ [rad/s]	$f_{n,a}$ [Hz]	Damping ratio ζ_a
35	0.52	1.10	8.65	1.38	0.030
45	0.35	1.15	8.35	1.33	0.035
55	0.27	1.20	8.01	1.27	0.031
65	0.22	1.26	7.74	1.23	0.030
75	0.18	1.31	7.52	1.20	0.031
85	0.15	1.36	7.33	1.17	0.026
95	0.14	1.41	7.22	1.15	0.030
105	0.12	1.47	7.02	1.12	0.048

8.3 Structural dynamic response with a TLCD

After the dynamic parameters have been characterized, an experimental study is performed to identify the structure dynamic response with a TLCD, which is rigidly connect to the structure upper plate.

The test procedure can follow two approaches. The first approach begins by first tuning the TLCD to the structure first natural frequency. The tuning can be done by varying the water column height following the data presented in Table 8.2. The exact values for optimized tuning are obtained through the computer algorithm from Chapter 6.

The second and alternative approach follows an inverse procedure where the water column is known a priori and the structures is tuned accordingly by changing its height. This approach is chosen because the TLCD reservoir has a fixed construction, whereas the experimental structure can have its height easily adjust. However, in a real word scenario the opposite would be the case, the structure would have a fixed construction and the TLCD would be tuned accordingly.

This approach starts by choosing the appropriate water column height. The column height should be high enough so the effects of water displacement are relevant, but it cannot be too high so there is water spill. From experimental observation, the best height is around $h_a = 65$ mm. Then, the TLCD geometric parameters are used to obtain the dimensionless parameters α and μ. Since the actual structure length in unknown, we arbitrarily estimate it for the first iteration and calculate a theoretical value for the stiffness k_{teo}. Using α, μ and k_{teo} as input in the optimization algorithm we get as output the optimized tuning ratio. Next, the structure and the TLCD natural frequency can be calculated and from the structure's natural frequency, its stiffness can be obtained. If the obtained structure's stiffness is not equal the theoretical stiffness, the structure's length is updated and the whole process is repeated, otherwise, the optimized length is obtained. The iterative process is summarized in Figure 8.9.

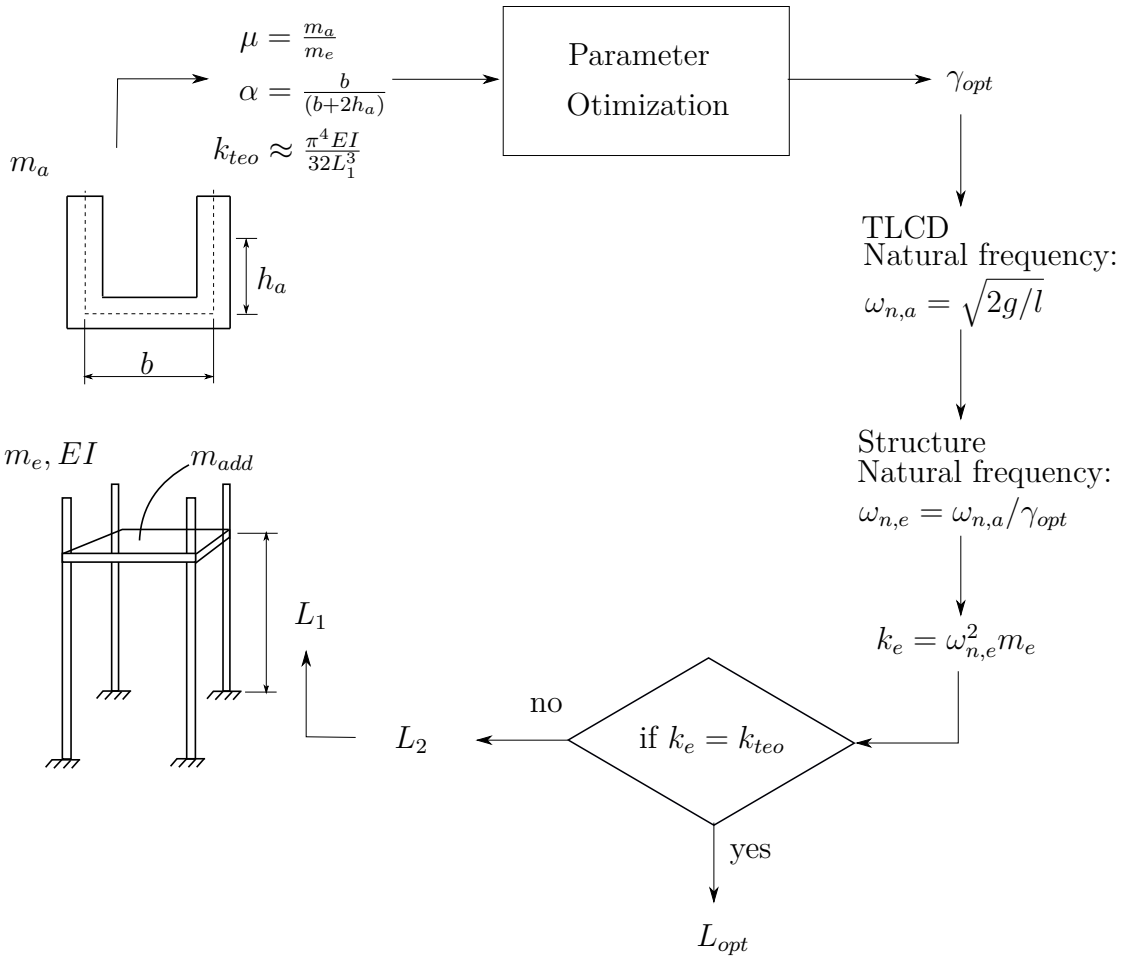

Figure 8.9 – Diagram for the inverse approach for the testing procedure. An iterative process is used to determine the optimized structure length based on the TLCD's geometry.

For a TLCD column of $h_a = 65$ mm, we obtain the values for the length ratio $\alpha = 0.63$ and mass ratio $\mu = 0.14$ considering an added mass of $m_{add} = 5kg$. The results from the parameter optimization gives $\gamma_{opt} = 0.92$, then from the calculated TLCD's natural frequency of $\omega_{n,a} = 1.23$ Hz we obtain the structure's natural frequency of $\omega_{n,e} = 1.21$ Hz. Finally, the structures stiffness is calculated which gives a values of $k_e = 490$ N/m and the structure height is found to be $L = 79.3$ cm (the subscript *opt* is omitted from now on). This result is in accordance with the structure's natural frequency from Figure 8.5 and with the TLCD's natural frequency from Table 8.2, both at about 1.3 Hz.

A procedure to allow a comparison between the system with and without absorber are proposed through two experiments.

8.3.1 Experiment 1: root mean square method

This procedure consist of calculating the root mean square (RMS) ratio of the amplitude between the output signal from the accelerometer and input signal from the function generator for a range of frequencies. The RMS is a way of expressing its average

(mean) power of a signal. The input and output signals are sinusoidal waves in the time domain as shown in Figure 8.10.

Figure 8.11 shows the experimental data for the RMS ratio between the output and input signal for three configurations, $m_{add} = 6$ kg, $m_{add} = 5$ kg with TLCD (1.1 kg), $m_{add} = 3$ kg with TLCD for reference. It can be noticed the effect of added mass is predominant when comparing the curve with 5 kg and 3 kg. The TLCD, however, does not seem to be a major influence in the damping although its tuned frequency is correctly showing a decrease in the amplitude value for the RMS ratio at about 1.3 Hz which is the TLCD's tuning frequency. From the plot trend, a second peak might exist at a frequency bellow 1 Hz. Even so, due the accelerometer limitations which has minimum frequency range of 1 Hz, the data for small frequencies could not be acquired.

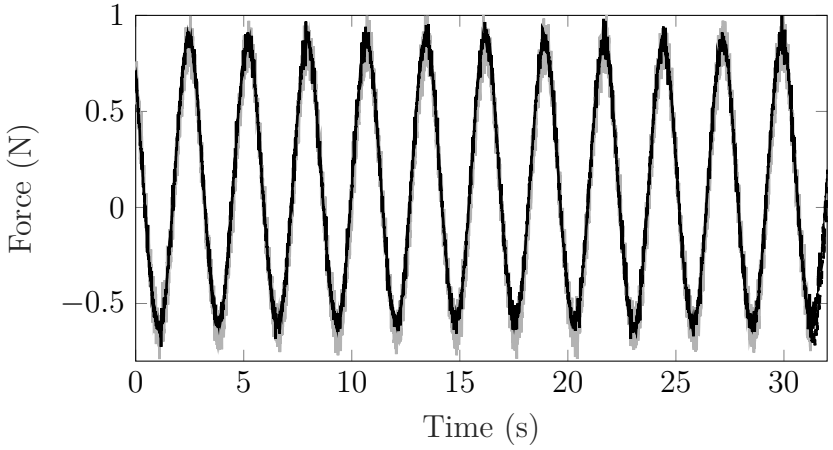

Figure 8.10 – Experimental input (gray) and output (black) normalized sinusoidal functions.

8.3.2 Experiment 2: structure free response

A second experiment is performed to investigate the transient free vibration response of the structure with and without TLCD. A similar setup to calculate the TLCD natural frequency using a recording camera is used. This methodology is chosen due to the low natural frequency of the system and limitation of the accelerometer frequency resolution observed in experiment 1. An initial condition is impose to the structure using a string. Each experiment is done considering the same initial condition. The camera captures the structure's displacement for both cases, with and without TLCD as shown in Figure 8.12. A 40 second video is recorded for both cases generating data with 1024 samples each.

In this case, the structure is tuned to the TLCD frequency using experimental data only. The TLCD column height used is $h_a = 65$ mm, which from Table 8.2 has a natural frequency of $f_{n,a} = 1.23$ Hz. The chosen length for the structure is $L = 0.98$ m and added mass at the top is $m_{add} = 8.4$ kg which gives a natural frequency of $f_{n,e} = 1.93$ Hz. The ratio between natural frequency is $\gamma = 0.7$ which is not ideal but is still considered

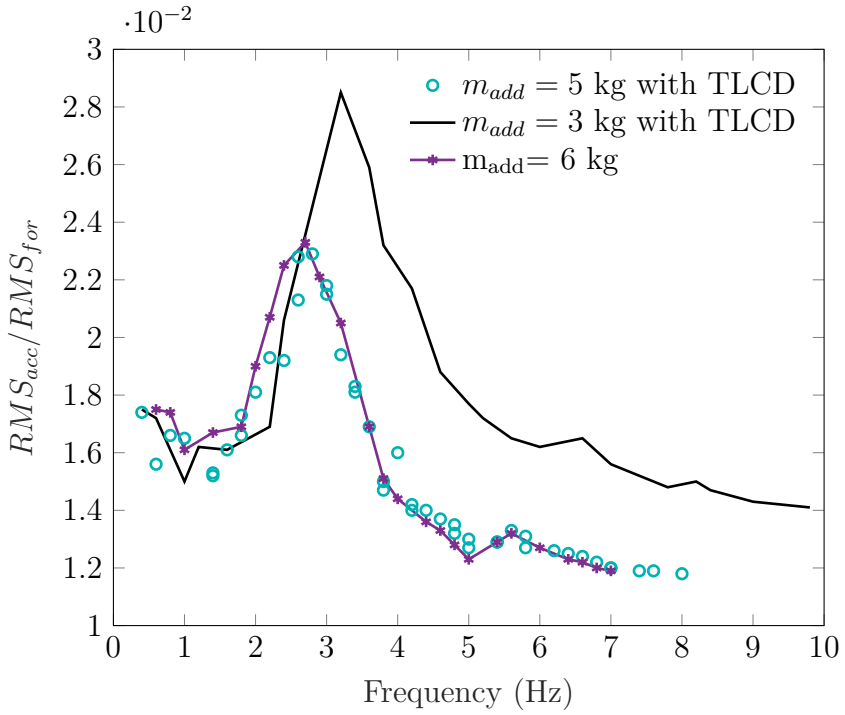

Figure 8.11 – Experimental data for the RMS ratio between the output and input signal from three configurations, $m_{add} = 6$ kg, $m_{add} = 5$ kg with TLCD, $m_{add} = 3$ kg with TLCD.

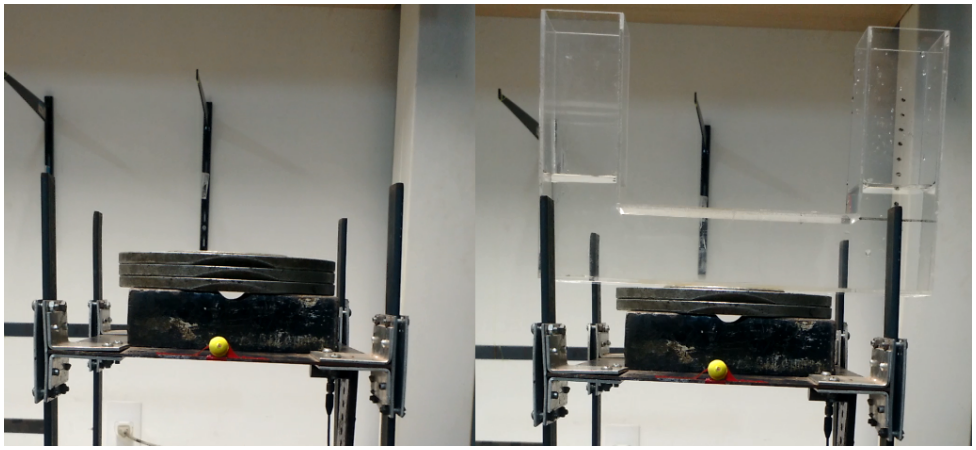

Figure 8.12 – Experimental structure with and without TLCD for tracking the structure displacement.

nonetheless given the structure and TLCD physical constraints (maximum length and fixed construction, respectively).

Figure 8.13 (a) shows the structure displacement with and without TLCD. A decrease in the structure displacement amplitude is seen at about 20%. Additionally, a slight shift in phase is seen as the time increase. This can be attributed to the elements off-tuning during design phase and nonlinearities present in the TLCD.

Figure 8.13 (b) shows the response PSD of the structure with and without TLCD. The output PSD is constructed by performing the Discrete Fourier transform (DFT) of the displacement and calculating the quantity $|X(f)|^2$ which is an energy spectral density.

A decrease in the PSD amplitude occurs at the structure resonance peak. A second peak seems to occur at around 4 Hz and the presence of the TLCD shift the peak slightly and decreases its amplitude. Moreover, Figure 8.13 (b) shows a decrease in amplitude near 1.3 Hz which is the proposed tuned frequency of the TLCD.

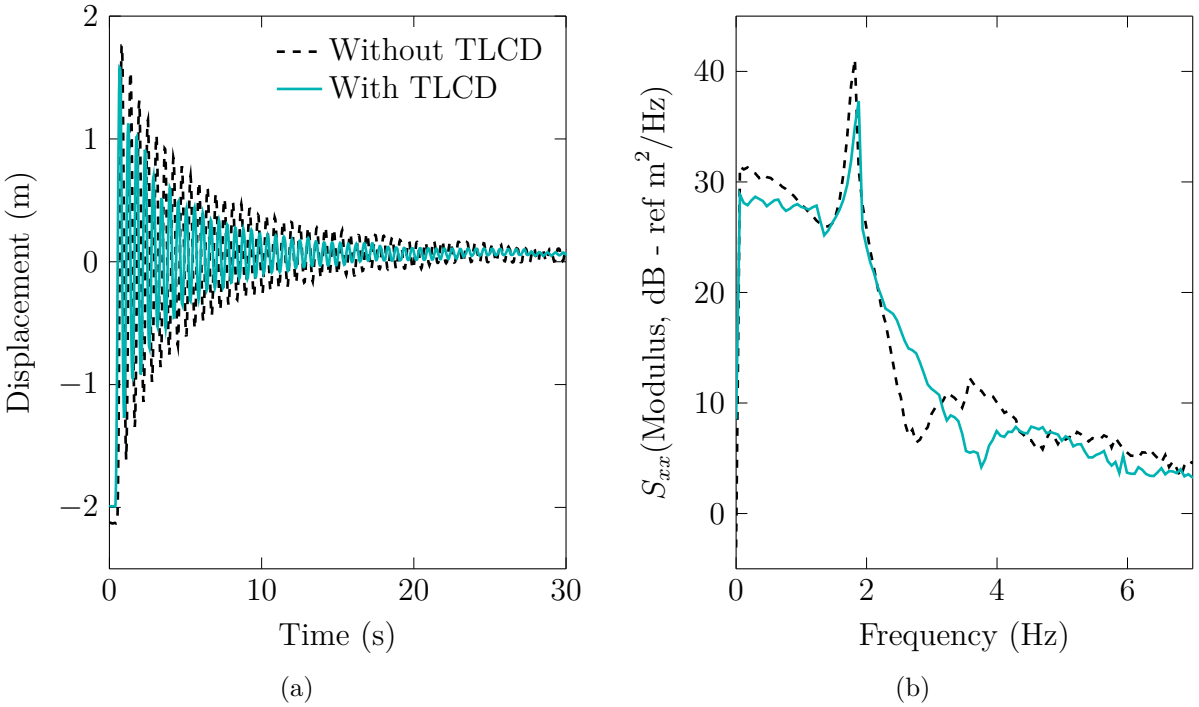

Figure 8.13 – Experimental (a) displacement and (b) output PSD of structure with length $L = 0.98$ m for the case without TLCD with added mass $m_{add} = 8.4$ kg and configuration using a TLCD (1.1 kg) with added mass $m_{add} = 7.3$.

A second configuration is now investigated. In order to obtain a smaller structure natural frequency, the added mass to the tip mass is increased to $m_{add} = 10$ kg. Figure 8.14 shows the output PSD for different liquid column heights. The fundamental frequency of the structure can be obtained from Figure 8.14 which is around 1.71 Hz. In this configuration, the natural frequency shows a difference between the previous case with 2 kg less mass as expected. Moreover, a decrease in the PSD amplitude is seen both at the structure resonance peak and near the TLCD natural frequency. Comparing the three different liquid column height, an optimum height can be established. The liquid column height cannot be neither too high not too low. A liquid column height of about 55 cm showed overall better results.

In the case of small liquid column height, the sharp edges of the tube's columns create a region propitious for the appearance of air bubbles and turbulence effects, which are not ideal and in most cases undesirable. Another observation about Figure 8.14 concerns the region of decrease in amplitude around 1.3 Hz. As the liquid column increases, it can be noticed the frequency in which there are a decrease in amplitude also decreases. This is in agreement with the fact that the TLCD natural frequency decrease with an increase of the liquid column.

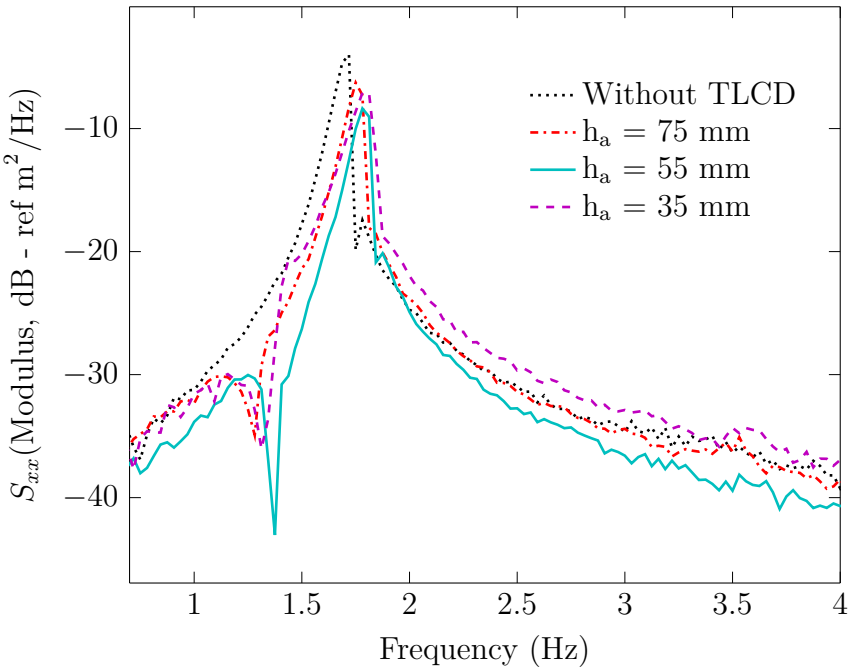

Figure 8.14 – Output PSD of structure with length $L = 0.98$ m for the case without TLCD with added mass $m_{add} = 10$ kg and configuration using a TLCD (1.1 kg) with different column heights.

8.4 Concluding remarks

In this Chapter, the structure and the TLCD were characterized through an experimental procedures. We successfully characterized the structure and the TLCD and the main modal parameters were found. A procedure with the TLCD attached to the structure was done to investigated the effect of the damper in the structure.

Two methodology were then investigated, the RMS method and the structure free response. In the RMS method, the RMS value for the excitation and the structure response were calculated using an accelerometer and a function generator. For this case, results showed that the effect of added mass were predominant. Even though the effects of TLCD were minimal, it still showed a vibration reduction (RMS amplitude) which validated the correctly tuned TLCD near its natural frequency. Even though this methodology indicates correctly TLCD behavior, due the accelerometer limitations, the data for small frequencies could not be acquired. A second methodology was then proposed using a recording camera.

In the second method, the structure free response is investigated using a recording camera. This methodology was chosen due to the low natural frequency of the system and limitation of the accelerometer frequency resolution observed in experiment 1. Results for two configurations were shown, the first configuration consisting of a test to investigate the efficacy of the TLCD even though the elements were not completely tuned and a second configuration with more added mass to decrease the structure's natural frequency in order to investigate the effects of different liquid column height in the structure's response. A decrease in the structure displacement amplitude is seen at about 20% for the first

configuration. The second configuration showed the impact of different heights to the structure response, which cannot be neither too high nor too low. A liquid column height of about 55 cm showed overall better results. Moreover, results showed a decrease in the PSD amplitude at the structure resonance peak and near the TLCD natural frequency.

As suggestions for future works, a new TLCD model could be constructed with higher operation frequency and with more construction modularity. Further tests with more sensible equipment with lower frequency range can also be investigated.

9 Final Remarks

The main objective of this thesis was to develop a numerical and experimental analysis to study a tuned liquid column damper (TLCD) subjected to random wind loads with particular application in wind turbines. The numerical analysis in this thesis was divided in two stages. The first stage consider the deterministic model of the wind turbine and TLCD. The wind turbine model was derived from a simplified one degree of freedom wind turbine using the virtual work method. The goal was to control the structure for small displacement without considering the rotational inertia from the blades. The numerical study then followed the derivation of the TLCD model in accordance with the fluid dynamics theory of a liquid oscillating in a tube, where the liquid's motion can be derived from the Bernoulli equation. An optimization approach was adopted which allows the search of optimized parameter considering different wind spectrums. The second stage concentrated in study the nondeterministic model aiming to quantify uncertainties in the damper and structure parameters. An experimental phase was then carried out in the Dynamic Systems Group (GDS) facilities. The characterization of the TLCD and structure are carried out and the coupled problem is compared with the numerical results.

Chapter 2 presented some of the main structural control techniques in suppressing vibration of structures. First, the state of the art of structural control was presented. Then, the relevant types of control systems were discussed. Emphasis was given to passive controls and more specifically on the tuned liquid absorbers and their use in wind turbines which is the subject of this work. A brief bibliographic review was made about the use of absorbers in several applications and their development in recent years. Chapter 3 consisted of a first exposition of the fundamental concepts of random vibration and probability theory. The aim was to review the key principles of the probability theory and thus facilitate its application to solve problems in the random vibration.

Chapter 4 dealt with the effects of the probabilistic aspect of wind in low atmospheric layers on flexible structures. The problems is confined to along-wind response of structures. Moreover, cross-wind response or aero-elastic coupled problems were left out of discussion. The idea was discuss some general notions, which should cast some light on the complexity of the phenomenon. In Chapter 5, the influence of the wind in the structural dynamic behavior was of interest. It was therefore of interest study how good a simplified dynamic model could estimate the structural response. The simplified model had to be reduced to

the elementary coordinates but still had to describe the relevant physical process under consideration with good accuracy. Such a simplified model can be used as an early design of new wind turbines. This work focused on the structural dynamic aspect of structures such as lattice towers with concentrated mass at the top, hence, the model does not include the gyroscopic effects due to turbine blade rotation.

In Chapter 6, it was proposed a global direct search optimization algorithm for the TLCD's parameters subjected to an arbitrary wind spectra, given by its power spectral density (PSD). A simple verification was made considering the analytical solution of undamped primary structure under white noise excitation. Finally, a numerical example with a simplified wind turbine model was given to illustrate the efficacy of TLCD and it was shown that different wind spectra can significantly affect the optimization results, i.e. the TLCD parameters. Time and frequency domain results from the random vibration analysis were shown. Satisfactory reduction of the response vibration levels is found and it is shown that different wind profiles can significantly affect the optimum TLCD parameters.

Chapter 7 parametric uncertainties were investigated in a wind turbine with TLCD. The assumption that uncertainties in structures have negligible response can be unacceptable in real situations and, beside that, uncertainties in the performance-related cannot be included in the damper parameter optimization. For this reason, to increase the credibility of the model, these uncertainties were included to help describe the range of potential outputs of the system at some probability level and estimating the relative impacts of input variable uncertainties. Two different cases were studied, the first one only considering uncertainties in the absorber damping ratio and the second case considering both uncertainties in the absorber damping ratio and the structural stiffness. The results showed that the uncertainties can indeed interfere in the TLCD performance since it change the FRF amplitude considerably in both cases and that uncertainty in the primary-system stiffness is relatively more significant than uncertainty in the damping ratio parameter although the last one interferes in the design performance.

Finally, Chapter 8 focused on understand the vibration phenomena through experimental observation. The experimental setup built in the Dynamic Systems Group (GDS) Vibrations Laboratory was proposed. An experimental procedure was carried out to characterize the system and a comparison with the numerical analysis was then performed. A procedure with the TLCD attached to the structure was done to investigated the effect of the damper in the structure. In the RMS method, the RMS value for the excitation and the structure response were calculated using an accelerometer and a function generator. Results from Figure 8.11 showed that the effect of added mass was predominant. Even though the effects of TLCD were minimal, it still showed a vibration reduction (RMS amplitude) which validated the correctly tuned TLCD near its natural frequency. Even though this methodology indicates correctly TLCD behavior, due the accelerometer limitations, the data for small frequencies could not be acquired. A second methodology was then proposed using a recording camera.

In the second method, the structure free response is investigated using a recording camera. This methodology was chosen due to the low natural frequency of the system and limitation of the accelerometer frequency resolution observed in experiment 1. Results for two configurations were shown, the first configuration consisting of a test to investigate the efficacy of the TLCD even though the elements were not completely tuned and a second configuration with more added mass to decrease the structure's natural frequency in order to investigate the effects of different liquid column height in the structure's response. A decrease in the structure displacement amplitude is seen at about 20% for the first configuration. The second configuration showed the impact of different heights to the structure response, which cannot be neither too high nor too low. A liquid column height of about 55 cm showed overall better results.

9.1 Future works

Some future works that may contribute to the research.

- increase structure model complexity by
  - including rotational effects from the blade,
  - adding more degree of freedom
- compare the mathematical model with finite element analysis
- compare the mathematical model with FAST wind turbine simulator
- compare the TLCD with other damper strategies
- introduce different optimization solutions with multiple TLCDs
- introduce different stochastic wind models
- introduce different methodologies to quantify uncertainties in the system
- improvements to the experimental setup

9.2 List of publications

Work submitted to Journals

Alkmim, M. H., M. V. G. de Morais, and A. T. Fabro. Optimum Parameters of a Tuned Liquid Column Damper in a Wind Turbine Subject to Stochastic Load. Submitted to *Engineering Structures*, 2017.

Conference proceedings:

Alkmim, M. H., M. V. G. de Morais, and A. T. Fabro. Vibration Reduction of Wind Turbines Using Tuned Liquid Column Damper Using Stochastic Analysis. Journal of Physics: Conference Series. Vol. 744. No. 1. IOP Publishing, 2016.

Alkmim, M. H., M. V. G. de Morais, and A. T. Fabro. Response Variability of a Tuned Liquid Column Damper Applied to a Wind Turbine. 5^{th} International Conference on Engineering Optimization (EngOpt), Iguassu Falls, Brazil, 2016.

Alkmim, M. H., M. V. G. de Morais, and A. T. Fabro. Response Variability with Random Uncertainty in a Tuned Liquid Column Damper. XXXVII Ibero-Latin American Congress on Computational Methods in Engineering (CILAMCE), Brasília, Brazil, 2016.

References

AGEZE, M. B.; HU, Y.; WU, H. Wind turbine aeroelastic modeling: Basics and cutting edge trends. *International Journal of Aerospace Engineering*, Hindawi Publishing Corporation, v. 2017, 2017.

ALKMIM, M.; MORAIS, M. de; FABRO, A. Vibration reduction of wind turbines using tuned liquid column damper using stochastic analysis. In: IOP PUBLISHING. *Journal of Physics: Conference Series*. [S.l.], 2016. v. 744, n. 1, p. 012178.

ALTAY, O. et al. Vibration mitigation of wind turbine towers by tuned liquid column dampers. In: *Proceedings of the IX international conference on structural dynamics, Porto, Portugal*. [S.l.: s.n.], 2014. v. 12.

AUCIELLO, N. Transverse vibrations of a linearly tapered cantilever beam with tip mass of rotary inertia and eccentricity. *Journal of Sound and Vibration*, Elsevier, v. 194, n. 1, p. 25–34, 1996.

AVILA, S. et al. Numerical modeling of the dynamic behavior of a wind turbine tower. *Journal of Vibration Engineering & Technologies*, v. 4, p. 249–257, 2016.

BAUMGART, A.; LARSEN, G. C.; HANSEN, M. H. *Models for wind turbines-a collection*. [S.l.], 2002.

BURTON, T. et al. *Wind energy handbook*. [S.l.]: John Wiley & Sons, 2001.

CATALDO, E.; BELLIZZI, S.; SAMPAIO, R. Taking into account uncertainties to analyze the robustness of an energy pumping system. In: *IX Argentinean Congress on Computational Mechanics y II South American Congress on Computational Mechanics (MECOM 2010)*. [S.l.: s.n.], 2010. p. CD–ROM.

CHAKRABORTY, S.; ROY, B. K. Reliability based optimum design of tuned mass damper in seismic vibration control of structures with bounded uncertain parameters. *Probabilistic Engineering Mechanics*, Elsevier, v. 26, n. 2, p. 215–221, 2011.

CHANG, C.; QU, W. Unified dynamic absorber design formulas for wind-induced vibration control of tall buildings. *The structural design of tall buildings*, John Wiley & Sons, Ltd., v. 7, n. 2, p. 147–166, 1998.

COLWELL, S.; BASU, B. Tuned liquid column dampers in offshore wind turbines for structural control. *Engineering Structures*, Elsevier, v. 31, n. 2, p. 358–368, 2009.

CONSTANTINOU, M. C.; SOONG, T. T.; DARGUSH, G. F. *Passive energy dissipation systems for structural design and retrofit*. [S.l.]: Multidisciplinary Center for Earthquake Engineering Research Buffalo, New York, 1998.

DAVENPORT, A. G. The spectrum of horizontal gustiness near the ground in high winds. *Quarterly Journal of the Royal Meteorological Society*, Wiley Online Library, v. 87, n. 372, p. 194–211, 1961.

ENEVOLDSEN, I.; MØRK, K. Effects of a vibration mass damper in a wind turbine tower*. *Journal of Structural Mechanics*, Taylor & Francis, v. 24, n. 2, p. 155–187, 1996.

ERTURK, A.; INMAN, D. J. *Piezoelectric energy harvesting*. [S.l.]: John Wiley & Sons, 2011.

EWINS, D. J. *Modal testing: theory and practice*. [S.l.]: Research studies press Letchworth, 1984. v. 15.

FARSHIDIANFAR, A. Tuned liquid column dampers with period adjustment equipment for earthquake vibrations of high-rise structures. In: *6th National Congress on Civil Engineering, 6NCCE*. [S.l.: s.n.], 2011.

FRAHM, H. *Device for damping vibrations of bodies*. [S.l.]: Google Patents, 1911. US Patent 989,958.

FU, Z.-F.; HE, J. *Modal analysis*. [S.l.]: Butterworth-Heinemann, 2001.

GAO, H.; KWOK, K.; SAMALI, B. Optimization of tuned liquid column dampers. *Engineering structures*, Elsevier, v. 19, n. 6, p. 476–486, 1997.

GHANEM, R. G.; SPANOS, P. D. *Stochastic finite elements: a spectral approach*. [S.l.]: Courier Corporation, 2003.

GUIMARAES, P. V. et al. Vibration control of an offshore wind turbine modeled as an inverted pendulum. 2014.

HALFPENNY, A. *Dynamic analysis of both on and offshore wind turbines in the frequency domain*. Tese (Doutorado) — University of London, 1998.

HARTOG, J. P. D. *Mechanical vibrations*. [S.l.]: Courier Corporation, 1985.

HATCH, M. R. *Vibration simulation using MATLAB and ANSYS*. [S.l.]: CRC Press, 2000.

HOOKE, R.; JEEVES, T. A. Direct search solution of numerical and statistical problems. *Journal of the ACM (JACM)*, ACM, v. 8, n. 2, p. 212–229, 1961.

JONG, P. D. et al. Solar and wind energy production in relation to the electricity load curve and hydroelectricity in the northeast region of brazil. *Renewable and Sustainable Energy Reviews*, Elsevier, v. 23, p. 526–535, 2013.

KANG, N. et al. Dynamics of flexible tower-blade and rigid nacelle system: dynamic instability due to their interactions in wind turbine. *Journal of Vibration and Control*, SAGE Publications, v. 22, n. 3, p. 826–836, 2016.

KAPUR, J. N.; KESAVAN, H. K. *Entropy optimization principles and their applications*. [S.l.]: Springer, 1992.

KAREEM, A. Model for predicting the acrosswind response of buildings. *Engineering Structures*, Elsevier, v. 6, n. 2, p. 136–141, 1984.

KIM, J. E. On the equivalent mass-spring parameters and assumed mode of a cantilevered beam with a tip mass. *Journal of Mechanical Science and Technology*, Springer, v. 31, n. 3, p. 1073–1078, 2017.

KOLDA, T. G.; LEWIS, R. M.; TORCZON, V. Optimization by direct search: New perspectives on some classical and modern methods. *SIAM review*, SIAM, v. 45, n. 3, p. 385–482, 2003.

KRÉE, P.; SOIZE, C. *Mathematics of random phenomena: random vibrations of mechanical structures*. [S.l.]: Springer Science & Business Media, 2012. v. 32.

LACKNER, M. A.; ROTEA, M. A. Structural control of floating wind turbines. *Mechatronics*, Elsevier, v. 21, n. 4, p. 704–719, 2011.

LEE, C.-L. et al. Optimal design theories and applications of tuned mass dampers. *Engineering structures*, Elsevier, v. 28, n. 1, p. 43–53, 2006.

LEE, S.-K. et al. Experimental implementation of a building structure with a tuned liquid column damper based on the real-time hybrid testing method. *Journal of mechanical science and technology*, Springer, v. 21, n. 6, p. 885–890, 2007.

LI, J.; ZHANG, Z.; CHEN, J. Experimental study on vibration control of offshore wind turbines using a ball vibration absorber. *Energy and Power Engineering*, Scientific Research Publishing, v. 4, n. 03, p. 153, 2012.

MARANO, G. C.; GRECO, R.; SGOBBA, S. A comparison between different robust optimum design approaches: application to tuned mass dampers. *Probabilistic Engineering Mechanics*, Elsevier, v. 25, n. 1, p. 108–118, 2010.

MATTEO, A. D. et al. The control performance of tlcd and tmd: experimental investigation. In: *5th European Conference on Structural Control*. [S.l.: s.n.], 2012. p. 18–20.

MAYNE, J. The estimation of extreme winds. *Journal of Wind Engineering and Industrial Aerodynamics*, Elsevier, v. 5, n. 1-2, p. 109–137, 1979.

MCNAMARA, R. J. Tuned mass dampers for buildings. *Journal of the structural Division*, ASCE, v. 103, n. 9, p. 1785–1798, 1977.

MIN, K.-W.; KIM, J.; LEE, H.-R. A design procedure of two-way liquid dampers for attenuation of wind-induced responses of tall buildings. *Journal of Wind Engineering and Industrial Aerodynamics*, Elsevier, v. 129, p. 22–30, 2014.

MURTAGH, P.; BASU, B.; BRODERICK, B. Wind force time-history generation by discrete fourier transform (dft). *Multi-Body Dynamics: Monitoring and Simulation Techniques III 3rd*, 2004.

MURTAGH, P.; BASU, B.; BRODERICK, B. Along-wind response of a wind turbine tower with blade coupling subjected to rotationally sampled wind loading. *Engineering structures*, Elsevier, v. 27, n. 8, p. 1209–1219, 2005.

NEWLAND, D. E. *An introduction to random vibrations, spectral & wavelet analysis*. [S.l.]: Courier Corporation, 2012.

PAZ, M. *Structural dynamics: theory and computation*. [S.l.]: Springer Science & Business Media, 2012.

POTTMAIER, D. et al. The brazilian energy matrix: from a materials science and engineering perspective. *Renewable and Sustainable Energy Reviews*, Elsevier, v. 19, p. 678–691, 2013.

ROBERTS, J. B.; SPANOS, P. D. *Random vibration and statistical linearization*. [S.l.]: Courier Corporation, 2003.

RUBINSTEIN, R. Y.; KROESE, D. P. *Simulation and the Monte Carlo method*. [S.l.]: John Wiley & Sons, 2016. v. 10.

SAAED, T. E. et al. A state-of-the-art review of structural control systems. *Journal of Vibration and Control*, Sage Publications Sage UK: London, England, v. 21, n. 5, p. 919–937, 2015.

SAKAI, F.; TAKAEDA, S.; TAMAKI, T. Tuned liquid column damper-new type device for suppression of building vibrations. In: *International Conference on Highrise Buildings, Nanjing, China, Mar*. [S.l.: s.n.], 1989. p. 25–27.

SAKAI, F.; TAKAEDA, S.; TAMAKI, T. Tuned liquid column dampers (tlcd) for cable-stayed bridges. In: *Proc. Specialty Conf. Innovation in Cable-Stayed Bridges*. [S.l.: s.n.], 1991. p. 197–205.

SAMPAIO, R.; RITTO, T. Dinâmica de estruturas flexíveis análise determinística e estocástica. In: . [S.l.: s.n.], 2008. p. 3–5.

SHUM, K. Closed form optimal solution of a tuned liquid column damper for suppressing harmonic vibration of structures. *Engineering Structures*, Elsevier, v. 31, n. 1, p. 84–92, 2009.

SOIZE, C. Maximum entropy approach for modeling random uncertainties in transient elastodynamics. *The Journal of the Acoustical Society of America*, Acoustical Society of America, v. 109, n. 5, p. 1979–1996, 2001.

SOIZE, C. A comprehensive overview of a non-parametric probabilistic approach of model uncertainties for predictive models in structural dynamics. *Journal of sound and vibration*, Elsevier, v. 288, n. 3, p. 623–652, 2005.

SOONG, T. T.; DARGUSH, G. F. *Passive energy dissipation systems in structural engineering*. [S.l.]: Wiley, 1997.

STEWART, G. M. Load reduction of floating wind turbines using tuned mass dampers. 2012.

STREETER, V. L.; WYLIE, E. B.; BEDFORD, K. W. *Fluid mechanics, WCB*. [S.l.]: McGraw-Hill, 1998.

THRÁINSSON, H.; KIREMIDJIAN, A. S.; WINTERSTEIN, S. R. *Modeling of earthquake ground motion in the frequency domain*. [S.l.]: John A. Blume Earthquake Engineering Center, 2000.

TORCZON, V. On the convergence of pattern search algorithms. *SIAM Journal on optimization*, SIAM, v. 7, n. 1, p. 1–25, 1997.

VANDERPLAATS, G. N. *Numerical optimization techniques for engineering design: with applications*. [S.l.]: McGraw-Hill New York, 1984. v. 1.

WU, J.; YANG, J. Active control of transmission tower under stochastic wind. *Journal of Structural Engineering*, American Society of Civil Engineers, v. 124, n. 11, p. 1302–1312, 1998.

XU, Y.; SAMALI, B.; KWOK, K. Control of along-wind response of structures by mass and liquid dampers. *Journal of Engineering Mechanics*, American Society of Civil Engineers, v. 118, n. 1, p. 20–39, 1992.

YALLA, S. K.; KAREEM, A. Optimum absorber parameters for tuned liquid column dampers. *Journal of Structural Engineering*, American Society of Civil Engineers, v. 126, n. 8, p. 906–915, 2000.

ZUO, L.; NAYFEH, S. A. Minimax optimization of multi-degree-of-freedom tuned-mass dampers. *Journal of Sound and Vibration*, Elsevier, v. 272, n. 3, p. 893–908, 2004.

Appendix